Department of Physics and Astronomy

University of Heidelberg

Diploma thesis

in Physics

submitted by

Lisa Michaels

born in Berlin

2012

Phenomenology of Sterile Neutrinos at different Scales

This diploma thesis has been carried out by

Lisa Michaels

at the

Max Planck Institute for Nuclear Physics

under the supervision of

Prof. Dr. Manfred Lindner

Fakultät für Physik und Astronomie

Ruprecht-Karls-Universität Heidelberg

Diplomarbeit

Im Studiengang Physik

vorgelegt von

Lisa Michaels

geboren in Berlin

2012

Phänomenologie von sterilen Neutrinos an verschiedenen Skalen

Die Diplomarbeit wurde von

Lisa Michaels

ausgeführt am

Max-Planck-Institut für Kernphysik

unter der Betreuung von

Herrn Prof. Dr. Manfred Lindner

Phänomenologie von sterilen Neutrinos an verschiedenen Skalen

Sterile Neutrinos sind eine sehr einfache Erweiterung des Standardmodells der Teilchenphysik und führen dennoch zu Veränderungen in vielen physikalischen Beobachtungsgrößen. Da sie durch ihre Mischung mit den aktiven Neutrinos mit den anderen Teilchen des Standardmodells wechselwirken, beeinflussen sie Prozesse der schwachen Wechselwirkung. Die Art der Veränderungen hängt von der Masse der sterilen Neutrinos ab und von ihrer Mischung mit den aktiven Neutrinos. Zwei Massenskalen werden in dieser Arbeit aufgegriffen: Für ein sehr leichtes steriles Neutrino, welches mit den aktiven Neutrinos oszilliert, wird untersucht, ob diese Oszillation durch Wechselwirkungen mit Materie verstärkt werden kann. Wenn die Mischung von den aktiven und dem sterilen Neutrino groß ist, kann der Fluß atmosphärischer aktiver Neutrinos um bis zu 80% verringert werden, wenn sie die Erde durchqueren. Der zweite Teil dieser Arbeit befasst sich mit indirekten Effekten schwerer steriler Neutrinos auf elektroschwache Beobachtungsgrößen. Wenn sowohl Korrekturen nullter als auch erster Ordnung einbezogen werden, können sich die Beiträge der sterilen Neutrinos in einigen Parametern aufheben. Dadurch werden größere Mischungsparameter erlaubt, die dann zu in Zukunft messbaren Effekten in anderen Prozessen führen können.

Phenomenology of sterile Neutrinos at different Scales

Sterile neutrinos are one of the most simple extensions of the Standard Model (SM), but they can still have a rich variety of phenomenological implications on physical observables. As they interact with other SM particles through their mixing with the active neutrinos, they modify processes of the weak interaction. The signatures of the sterile neutrinos depend on their masses and their mixing to the active neutrinos. Two mass scales are picked up in this thesis: First, a very light sterile neutrino that oscillates with the active neutrinos is considered and it will be analyzed, whether the oscillations can be resonantly enhanced when interacting with a matter background. For a large active–sterile mixing the deficit in the atmospheric active neutrino flux after crossing the Earth could be up to 80%. In the second part indirect effects of heavy sterile neutrinos on electroweak observables are examined. When tree-level and one-loop effects are taken into account, a cancellation of the contributions of the sterile neutrinos can be present in some observables. Therefore, a larger active–sterile mixing is allowed that can then lead to sizeable influence on other processes, which can be detected in the near future.

Contents

Acknowledgements

First of all I would like to thank Manfred Lindner for giving me the opportunity to work in his group and to write this diploma thesis. It was him who directed my attention to sterile neutrinos in the first place. I am very grateful for his encouragement and guidance. Moreover, I am very thankful that Manfred Lindner sent me to the Schladming winter school, where I learned a lot about Quantum Field Theory and LHC physics.

I am very grateful to Evgeny Akhmedov, Alexander Kartavtsev and Juri Smirnov for supervising my work and answering patiently all my questions. Evgeny Akhmedov explained me the field of neutrino oscillation, what I am very thankful for. Alexander Kartavtsev and Juri Smirnov were always available if I had a question.

For proof-reading my thesis I have to thank Johanna Gramling, Julian Heeck, Evgeny Akhmedov, Juri Smirnov, Alexander Kartavtsev, Alexander Dück and Stefan Brünner. I appreciate their help for disentangling my confused thoughts, finding all the errors and misspelling in my text.

I am deeply grateful to Werner Rodejohann, Joachim Kopp, Thomas Schwetz-Mangold, He Zhang, Yasutaka Takanishi, Michael Dürr, James Barry, Tibor Frossard and Kher Sham Lim that their office was always open for me and I could come with questions.

Next, I would like to thank all the Diploma, Master and Bachelor students I had the pleasure to share the office with: Stefan Brünner, Philipp Grothaus, Nina Memenga, Alina Wilhelm, Dominik Neuenfeld, Dominik Stolzenburg, David Mitrouskas, Dominik Skala, Pascal Humbert, Steffen Schmidt, Johannes Welter and Gianna Marschmann. I wish to thank them for the interesting discussions and the support.

I would like to express my gratitude to Anja Berneiser and Britta Schwarz for taking care of all the bureaucracy and helping me with all the forms I had to fill out.

My studies would not have been possible without the support of my parents Sabine Sültrup and Kai Michaels and my boyfriend Alexander Schuster.

Finally, I would like to say that I really enjoy working in this group.

CHAPTER 1

Outline

In the course of time, many descriptions of the laws of nature have been thought up and discarded again. While some new theories just took the old ideas a few steps further, others led to an entire new understanding of nature, changing the philosophical view on its relations. General relativity, for example, redefined the understanding of space and time, revising them from being mathematical concepts to being physical objects that are influenced by the existence of matter. The basis of quantum mechanics, contradicting the idea of determinism in the range of its validity, was even rejected by some great minds for its philosophical implications.

These two theories, both revolutionary in their underlying assumptions, are the fundamentals of today's physics. While general relativity describes the dynamics at large scales, e.g. the evolution of galaxies, quantum mechanics was extended to quantum field theory, describing mainly the physics at small scales. It is the basis of the Standard Model (SM) of particle physics, one of the most successful theories so far. Numerous experiments have been built in the last decades to test the SM, having reached an impressive precision. Although there are hints for physics beyond the SM, most new theories only extend the SM by new particles of new symmetry groups.

The most firmly established phenomenon in particle physics, which is clearly in need of physics beyond the SM, is the oscillation of neutrinos. As will be explained in chapter 2,

neutrinos must thus have tiny, but nonvanishing masses. In the SM, however, neutrinos are massless by construction. This motivates the introduction of so-called sterile neutrinos, as this is the straightforward way to generate neutrino masses. These sterile states are singlets under the SM gauge group and in the most general case Majorana particles, meaning they are their own antiparticles. But they can actually have a rich phenomenology. Via the Yukawa coupling – the coupling of the Higgs field to fermions – they interact with the SM neutrinos. When the electroweak symmetry is broken and the Higgs field acquires a vacuum expectation value, this leads to a mixing of the sterile with the SM neutrinos. Through the mixing they then also couple to other SM particles.

Other hints to physics beyond the SM come for example from large scale observations, from the dynamics of galaxies and stars. The incompatibilities with theory could most easily be explained by the existence of one or more particles that do not interact electromagnetically, being therefore called "Dark Matter". On the other hand, the SM also fails to explain the baryon asymmetry of the universe, i.e. the fact that the universe is made up of particles and not antiparticles.

Sterile neutrinos could also solve these other two problems. They could be a warm dark matter candidate and heavy sterile neutrinos could provide a mechanism causing a lepton asymmetry in the universe (called leptogenesis), which is then transferred to baryons via sphaleron processes.

In this work the phenomenology of sterile neutrinos at different mass scales will be discussed. The motivation for the introduction of sterile neutrinos will be revisited in more detail in chapter 2. Chapter 3 is devoted to the possibilities of observing sterile neutrinos in different processes and phenomena. These may vary depending on the mass of the sterile neutrino. Some processes are only sensitive to light, others to heavy sterile neutrinos, since the contribution of the sterile states can change depending on their mass. In chapters 4 and 5 two mass scales are taken up. First, one very light sterile neutrino with a mass at the eV scale is treated. This neutrino can oscillate with the SM neutrinos and it will be analyzed whether the oscillation could be enhanced by matter effects, thus facilitating their detection. The calculation will be done especially for the oscillation of electron neutrinos to sterile neutrinos, as there are some hints to the disappearance of electron (anti)neutrinos into a sterile state coming from reactor experiments with electron antineutrinos and calibrations of detectors with radioactive sources. Chapter 5 will turn to a discussion of heavy sterile neutrinos, whose masses are above the Z boson mass. These neutrinos are not produced via weak interactions at tree-level and leave a trace just by the non-unitarity of this effective theory. Since they may however propagate in loops, they contribute to the oblique correction parameters. These

two indirect effects – the non-unitarity and the loop contributions – are summarized in corrections to electroweak precision observables. This analysis is motivated by e.g. the NuTeV anomaly, where the ratios of neutral to charged current cross-sections in (anti)neutrino–nucleon scattering were smaller than predicted and the measurement of the Z decay width into invisible particles resulting in a number of neutrino species slightly smaller than three. It will be examined, whether the agreement of the data with the theoretical predictions can be improved by the introduction of heavy sterile neutrinos as an addition to the SM. In chapter 6 the results will be summarized and an outlook to future prospects of these topics is given.

CHAPTER 2

An Introduction to Sterile Neutrinos

Sterile neutrinos have been introduced as an extension of the Standard Model (SM) in order to describe neutrino masses. Hints for the existence of neutrino masses have been found only recently, so that in the formulation of the SM neutrinos are purely left-handed and one cannot write down a mass term in the Lagrangian; neutrinos are thus massless. In the following, the experimental evidence for massive neutrinos will be discussed and mass terms in the Lagrangian introduced using sterile neutrinos.

Neutrino masses are so far only observed via neutrino oscillations. Oscillations can occur when the mass eigenstates (propagating states) differ from the flavor eigenstates (being the interacting states), disproving the hypothesis that neutrinos are massless. First hints came from the Homestake experiment [1], which was taking data from 1970 to 1994, observing the electron neutrino flux from the Sun. The measured flux was about 1/3 of the flux predicted by the Standard Solar Model; oscillations would give an explanation of this deficit, as the electron neutrinos that are produced in the Sun could oscillate to other flavors and would thus be missed by the detector, which was sensitive to electron neutrinos only. The SNO experiment (Sudbury Neutrino Observatory, see [2]) measured the neutrino flux via neutral current interactions (being thus sensitive to all three neutrino flavors) and ultimately confirmed the hypothesis of oscillating neutrinos in 2001. How the observation of neutrino oscillations necessarily leads to the fact that

they are massive, will now be explained in more detail.

Neutrinos are produced via a charged or neutral current interactions as flavor eigenstates, but they propagate as mass eigenstates. For massless particles these states coincide, otherwise one can write the flavor eigenstate α as a superposition of mass eigenstates i and vice versa. The matrix transforming from flavor ($\alpha = e, \mu, \tau$) to mass basis ($i = 1, 2, 3$) of neutrinos is the so called PMNS matrix $U^P_{\alpha i}$ (namend after Pontecorvo, Maki, Nakagawa and Sakata). It is unitary in case of only three mass eigenstates ν_i:

$$|\nu_\alpha\rangle = \sum_i U^{P*}_{\alpha i} |\nu_i\rangle \,. \tag{2.1}$$

If at a time $t = 0$ the initial state $|\nu_\alpha\rangle$ is produced, the evolution over a time interval t is given by

$$|\nu(t)\rangle = \sum_i e^{-i(E_i t - p_i x)} U^{P*}_{\alpha i} |\nu_i\rangle \,, \tag{2.2}$$

where the propagation of the mass eigenstates can be described by a plane wave (see for example [3] or [4]). E_i and p_i are energy and momentum of the respective mass eigenstate.

As neutrino masses are tiny (they have escaped direct detection so far), their velocity is approximately the speed of light, meaning $E_i \gg m_i$ (and one can identify distance travelled with time $x = t$ in natural units), so the momentum can be expanded to

$$p_i = \sqrt{E_i^2 + m_i^2} \approx E_i - \frac{m_i^2}{2E_i} \,. \tag{2.3}$$

If assuming that the neutrino mass eigenstates have the same energy E, one can calculate the probability P to find the neutrino that had flavor α at $x = 0$ ($t = 0$) to be of flavor β at length $x = L$ (time $t = T$) using the orthogonality of the mass eigenstates:

$$P(\nu_\alpha \to \nu_\beta, T) = |\langle \nu_\beta | \nu(T) \rangle|^2 = \left| \sum_i U^P_{\beta i} U^{P*}_{\alpha i} e^{-i \frac{m_i^2}{2E} L} \right|^2 \,. \tag{2.4}$$

The probability is therefore a function of the mass squared differences $\Delta m^2_{ij} = m_i^2 - m_j^2$, meaning that if an oscillation of two eigenstates is observed, one of them has to have a nonzero mass. Thereby the mass splitting of the different states can be measured; the current best fit values from solar and atmospheric neutrinos are (PDG [5])

$$|\Delta m^2_\odot| = (7.58^{+0.22}_{-0.26}) \times 10^{-5} \mathrm{eV}^2 \,, \tag{2.5}$$

$$|\Delta m^2_{atm}| = (2.35^{+0.12}_{-0.09}) \times 10^{-3}\text{eV}^2\,. \tag{2.6}$$

By convention the mass eigenstate ν_1 is defined to consist mostly of the flavor component ν_e and the solar mass squared difference $\Delta m_\odot$ is identified with Δm^2_{21}. This makes $\Delta m^2_{21} > 0$, as the interaction of the neutrinos with matter in the Sun has to be resonant (see introduction to the MSW – the Mikheyev–Smirnov–Wolfenstein – effect in section 3.1). The sign of the atmospheric mass squared difference Δm^2_{atm} depends on which mass eigenstate is the lightest, m_1 or m_3. The case of $m_1 < m_2 < m_3$ is called normal hierarchy (NH) and makes $\Delta m^2_{atm} = \Delta m^2_{31} > 0$. In the inverted hierarchy (IH) $m_3 < m_1 < m_2$ and $\Delta m^2_{atm} = \Delta m^2_{32} < 0$.

The observation of neutrino oscillations imply at least two massive neutrinos. This motivates the introduction of sterile neutrinos ν_R, extending the particle content of the SM to create neutrino masses analogously to the other fermion masses in the SM. The right-handed neutrinos ν_R are called sterile as they cannot interact with other SM particles via gauge interactions: They are electrically neutral (no electromagnetic interactions), not strongly charged (no strong interactions) and do also not interact via weak interactions with $W^\pm$ or Z bosons. The left-handed neutrinos of the SM are then referred to as active neutrinos. In the SM, fermion mass terms arise from the coupling of a left-handed $SU(2)_L$-doublet with a Higgs $SU(2)_L$-doublet Φ and a right-handed $SU(2)_L$-singlet, where the neutral component of the Higgs boson acquires a vacuum expectation value (VEV) v after electroweak symmetry breaking. In order to formulate such a mass term for neutrinos, one needs right-handed singlets ν_R. To satisfy the observed mass squared differences there must be at least two such states, but there could be more, say n_R. The Dirac mass term in the Lagrangian then becomes

$$\mathscr{L}_{Dirac} = -y_{ab}\bar{\nu}_{Ra}\tilde{\Phi}^\dagger L_b + h.c. = -y_{ab}\frac{v}{\sqrt{2}}\,\bar{\nu}_{Ra}\nu_{Lb} + h.c.\,, \tag{2.7}$$

where a is the index of the right-handed singlets ν_{Ra}, $a = 1, 2, ..., n_R$, L_b are the left-handed lepton doublets, $b = e, \mu, \tau$, and y_{ab} are the Yukawa couplings, forming an $n_R \times 3$ matrix. In the broken phase the neutral component of the Higgs doublet acquires a vacuum expectation value (VEV) v and the second expression is valid.

When only this neutrino mass term is present in the Lagrangian, the neutrinos are Dirac particles like the other fermions of the SM.

But as the right-handed neutrinos ν_R are not charged under a symmetry, one can also

write down additional mass terms

$$\mathscr{L}_{Majorana} = -\frac{1}{2} M_{Rab} \nu_{Ra}^T C^{-1} \nu_{Rb} + h.c.\,, \tag{2.8}$$

where C is the charge conjugation operator. M_{Rab} can be taken as diagonal, since the states ν_R do not couple to any SM gauge bosons, so any rotations among the ν_{Ra} necessary for a diagonalization of M_R merely results in a redefinition of y_{ab}. For nonzero M_R, the right-handed neutrinos are Majorana particles, which means that they are their own antiparticles, i.e. the mass eigenstates are self-conjugate fields. For charged SM particles such mass terms would violate charge conservation and are thus forbidden. To introduce a similar mass term for the left-handed neutrinos, which are also electrically neutral, one would need an additional Higgs triplet Δ to conserve isospin, as ν_L is part of the lepton doublet L. The neutral component of the Higgs triplet acquires a VEV v_T, analogous to the Higgs doublet. The mass term in the Lagrangian would be

$$\mathscr{L}_{triplet} = -\frac{1}{2} f_{ab} L_a^T C^{-1} i\tau_2 \Delta L_b + h.c. = -\frac{1}{2} f_{ab} v_T \, \nu_{La}^T C^{-1} \nu_{Lb} + h.c.\,, \tag{2.9}$$

where f_{ab} is the symmetric Yukawa coupling matrix to the triplet Δ and τ_2 the second Pauli matrix acting on the $SU(2)$ indices. Note that in this case one would not need to introduce right-handed neutrinos, the active neutrinos become massive by their interaction with the triplet. Such models (so-called type II seesaw, see next section) are experimentally very restricted, as the well measured parameter

$$\rho = \frac{M_W^2}{M_Z^2 \cos^2(\theta_W)}\,, \tag{2.10}$$

which is equal to one in the SM at tree level, is modified. This restricts the new VEV v_T. There arise also additional couplings between the Higgs doublet and triplet, see for example [6] or [7] for an overview about the model and experimental bounds.

The right-handed neutrino fields are not charged under SM interactions and can therefore interact only via mixing to the active neutrinos and with the Higgs. The mass eigenstates (which are the propagating states) are again connected to the flavor eigenstates by a unitary mixing matrix U. The entries of the $(3 + n_R) \times (3 + n_R)$ matrix depend on the Dirac and Majorana mass terms and their size will determine the mixing of the neutrino states. The upper left 3×3 part of U is again the PMNS matrix, which then is non-unitary. The size of the entries describing the active-sterile mixing will fix the possibility of producing a sterile state in an interaction and the percentage of non-unitarity of the PMNS matrix. Many experiments have restricted the active-sterile mixing for

different mass ranges of the sterile neutrinos, see chapter 3.

In order to study the neutrino mass eigenstates theoretically, one can redefine the fields

$$\nu^M = \nu_L + \nu_L^c \,, \tag{2.11}$$

$$N^M = \nu_R + \nu_R^c \,, \tag{2.12}$$

where the upper index M refers to Majorana fermions, as these fields are invariant under charge conjugation, i.e. $(\nu^M)^c = \nu^M$. Note that ν^M and N^M are vectors of length 3 and n_R respectively. The three contributions from $\mathscr{L}_{Dirac}$, $\mathscr{L}_{Majorana}$, and $\mathscr{L}_{triplet}$ can be combined to obtain

$$\mathscr{L}_{mass} = -\frac{1}{2}(\bar{\nu}^M, \bar{N}^M) \begin{pmatrix} M_L & m_D^T \\ m_D & M_R \end{pmatrix} \begin{pmatrix} \nu^M \\ N^M \end{pmatrix} . \tag{2.13}$$

The mass matrices M_L and m_D are generated by spontaneous symmetry breaking:

$$M_{L_{ab}} = f_{ab} \cdot v_T \,, \tag{2.14}$$

$$m_{D_{ab}} = y_{ab} \cdot \frac{v}{\sqrt{2}} \,, \tag{2.15}$$

where $v \simeq 246$ GeV is the Standard Model Higgs VEV and the triplet VEV v_T is restricted by experiments to be below $\approx$ GeV (see again [6] or [7]). The indices are dropped in the following. The symmetric matrix

$$M_\nu = \begin{pmatrix} M_L & m_D^T \\ m_D & M_R \end{pmatrix} \tag{2.16}$$

is called the neutrino mass matrix, the entries M_L, m_D and M_R being matrices themselves. Note that in this notation (where the neutrinos are written as Majorana fields) the kinetic term acquires an additional factor 1/2:

$$\mathscr{L}_{kin} = \frac{1}{2} \left(\bar{\nu}^M i\partial\!\!\!/ \nu^M + \bar{N}^M i\partial\!\!\!/ N^M \right) . \tag{2.17}$$

The matrix U that diagonalises M_ν gives the mass eigenstates ν_i $(i = 1, ..., 3 + n_R)$

$$M_\nu^{diag} = U^T M_\nu U \tag{2.18}$$

$$\nu_i^M = \sum_{b=1}^{3} U_{ib} \nu_b^M + \sum_{c=4}^{3+n_R} U_{ic} N_c^M \,. \tag{2.19}$$

Here the indices of N^M were renumerated, so that those in U are continuous.

Experiments show that active neutrino masses are tiny. They are still escaping direct detection, apart from knowing the mass squared differences from neutrino oscillation measurements. The Troitsk and the Mainz experiments only give upper bounds of about 2 eV on the neutrino mass, using beta decay of tritium to measure the effective mass of the electron antineutrino (see [8] and [9]). New experiments are being built to improve these results; the Katrin experiment should be able to measure an effective electron antineutrino mass of about 0.2 eV (see [10] for a rough overview over Katrin, or [11] for a general summary of new experiments).

Compared to the other particles of the SM, the mass of the neutrinos is very small: In case of pure Dirac masses the Yukawa coupling would have to be of the order of $y \simeq 10^{-12}$, whereas the electron, the next heaviest SM particle, has a coupling of 10^{-6}. This is somewhat unnatural; the right-handed neutrinos however allow for an elegant mechanism to suppress the masses of the active neutrinos: the seesaw mechanism.

2.1 Generation of small Neutrino Masses – the Seesaw Mechanism

The seesaw mechanism is mainly categorized in type I and II depending on the presence of the Majorana mass term of the left-handed neutrinos, thus of the existence of a Higgs triplet. In the type I seesaw there is no triplet and the left-handed Majorana mass vanishes, $M_L = 0$. There are in general n_R sterile neutrinos, mixing with the active ones via the Dirac mass term m_D and having a Majorana mass M_R. The type II seesaw includes the Higgs triplet and thus gives the full neutrino mass matrix M_ν that was developed above. (This scenario is also called type I+II, then type II refers to the presence of the triplet term only.) The type I seesaw mechanism was first introduced by Minkowski [12] in 1977 and in [13], [14] and [15] in 1979. The seesaw II was motivated by Grand Unified Theories (GUTs), see [16], [17] and [18].[1]

If M_R is much larger than m_D (meaning the eigenvalues of these matrices), the neutrino mass matrix M_ν can be block-diagonalised, expanding in a series of $M_R^{-1} m_D$.

There are $3 + n_R$ mass eigenstates ν_i ($i = 1, ..., 3 + n_R$) that contain parts of all flavor eigenstates ($\alpha = e, \mu, \tau, s_1, s_2, ..., s_{n_R}$): $\nu_i = \sum_\alpha U^*_{i\alpha} \nu_\alpha$, where $\nu_{e,\mu,\tau}$ are the active neutrinos and $\nu_{s_i} \equiv N_{s_i}$ are the sterile neutrinos. The matrix M_ν, being the mass matrix in the flavor basis, can now be block-diagonalised so that there are three light states ν_{light}, containing almost only the active states, and n_R heavy states ν_{heavy}, containing almost

[1] GUTs usually contain a left–right symmetry and therefore M_L and M_R are created by Higgs VEVs.

only the sterile states (compare [19]).[2] The matrix that block-diagonalises M_ν is called W:

$$\begin{pmatrix} \nu^M \\ N^M \end{pmatrix} = W \begin{pmatrix} \nu_{light} \\ \nu_{heavy} \end{pmatrix} , \tag{2.20}$$

$$W^T \begin{pmatrix} M_L & m_D^T \\ m_D & M_R \end{pmatrix} W = \begin{pmatrix} M_{light} & 0 \\ 0 & M_{heavy} \end{pmatrix} , \tag{2.21}$$

where W is unitary and M_{light} (M_{heavy}) is a 3×3 ($n_R \times n_R$) matrix which is in general not diagonal. The condition of the off-diagonal submatrices on the right hand side of equation (2.21) being zero leads to $3 \cdot n_R$ degrees of freedom of W. One can therefore make the ansatz

$$W = \begin{pmatrix} \sqrt{1 - BB^\dagger} & B \\ -B^\dagger & \sqrt{1 - B^\dagger B} \end{pmatrix} , \tag{2.22}$$

where B is a $3 \times n_R$ matrix, being a function of M_L, m_D and M_R. The square root of the matrices has to be interpreted as a power series[3]

$$\sqrt{1 - BB^\dagger} = 1 - \frac{1}{2} BB^\dagger - \frac{1}{8} BB^\dagger BB^\dagger - ... \tag{2.23}$$

Putting the ansatz into equation 2.21, the vanishing off-diagonals give an equation for B that can be solved by expanding in orders of m_R^{-1}, where m_R is the scale of the eigenvalues of M_R.

$$B = B_1 + B_2 + B_3 + ... , \tag{2.24}$$

where $B_i \propto m_R^{-i}$. At first order

$$B \simeq (M_R^{-1} m_D)^\dagger . \tag{2.25}$$

The masses of the light neutrinos are given by

$$M_{light} \simeq M_L - m_D^T M_R^{-1} m_D , \tag{2.26}$$

[2] Note that the active–sterile mixing has to be small, it is constrained by experiments, as mentioned before (see chapter 3).

[3] This is possible, since the eigenvalues of B are small, see later in the text.

while the the first order contribution to the heavy states vanishes and at zero order

$$M_{heavy} \simeq M_R \,. \tag{2.27}$$

Note that the PMNS matrix is equal to the upper left part of W times the matrix that diagonalises M_{light}, say U_{light}: $U_{light}^T M_{light} U_{light} = M_{light}^d$. The PMNS matrix is then given by

$$U_{PMNS} = \sqrt{1 - BB^\dagger} U_{light} \approx \left(1 - \frac{1}{2} BB^\dagger\right) U_{light} \,. \tag{2.28}$$

Since U_{light} is a unitary matrix one can interpret $BB^\dagger$ as the unitarity violating part of the PMNS matrix. The non-unitarity of the PMNS matrix is therefore small in the seesaw mechanism, B is at first order given by $B^\dagger \simeq M_R^{-1} m_D$.

Since

$$\nu^M = \sqrt{1 - BB^\dagger} \nu_{light} + B \nu_{heavy}$$

the active-sterile mixing is proportional to B, so to $M_R^{-1} m_D$.

The necessary condition for this block-diagonalisation is that m_R^{-1} is small. When assuming $M_L \equiv 0$, so no triplet Higgs in the theory, the (active) neutrino masses are given by $M_{light} \simeq -m_D^T M_R^{-1} m_D$. Supposing for example, that the Yukawa couplings of the neutrinos are of order one (so the scale of m_D is about 10^2 GeV), and the scale of M_R were at 10^{15} GeV, the active neutrinos had masses of $\approx 10^{-2}$ eV. The Yukawa couplings could also be smaller, then the scale of M_R becomes lower in this scenario.

In summary one can state that in the seesaw mechanism, the possibly high scale of the right-handed neutrino Majorana mass gives a reason for the smallness of the active neutrino masses.

So far an overview over the contribution of sterile neutrinos to the mechanism of mass generation for the neutrinos was given. But the existence of sterile neutrinos would also manifest in the modification of the weak interactions. The weak neutral current interaction with some fermion Ψ_f is given by the Lagrangian:

$$\mathscr{L}_I^{NC} = -\frac{g}{\cos(\theta_W)} \bar{\Psi}_f \gamma_\mu \frac{1}{2} \left(c_V^f - c_A^f \gamma_5\right) \Psi_f Z^\mu + h.c. \,, \tag{2.29}$$

where g is the weak coupling constant and θ_W the Weinberg angle. The vector and axial couplings c_V and c_A are determined by the third component of the isospin I_3^f and the

charge Q^f of the fermion:

$$c_V^f = I_3^f - 2\,\sin^2(\theta_W)\,Q^f\,, \tag{2.30}$$

$$c_A^f = I_3^f\,. \tag{2.31}$$

For neutrinos ($c_V = c_A = 1/2$) one gets:

$$\mathscr{L}_{int}^{NC} = -\frac{g}{2\cos(\theta_W)}\bar{\nu}_\alpha\gamma_\mu\left(\frac{1-\gamma_5}{2}\right)\nu_\alpha Z^\mu + h.c. \tag{2.32}$$

The charged current interaction is given by

$$\mathscr{L}_{int}^{CC} = -\frac{g}{\sqrt{2}}\bar{\nu}_\alpha\gamma_\mu\left(\frac{1-\gamma_5}{2}\right)\ell_\alpha W^{+\mu} - \frac{g}{\sqrt{2}}\bar{\ell}_\alpha\gamma_\mu\left(\frac{1-\gamma_5}{2}\right)\nu_\alpha W^{-\mu}\,, \tag{2.33}$$

and changing to the mass basis gives:

$$\mathscr{L}_{int}^{NC} = -\sum_{i,j=1}^{3+n_R}\frac{g}{2\cos(\theta_W)}U_{\alpha i}^*\bar{\nu}_i\gamma_\mu\left(\frac{1-\gamma_5}{2}\right)U_{\alpha j}\nu_j Z^\mu + h.c.\,, \tag{2.34}$$

$$\mathscr{L}_{int}^{CC} = -\sum_{i=1}^{3+n_R}\frac{g}{\sqrt{2}}\left(U_{\alpha i}^*\bar{\nu}_i\gamma_\mu\left(\frac{1-\gamma_5}{2}\right)\ell_\alpha W^{+\mu} + \bar{\ell}_\alpha\gamma_\mu\left(\frac{1-\gamma_5}{2}\right)U_{\alpha i}\nu_i W^{-\mu}\right)\,. \tag{2.35}$$

The coupling of the (mainly sterile) states ν_i, where $i = 4, ..., 3+n_R$, depends thus on the mixing elements $U_{\alpha i}$ and on the kinematics of the interaction, which are determined by its mass.

The goal of this thesis is to explain how the phenomenology of sterile neutrinos varies on different scales. The possibility of detecting these neutrinos depends on their mixing to the active neutrinos (which can couple via the SM interactions), but also the sterile mass scale plays an important role. The experimental signatures differ strongly depending on whether the sterile states can be produced in an interaction or not.

For very small masses sterile neutrinos can oscillate with the active ones. This will be discussed in section 3.1. Many experiments have been built to measure these oscillations and there have even been indications for the existence of a light sterile neutrino.

In case the sterile states are too heavy and they can not produced in the observed processes, so-called non-unitarity effects appear: the mixing matrix of the three active neutrinos is not unitary in the presence of sterile neutrinos. The impact of these effects depends on the mixing of the sterile neutrinos to the active ones, see section 3.2.

Already the oscillations between the active neutrinos induce flavor violating decays, for

example $\mu \rightarrow e\,\gamma$, but the branching ratios are tiny and a detection almost impossible. Sterile neutrinos could enhance this ratio, depending on their masses and mixing. This will be analyzed in section 3.3.

A process that could determine the nature of neutrinos, i.e. whether they are Dirac or Majorana particles, is the neutrinoless double-beta decay. If this decay should be observed, lepton number is violated (by two units here) and neutrinos are of Majorana type. The process also induces an effective mass for the neutrinos, independent of the mechanism it is caused by[4], though this mass might be very small (Schechter-Valle-theorem [20]). The contribution of sterile neutrinos depends on their mass and mixing to the active neutrinos and on whether their mass is smaller or bigger than the energy scale of the process, see section 3.4.

Sterile neutrinos can also be produced in colliders, although they typically have only small interactions with matter, producing certain signatures when they decay. Section 3.5 will explain the collider signatures.

Finally, sterile neutrinos can propagate in loops, contributing to the self energies of the gauge bosons. This is expressed through the oblique correction parameters S, T and U, see section 3.6.

A subject that will not be touched in this work is the role of sterile neutrinos in cosmology and astrophysics. A keV sterile neutrino could, for example, be a warm dark matter candidate, but the mixing has to be very small, so that the life time is bigger than the age of the universe (see e.g. [21]). Also, heavier sterile neutrinos can cause leptogenesis (lepton-antilepton asymmetry), which can then transfer to baryons via sphaleron processes and account for the matter–antimatter asymmetry in the universe. Models combining sterile neutrinos as dark matter and for leptogenesis are for example the νMSM ([22], [23]) or a model by Bezrukov, Kartavtsev and Lindner [24].

Light sterile neutrinos are also constrained by cosmology, as they contribute as radiation to the cosmic microwave background (CMB). Assuming a specific model (e.g. the cosmological Standard Model ΛCDM) one can constrain the number of light neutrinos and their total mass (for an overview see [25]). As these bounds can only be obtained when assuming a model, they are not as stringend as direct searches.

Although the role of sterile neutrinos in cosmology is a very interesting topic for itself, it is beyond the scope of this work and will not be considered in detail. The following chapter will give an overview on the above mentioned signatures of sterile neutrinos at different scales.

[4] The neutrinoless double beta decay could be caused by the mechanism that generates neutrino masses, but it could also be independent new physics.

CHAPTER 3

Signatures of Sterile Neutrinos at different Scales

The sections of this chapter will provide the basic principles that will be used in the main parts of this work.

3.1 Neutrino Oscillations

Sterile neutrinos can oscillate with the active ones, when they have small masses. This phenomenon is restrained by the necessary coherence: the neutrino mass eigenstates have to be coherently produced and detected and also their propagation has to be coherent. For the production and detection this means that the intrinsic quantum mechanical energy uncertainty σ_E has to be big compared to the energy difference of the mass eigenstates ΔE_{ij}:

$$\Delta E_{ij} \approx \frac{\Delta m_{ij}^2}{2E} \ll \sigma_E \tag{3.1}$$

If this is not fulfilled, the different mass eigenstates can be identified and the oscillation is averaged out. Since the quantum mechanical energy uncertainty is determined by Heisenberg's uncertainty principle, the production and detection processes have to be well localized.

The different mass eigenstates propagate as wave packets with different group velocities and thus for long distances (long times) become separated and the interference is destroyed. For ultrarelativistic neutrinos one can approximate

$$\frac{\Delta m_{ij}^2}{2E^2} \cdot L \ll \sigma_x \approx \frac{v_g}{\sigma_E}\,, \tag{3.2}$$

where L is the travelled distance, σ_x the spacial width of the neutrino wave packets and v_g their group velocity.

This gives an upper bound on the mass squared difference for the oscillating neutrinos, which depends on the production and detection setup and the travelled distance. The second condition (coherent propagation) is usually satisfied unless the neutrinos are of astrophysical origin (meaning e.g. from supernova; the distances then become huge). As the (mostly active) neutrino masses are so small, in their case also the first condition is always fulfilled, but for sterile neutrinos it depends on the mass squared difference and on the experimental setup. The coherence conditions have been carefully examined in [26], where a proper quantum mechanical approach is used.

In order to observe neutrino oscillations with a sterile neutrino, its mass must therefore be in the eV range. There actually have been some hints to a sterile neutrino at a mass of about one to two eV, but they are controversial and should be taken with great care. These experiments will be discussed later in the section 3.1.2. First the formalism of neutrino oscillations is introduced in more detail, then the experimental evidence is summarized and finally oscillations in matter are discussed.

Neutrino oscillations were already mentioned in the beginning of this work, as oscillations between the active neutrinos led to the conclusion that neutrinos have to be massive. In the following the theoretical background will be developed in more detail, including also sterile neutrinos.

3.1.1 Theory of Neutrino Oscillations

In the introduction the general formula for the probability of a neutrino produced as flavor α at $t = 0$ to be detected as flavor β at $t = T$ was derived (equation (2.4)):

$$P(\nu_\alpha \to \nu_\beta, T) = |\langle \nu_\beta | \nu(T) \rangle|^2 = \left| \sum_{i=1}^{3} U_{\beta i}^P U_{\alpha i}^{P\,*} e^{-i\frac{m_i^2}{2E}L} \right|^2 , \tag{3.3}$$

where U^P is the PMNS mixing matrix. One can further develop this equation to clarify the dependencies of the oscillations:

$$P(\nu_\alpha \to \nu_\beta, L) = \delta_{\alpha\beta} - 4\sum_{i>j} \Re(U^{P\,*}_{\alpha i} U^P_{\beta i} U^P_{\alpha j} U^{P\,*}_{\beta j}) \sin^2\left(\frac{\Delta m^2_{ij} L}{4E}\right) + 2\sum_{i>j} \Im(U^{P\,*}_{\alpha i} U^P_{\beta i} U^P_{\alpha j} U^{P\,*}_{\beta j}) \sin\left(\frac{\Delta m^2_{ij} L}{2E}\right). \tag{3.4}$$

Depending on L/E, the ratio of the baseline of the experiment and the energy of the neutrinos, one can thus investigate different mass squared differences Δm^2_{ij}. Usually, at certain L/E, one can approximate this formula by a two flavor oscillation, when the other mass squared differences are either small or big enough.

The former expression can also be derived from the Schrödinger equation, a notation that will be useful when considering neutrino oscillations in matter. The evolution of the neutrinos is determined by

$$i\frac{d}{dx}\nu = H\nu\,, \tag{3.5}$$

where $\nu = (\nu_e, \nu_\mu, \nu_\tau)^T$ and the Hamiltonian contains the energies of the flavor states which can be rotated by the mixing matrix from the mass eigenbasis:

$$H = U^P \begin{pmatrix} E_1 & 0 & 0 \\ 0 & E_2 & 0 \\ 0 & 0 & E_3 \end{pmatrix} U^{P\,\dagger} \approx U \begin{pmatrix} p + \frac{m_1^2}{2E} & 0 & 0 \\ 0 & p + \frac{m_2^2}{2E} & 0 \\ 0 & 0 & p + \frac{m_3^2}{2E} \end{pmatrix} U^{P\,\dagger}\,. \tag{3.6}$$

The neutrinos are ultrarelativistic, therefore one can approximate the energy by $E_i \approx p + \frac{m_i}{2E}$, assuming all neutrino states to have the same momentum p and energy E. A term proportional to the unit matrix in the Hamiltonian can be absorbed into a redefinition of an overall phase of the neutrino states, which can be dropped because it is not physical. Use this to substract $p \cdot \mathbb{1}$:

$$H = U^P \begin{pmatrix} \frac{m_1^2}{2E} & 0 & 0 \\ 0 & \frac{m_2^2}{2E} & 0 \\ 0 & 0 & \frac{m_3^2}{2E} \end{pmatrix} U^{P\,\dagger}\,. \tag{3.7}$$

The evolution of the state ν can be expressed through the so-called S-matrix:

$$\nu(x) = S(x, x_0)\nu(x_0)\,, \tag{3.8}$$

$$i\frac{d}{dx}S(x,x_0) = H \cdot S(x,x_0)\,, \tag{3.9}$$

where the evolution of S is determined by the evolution of ν, see equation (3.5). Solving equation (3.9) with the initial condition $S(x_0,x_0) = \mathbb{1}$ gives

$$S(x,x_0) = e^{-iH\cdot(x-x_0)} = U^P \begin{pmatrix} e^{-i\frac{m_1^2}{2E}(x-x_0)} & 0 & 0 \\ 0 & e^{-i\frac{m_2^2}{2E}(x-x_0)} & 0 \\ 0 & 0 & e^{-i\frac{m_3^2}{2E}(x-x_0)} \end{pmatrix} U^{P\,\dagger}\,. \tag{3.10}$$

The oscillation probabilities are now given by the entries of the S-matrix. Setting (as before) $x_0 = 0$ and $x = L$, this leads to the probability

$$P(\nu_\alpha \to \nu_\beta, L) = |S_{\beta\alpha}(L)|^2 = \left| \sum_{i=1}^{3} U^P_{\beta i} U^{P\,*}_{\alpha i} e^{-i\frac{m_i^2}{2E}L} \right|^2 , \tag{3.11}$$

as above. The S-matrix formalism will become especially useful later on to study the propagation in matter.

The PMNS mixing matrix is usually written in terms of mixing angles θ_{ij} and phases δ and $\alpha_{1,2}$:

$$U^P = \begin{pmatrix} 1 & 0 & 0 \\ 0 & c_{23} & s_{23} \\ 0 & -s_{23} & c_{23} \end{pmatrix} \begin{pmatrix} c_{13} & 0 & s_{13}e^{-i\delta} \\ 0 & 1 & 0 \\ -s_{13}e^{i\delta} & 0 & c_{13} \end{pmatrix} \begin{pmatrix} c_{12} & s_{12} & 0 \\ -s_{12} & c_{12} & 0 \\ 0 & 0 & 1 \end{pmatrix} \begin{pmatrix} 1 & 0 & 0 \\ 0 & e^{i\frac{\alpha_1}{2}} & 0 \\ 0 & 0 & e^{i\frac{\alpha_2}{2}} \end{pmatrix} \tag{3.12}$$

$$= \begin{pmatrix} c_{12}c_{13} & s_{12}c_{13} & s_{13}e^{-i\delta} \\ -s_{12}c_{23} - c_{12}s_{23}s_{13}e^{i\delta} & c_{12}c_{23} - s_{12}s_{23}s_{13}e^{i\delta} & s_{23}c_{13} \\ s_{12}s_{23} - c_{12}c_{23}s_{13}e^{i\delta} & -c_{12}s_{23} - s_{12}c_{23}s_{13}e^{i\delta} & c_{23}c_{13} \end{pmatrix} \begin{pmatrix} 1 & 0 & 0 \\ 0 & e^{i\frac{\alpha_1}{2}} & 0 \\ 0 & 0 & e^{i\frac{\alpha_2}{2}} \end{pmatrix}, \tag{3.13}$$

with $c_{ij} = \cos(\theta_{ij})$ and sine respectively. The phase δ is the so-called Dirac phase, it is the only physical phase in case neutrinos are Dirac particles and the only phase observable in neutrino oscillations (although not conclusively determined yet). $\alpha_{1,2}$ are Majorana phases, which are physical if neutrinos are Majorana particles. As it is still not known whether neutrinos are Majorana or Dirac type, the Majorana phases are undetermined, too.

Many experiments have measured the values of the mixing angles and the mass squared

Parameter	best-fit ($\pm 1\sigma$)
$\Delta m^2_{\odot}$	$(7.58^{+0.22}_{-0.26}) \times 10^{-5}\text{eV}^2$
$\lvert\Delta m^2_{atm}\rvert$	$(2.35^{+0.12}_{-0.09}) \times 10^{-3}\text{eV}^2$
$\sin^2(\theta_{12})$	$0.312^{+0.018}_{-0.015}$
$\sin^2(\theta_{23})$	$0.42^{+0.08}_{-0.03}$
$\sin^2(\theta_{13})$	0.0251 ± 0.0034

Table 3.1: Neutrino oscillation parameters, global best fit values from the PDG [5].

differences from neutrino oscillations in different setups. Table 3.1 quotes the global best fit values from the Particle Data Group (PDG [5]).

The formula for the oscillation probability derived above describes neutrino oscillations, when only the three active neutrinos oscillate. In case there was an additional heavy sterile state (that does not oscillate because of the large mass squared difference), the PMNS matrix would be non-unitary. But the oscillation formula would essentially stay the same, apart from an overall normalization factor. This leads to a so called zero-distance effect, as even $P(\nu_\alpha \to \nu_\beta, T)$ at $T = 0$ could be nonzero (see section 3.2).

When the sterile neutrino is however light enough to oscillate with the active neutrinos, new mass squared differences and mixing angles appear. The oscillation probability now includes the sterile state s ($\alpha, \beta = e, \mu, \tau, s$) and the mixing matrix is no longer the PMNS, but the full 4×4 matrix U that diagonalises the 4×4 mass matrix $M_{\alpha\beta}$:

$$P(\nu_\alpha \to \nu_\beta, T) = \left| \sum_{i=1}^{4} U_{\beta i} U^*_{\alpha i} e^{-i \frac{m_i^2}{2E} L} \right|^2 . \tag{3.14}$$

This would introduce three additional mixing angles θ_{i4} and mass squared differences Δm^2_{4i} ($i = 1, 2, 3$), two additional Dirac and one Majorana phase. There could also be more light sterile neutrinos, then there are even more new parameters. More than two light additional neutrinos would be disfavored by cosmology, which restricts the effective number of light[1] neutrinos N_{eff} to about 3 to 5 (see e.g. [25]).

There have been by now a number of experiments that see hints for an oscillation with a mass squared difference in the eV range, which cannot be due to an active neutrino. These must therefore be taken as hints for the existence of (at least one) light sterile neutrino that oscillates with the active neutrinos. In the following, the experimental evidence will be summarized.

[1] For masses $m_\nu \gg 10$ eV, this bound is not valid.

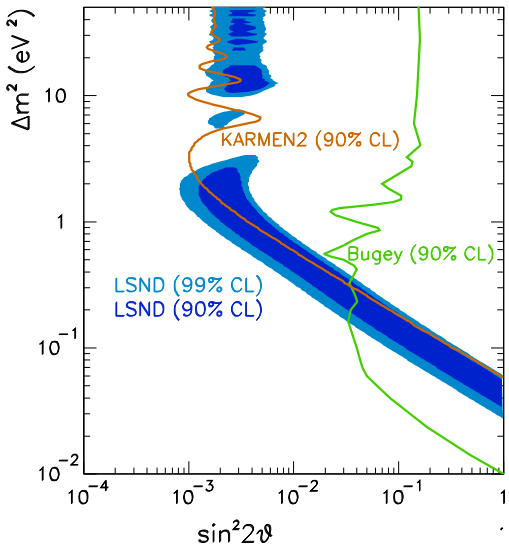

Figure 3.1: Combined analysis of the parameter space of LSND and KARMEN (from [25]).

3.1.2 Experimental Hints

As there are many experiments that have investigated the parameter space of a possible sterile neutrino oscillating with the active ones, this will be only a short overview. There are several experiments that have seen signs of an oscillation with a mass squared difference that is too big to fit into the three flavor oscillation scheme. Among these are LSND (Liquid Scintillator Neutrino Detector), MiniBooNE (Mini Booster Neutrino Experiment), experiments with radioactive sources and short-baseline reactor experiments. KARMEN (Karlsruhe Rutherford Medium Energy Neutrino experiment) and MINOS (Main Injector Neutrino Oscillation Search), on the other hand, observe no oscillation in that mass region. There is some tension between the results, which becomes clear when a global fit to all data is performed. KARMEN and LSND will be treated in one paragraph, as the experiments are similar, then the other experiments that were mentioned above are summarized and finally a global fit is discussed.

LSND and KARMEN

The LSND experiment [27] uses pion decay to produce mainly muon antineutrinos via $\pi^+ \rightarrow \mu^+ \nu_\mu \quad \Rightarrow \quad \mu^+ \rightarrow e^+ \nu_e \bar{\nu}_\mu$, and investigates $\bar{\nu}_\mu \rightarrow \bar{\nu}_e$ oscillations. KARMEN [28] also looks for $\bar{\nu}_\mu \rightarrow \bar{\nu}_e$ oscillations, but their baseline is slightly different, 30 m for LSND, 17.7 m for KARMEN. As the neutrino energies of both experiments are similar, the parameter space is slightly different. LSND obtained a positive signal of oscillations with

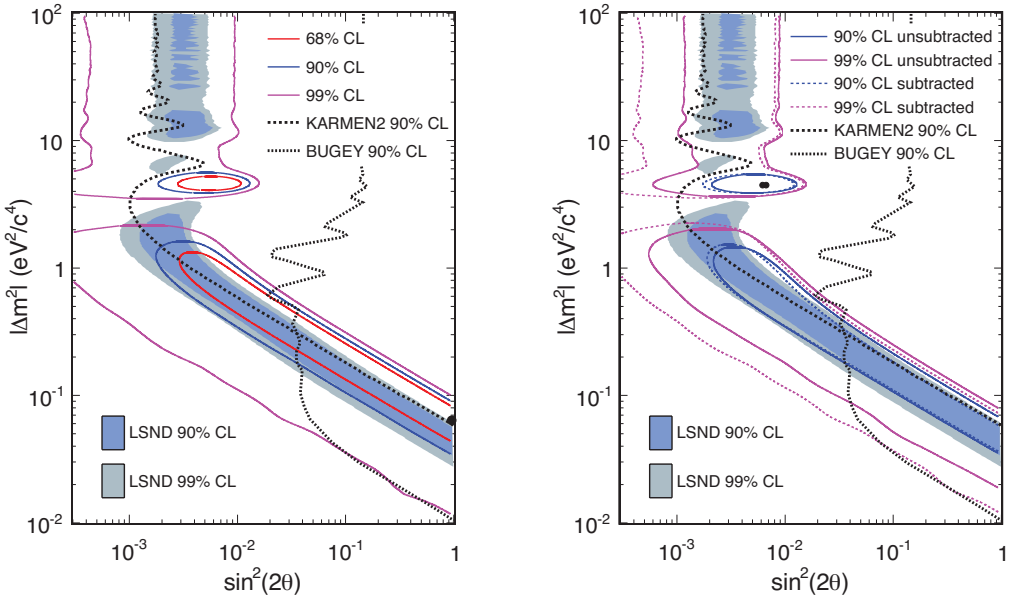

(a) neutrino mode

(b) antineutrino mode

Figure 3.2: MiniBooNE results compared to the former experiments. On the left the neutrino mode, on the right the antineutrino mode, where the first seems to be inconsistent with LSND data (taken from [32]).

over 3σ evidence [29], while KARMEN has seen no oscillations. A combined analysis has been done in [30], the results are shown in figure 3.1.

KARMEN does not exclude the whole parameter space of the LSND best fit, but at large mass squared differences Δm^2 the results are contradictory.

MiniBooNE

The MiniBooNE experiment [31] uses either a π^+ and K^+ or π^- and K^- beam. They search for $\nu_\mu \to \nu_e$ or alternatively for $\bar{\nu}_\mu \to \bar{\nu}_e$. The baseline is 541 m, but since the neutrino energies are also larger than at LSND, approximately the same mass range can be tested. Furthermore since the energies are different, MiniBooNE is an independent cross-check of LSND.

They observed only an excess at low energies, at high energies the measurement was consistent with the assumption of no oscillation in both the neutrino and antineutrino mode. The excess at low energies differed: in the antineutrino mode the results are consistent with LSND, which can be seen in figure 3.2. In the neutrino mode however the magnitude of the excess is consistent with LSND, but the shape suggests a more

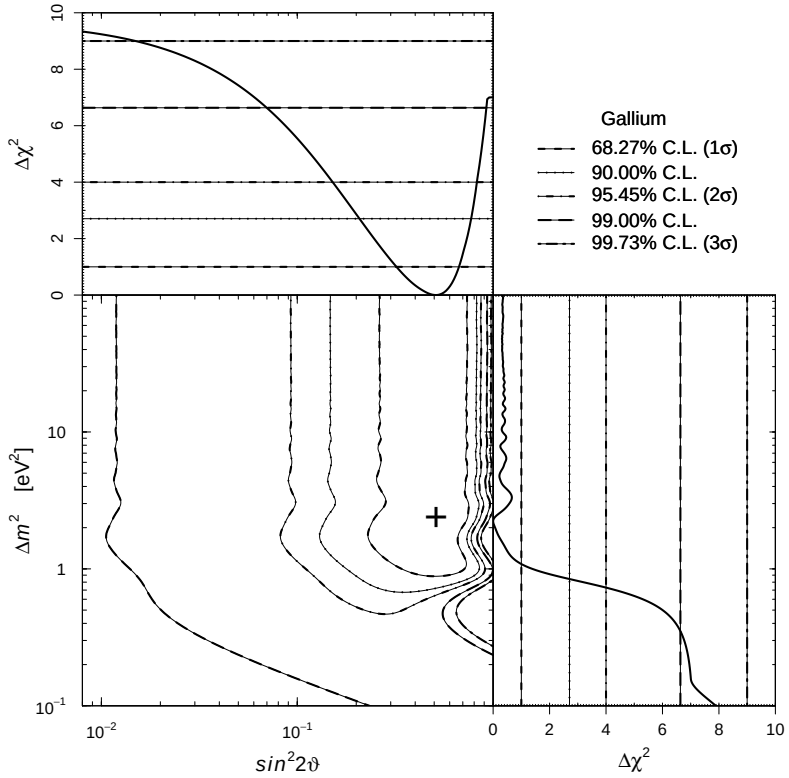

Figure 3.3: χ^2 analysis of the event deficit in the two Gallium detectors. Best fit values correspond to $\sin^2(2\theta) = 0.50$, $\Delta m^2 = 2.24$ eV^2 (from [33]).

complicated picture than simple two neutrino oscillations. A difference in the neutrino and antineutrino mode might be explained by oscillation structures that can include CP violation; in order to get CP violation there have to be at least two relevant mass squared differences, i.e. two sterile neutrinos.

The Gallium Anomaly

The two detectors GALLEX (Gallium Experiment) and SAGE (Soviet-American Gallium Experiment) were built to measure solar neutrinos and have been calibrated by radioactive sources (^{51}Cr and ^{37}Ar) that were placed inside the detectors. The electron neutrinos were detected by the decay $\nu_e + {}^{71}\mathrm{Ga} \rightarrow {}^{71}\mathrm{Ge} + e^-$. The activity of the source was known very precisely and both experiments observed less events than expected. The detection cross section has been calculated in two different ways with a similar outcome: the measured rates have a deficit compared to the expected ones of about 3σ.[2]

[2] An important remark to make here is that when the detectors were used to measure the solar neutrino parameters, their results were compatible with a number of other experiments.

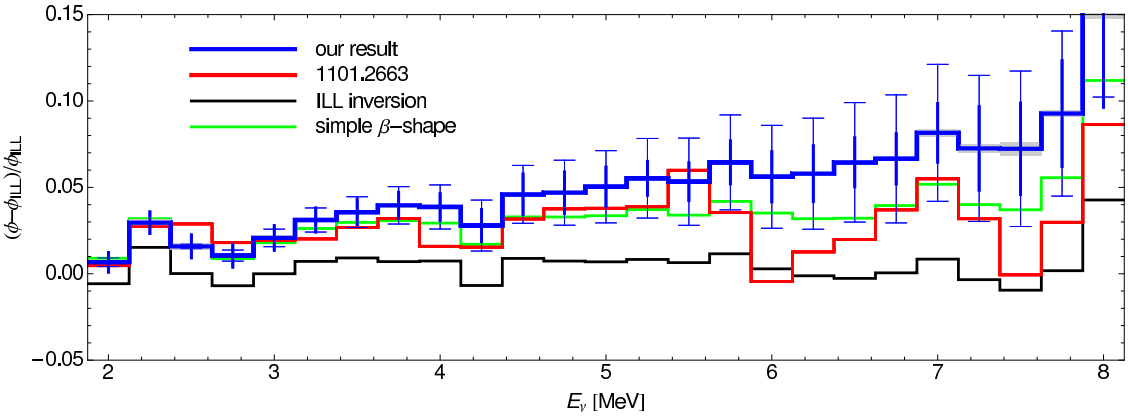

Figure 3.4: Flux of antineutrinos: former results compared to new analyses (from [34]). The black curve is the former result, the colored curves are new analyses (see references in [34]).

This electron neutrino disappearance could again be explained by an oscillation with a mass squared difference of a few eV^2. The fit (done in [33]) is shown in figure 3.3. The best fit values correspond to $\sin^2(2\theta) = 0.50$, $\Delta m^2 = 2.24$ eV^2 and the oscillation hypothesis is clearly favored compared to no oscillation at about 3σ.

The Reactor Anomaly

Nuclear reactors are an excellent source for electron antineutrinos with energies of a few MeV. Various experiments have measured the rate of antineutrino events at different reactors, they all agree quite well. There have also been analyses of the neutrino spectra leading to the expected flux, which were consistent with the measurements.

However, the expected energy spectrum of the neutrinos has been reevaluated recently (see e.g. [34]). The fission products have to be known very precisely: their β-decay spectra have been calculated and were then converted to $\bar{\nu}_e$ spectra. Compared to the old spectra (that were compatible with the measurements) the new predicted neutrino flux is about 3% higher (see figure 3.4). The main excess is at high energies and one has to note that especially the high energy part of the spectrum is difficult to estimate.

A 3% deficit in the antineutrino flux could point to an oscillation with a Δm^2 again in the eV^2 range. The χ^2 analysis is shown in figure 3.5, it includes the two source experiments GALLEX and SAGE. The no oscillation hypothesis is disfavored at almost 4σ. If an L/E-dependence would be observed, this would be a clear signal for oscillations. The Nucifer experiment [35] is being constructed very close to a reactor in order to measure a possible effect of the shorter baseline.

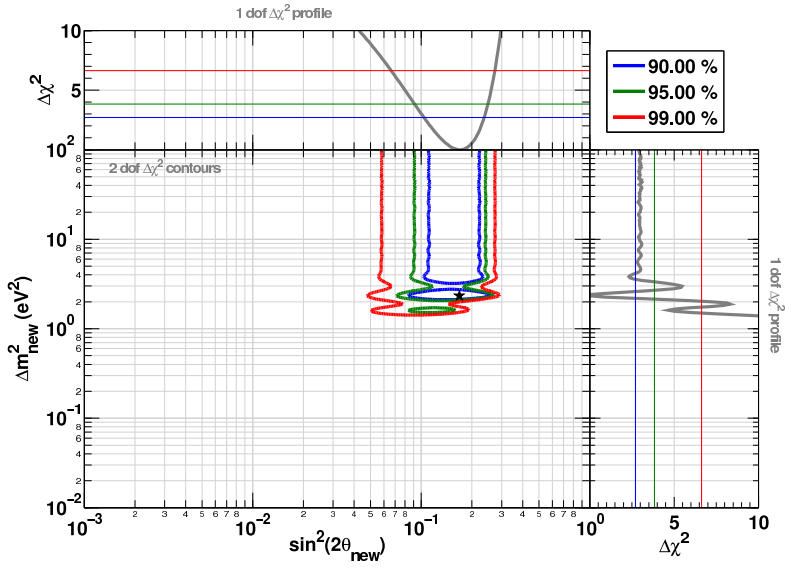

Figure 3.5: χ^2 analysis of the reactor anomaly with the assumption of one sterile neutrino (from [25]).

MINOS

The MINOS experiment [36] has two detectors, one is 1.04 km and the other 735 km away from the beam target. They can measure the neutrino flux in NC events and since sterile neutrinos do not interact via NC, but all active neutrinos do, an oscillation of active neutrinos to a sterile state would manifest as an energy dependent decrease of the flux.

The data are compatible with the usual three neutrino picture. For a mass region of $0.3\,\mathrm{eV}^2 < \Delta m^2_{43} < 2.5\ \mathrm{eV}^2$ MINOS excludes a sterile neutrino at 90% confidence level (but these limit were obtained assuming a certain model, see [25]).

The last paragraphs have shown that there is both evidence for and against the existence of a light sterile neutrino oscillating with the active neutrinos and the results of different experiments partly contradict each other. The existing evidence is therefore not compelling, but the hypothesis can also not be excluded so far. This summary has been very short, for detailed information see the broad overview provided in [25] (and references therein). The different results can be summarized in one model, performing a global fit to all data (based here on the work in [37]).

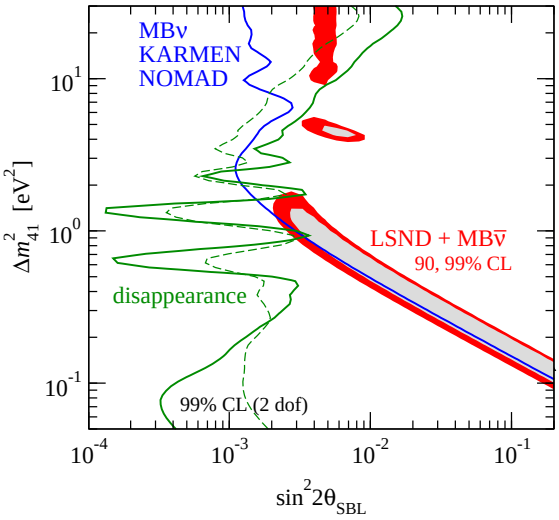

Figure 3.6: Constraints and allowed regions from the experiments mentioned in the text. The green dashed line marks the results of the "old" reactor neutrino fluxes, the solid line the new calculation. LSND and MiniBooNE favored regions (at 99% CL) are almost completely ruled out (taken from [37]).

	Δm^2_{41}	$\lvert U_{e4}\rvert$	$\lvert U_{\mu 4}\rvert$	Δm^2_{51}	$\lvert U_{e5}\rvert$	$\lvert U_{\mu 5}\rvert$	δ/π	χ^2/dof
3+2	0.47	0.128	0.165	0.87	0.138	0.148	1.64	110.1/130
1+3+1	0.47	0.129	0.154	0.87	0.142	0.163	0.35	106.1/130

Table 3.2: Parameter values and χ^2 at the global best fit points for 3+2 and 1+3+1 oscillations (Δm^2 in eV^2), taken from [37].

Global Fit

In the global fit from Kopp, Maltoni and Schwetz [37] the first analysis includes only short baseline reactor experiments (thus fitting the reactor anomaly only). They find that the no oscillation case is disfavored at about 98% in both a 3+1 and 3+2 scenario, where 3+1 means that there are the three active neutrinos and one heavier sterile state, in 3+2 there are two heavier steriles. In a second fit the results from LSND [29] and MiniBooNE [32] are included, as well as the constraints from KARMEN [30], NOMAD [38] and CERN [39].

In the 3+1 scheme, figure 3.6 shows the regions at 90 and 99% confidence level (CL) for LSND and MiniBooNE combined and the exclusion limits at 99% CL from disappearance experiments (green line) and appearance experiments (blue line). Except for a spot at $\Delta m^2 \approx 1$ eV^2 one can find no agreement of the data in this scenario.

Furthermore they analyzed a 3+2 and 1+3+1 scheme, where in the latter one sterile

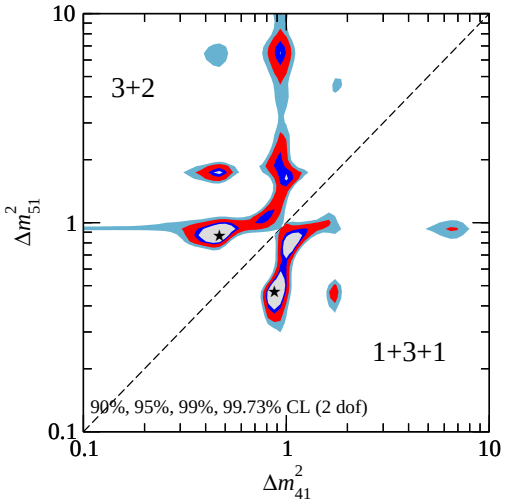

Figure 3.7: Preferred region for the mass squared differences in 3+2 and 1+3+1 (taken from [37]).

neutrino is lighter than the active neutrinos and one heavier. The 1+3+1 fit is slightly better than 3+2 (see table 3.2), although it is in even more tension with cosmology than 3+2, because of the large total neutrino mass (sum of light neutrino masses). Both improve the results drastically compared to the 3+1 case, which is disfavored at 97% CL compared to two steriles. The preferred mass-squared differences are shown in figure 3.7.

Overall there remains some tension between the data sets, even though there are many hints to the existence of one or two light sterile neutrinos. New experiments can hopefully clear up the view on these signs and maybe proof that there is a sterile neutrino mixing with the active ones.

Some recent updates have been made since the discussed global fit. The MiniBooNE collaboration has reanalyzed its data in [40], combining the analysis of the neutrino and antineutrino appearance data. The former agreement of the antineutrino channel with the LSND result becomes worse, the best fit regions now overlap only little in a region of small mass-squared differences below 1 eV^2. Moreover, the disagreement of the neutrino and antineutrino channel almost vanishes and with it the indication for CP violation. This supported the introduction of two sterile neutrinos, which is now not only in tension with cosmology, but also no longer preferred by the MiniBooNE measurement.

Another experiment searching for $\nu_\mu \to \nu_e$ oscillations is the ICARUS (Imaging Cosmic And Rare Underground Signals) experiment. Their recent publication [41] placed strong bounds on sterile neutrinos with large mixing, excluding the parameters space where $\sin^2(2\theta) \gtrsim 10^{-2}$, see figure 3.8. Note that global fits preferred exactly the parameter

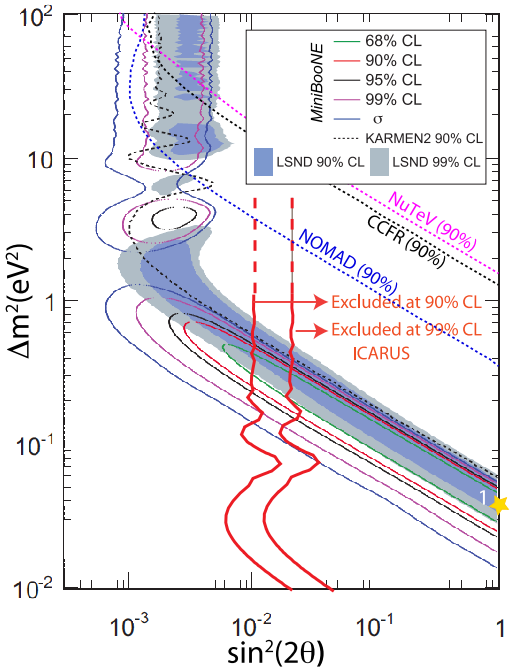

Figure 3.8: Exclusion limits from ICARUS including the new MiniBooNE analysis, taken from [41].

space of large mixing. The $\nu_\mu \rightarrow \nu_e$ oscillation data seems to become more and more inconsistent.

3.1.3 MSW Effect

A mechanism one could use to detect a sterile state could be the interaction with matter, as it can significantly enhance mixing angles. Therefore, the MSW effect will be explained in the following. In this section it will however be described only for the active neutrinos, in chapter 4 the equations will be derived in case there is one additional sterile neutrino. The formalism is introduced here and will be used later.

When neutrinos pass through matter they interact with the neutrons, protons and electrons of the medium via neutral or charged currents. For neutrino oscillations incoherent scattering manifests as a decrease of the flux and can be described by a complex damping term in the Hamiltonian. As it is proportional to the Fermi constant G_F, the contribution is negligible and will not be considered here. But in coherent elastic forward scattering, contributions from different collisions can add up coherently and must thus be considered although they are also proportional to G_F (for the original papers see [42], [43]). While only electron neutrinos can interact via charged currents (CC), as

matter usually does not contain muons and tauons but electrons, all flavors, ν_e, ν_μ and ν_τ, interact via neutral currents. The currents lead to interaction Hamiltonians.

For charged current (CC) interactions the Hamiltonian is given by

$$H_{CC} = \frac{G_F}{\sqrt{2}}[\bar{e}\gamma^\mu(1-\gamma_5)\nu_e][\bar{\nu}_e\gamma_\mu(1-\gamma_5)e] \tag{3.15}$$

$$= \frac{G_F}{\sqrt{2}}[\bar{e}\gamma^\mu(1-\gamma_5)e][\bar{\nu}_e\gamma_\mu(1-\gamma_5)\nu_e]\,, \tag{3.16}$$

where from the first to the second line Fierz transformations were applied. The electron contributions have to be averaged over the matter background:

$$\langle\bar{e}\gamma^\mu(1-\gamma_5)e\rangle = \langle\bar{e}\left(\begin{pmatrix}\gamma^0\\ \gamma^i\end{pmatrix} - \begin{pmatrix}\gamma^0\gamma_5\\ \gamma^i\gamma_5\end{pmatrix}\right)e\rangle\,. \tag{3.17}$$

These terms give the following contributions:

The first one gives the electron density $\langle\bar{e}\gamma^0 e\rangle = \langle e^\dagger e\rangle = N_e$, the second term the mean electron velocity $\langle\bar{e}\gamma^i e\rangle = \langle\boldsymbol{v}_e\rangle$, which is zero in the rest frame of the considered medium. The third term yields the mean helicity $\langle\bar{e}\gamma^0\gamma_5 e\rangle = \langle\frac{\boldsymbol{\sigma}_e\boldsymbol{p}_e}{E_e}\rangle$, which is negligible for a non-relativistic medium. The last term gives the polarization of the medium $\langle\bar{e}\gamma^i\gamma_5 e\rangle = \langle\boldsymbol{\sigma}_e\rangle$, which is also taken to be zero in the following.

As the active neutrinos are left-handed, the projection operator $(1-\gamma_5)$ becomes a factor 2 and the effective interaction Hamiltonian becomes

$$H_{CC}^{\text{eff}} = \langle H_{CC}\rangle = \bar{\nu}_e\sqrt{2}\,G_F N_e\nu_e = \bar{\nu}_e V_{CC}\nu_e \tag{3.18}$$

$$\text{with}\quad V_{CC} = \sqrt{2}\,G_F N_e \approx 7.63\cdot 10^{-14}\text{eV}\cdot\rho[\frac{\text{g}}{\text{cm}^3}]\cdot Y_e\,, \tag{3.19}$$

where Y_e is the number of electrons per nucleon which is about $\frac{1}{2}$ for media like e.g. the Earth.

The calculation is analogous for neutral current (NC) interactions and gives:

$$V_{NC} = -\frac{G_F}{\sqrt{2}}N_n\,, \tag{3.20}$$

where N_n is the neutron density. Contributions from electrons and protons to NC interactions cancel when assuming the medium to be electrically neutral, which is done in the following. This makes

$$V_{NC} = -\frac{G_F}{\sqrt{2}}N_n \approx \frac{1}{2}\cdot 7.63\cdot 10^{-14}\text{eV}\cdot\rho[\frac{\text{g}}{\text{cm}^3}]\cdot Y_n \tag{3.21}$$

$$= 7.63 \cdot 10^{-14}\text{eV} \cdot \rho[\frac{\text{g}}{\text{cm}^3}] \cdot \frac{1 - Y_e}{2}\,, \tag{3.22}$$

where Y_n is the number of neutrons per nucleons, which is equal to $1 - Y_e$, since there are as many electrons as protons, $N_e = N_p$. The matter density ρ is in grams per cubic centimeter. ρ and Y_e contain the coordinate dependence of the potential: $\rho = \rho(x)$, $Y_e = Y_e(x)$.

This section showed that there are various signs of a light sterile neutrino, but they remain very contradictory and inconclusive. It is therefore an interesting topic to be further investigated in order to find possibilities to detect such a sterile state. In chapter 4 a possible enhancement (due to the MSW effect) of the oscillation of the electron neutrino with a sterile state is studied, where the mass of the fourth state is in the eV range. Atmospheric neutrinos traversing the earth can have the right energies to undergo such an enhancement and they could be detected at the IceCube experiment.

3.2 Non-Unitarity

In the presence of sterile neutrinos, the mixing matrix of the three light (mainly active) neutrinos becomes non-unitary. If the sterile neutrinos are very light, they oscillate with the active neutrinos and the phenomenology changes as described above. But also if the sterile states are too heavy to oscillate or even be produced in the processes, they affect the low energy observables. Since the complete theory has to be unitary, the low energy part becomes non-unitary. This was already shown in section 2.1, where the non-unitarity caused by the heavy sterile neutrinos in the seesaw mechanism was calculated (see equation (2.28)). The non-unitarity of the PMNS mixing matrix then changes the low-scale phenomenology and this effect could be observed in various electroweak processes involving neutrinos. Different experiments, from neutrino oscillations to electroweak precision measurements, constrain the size of the effect, as no clear sign has been observed so far that would confirm that the PMNS matrix were non-unitary. In this section the effects of non-unitarity on electroweak processes will be analyzed, assuming there are only three light neutrinos and the sterile states are heavy, see [44].

When new physics are introduced at a scale M far beyond the scale that is tested in experiments, usually meaning $M \gg M_Z$, one can treat it as an effective theory at low energies. This means that parameters in the SM Lagrangian have to be corrected and higher dimensional, non renormalizable operators are introduced, whose coefficients are suppressed by the scale of new physics: $\propto 1/M$. In the following, the effects of

non-unitarity of the PMNS matrix are studied, thus only the corrections of the SM parameters are considered.

In chapter 2 the Lagrangians for the neutral and charged current interaction were introduced, including the possible presence of sterile neutrinos, see equations (2.34) and (2.35). In this section the sterile states should not be considered, but instead an effective Lagrangian, where the PMNS matrix U^P becomes non-unitary. The interaction Lagrangians then read

$$\begin{aligned}\mathscr{L}^{NC}_{int,\,\text{eff}} &= -\sum_{\alpha}\sum_{i,j=1}^{3}\frac{g}{2\cos(\theta_W)}U^{P\,*}_{\alpha i}\bar{\nu}_i\gamma_\mu P_L U^{P}_{\alpha j}\nu_j Z^\mu + h.c. \\ &= -\sum_{i,j=1}^{3}\frac{g}{2\cos(\theta_W)}\bar{\nu}_i\gamma_\mu P_L (U^{P\,\dagger}U^P)_{ij}\nu_j Z^\mu + h.c. \qquad (3.23)\end{aligned}$$

$$\mathscr{L}^{CC}_{int,\,\text{eff}} = -\sum_{\alpha}\sum_{i=1}^{3}\frac{g}{\sqrt{2}}\left(U^{P\,*}_{\alpha i}\bar{\nu}_i\gamma_\mu P_L \ell_\alpha W^{+\mu} + \bar{\ell}_\alpha\gamma_\mu P_L U^{P}_{\alpha i}\nu_i W^{-\mu}\right)\,, \qquad (3.24)$$

with the projection operator $P_L = \left(\frac{1-\gamma_5}{2}\right)$. In the neutral current the PMNS matrix would cancel out if it were unitary. These modifications in the neutral and charged current Lagrangians lead to modifications in electroweak processes. To give an example: For one heavy sterile neutrino s with mixing U_{si} to the mass eigenstates, the non-unitary contribution to the neutral current is given by

$$\begin{aligned}(U^{P\,\dagger}U^P)_{ij} &= \sum_{\alpha=e,\mu,\tau}U^{P\,*}_{\alpha i}U^P_{\alpha j} = \sum_{\alpha=e,\mu,\tau,s}U^*_{\alpha i}U_{\alpha j} - U^*_{si}U_{sj} \\ &= 1 - U^*_{si}U_{sj}\,, \qquad (3.25)\end{aligned}$$

where U is the full 4×4 unitary mixing matrix (and U^P its 3×3 upper left corner) and the indices $i,j = 1,...,3$ denote only the three light mass eigenstates.

Furthermore, the orthonormality of the flavor eigenstates is modified. The neutrino states in case of a full theory are normalized and orthogonal to each other in the flavor and mass basis. When the PMNS matrix U^P becomes non-unitary, this is no longer true. In the mass eigenbasis the states are still orthonormal:

$$\langle\nu_i|\nu_j\rangle = \delta_{ij}\,. \qquad (3.26)$$

The quantum states and fields have to be consistent, therefore the flavor eigenstates

have the normalization

$$|\nu_\alpha\rangle = \left((U^P U^{P\dagger})_{\alpha\alpha}\right)^{-\frac{1}{2}} \sum_{i=1}^{3} U^{P*}_{\alpha i} |\nu_i\rangle \,, \tag{3.27}$$

where $U^P U^{P\dagger}$ is not the unit matrix, as U^P is assumed to be non-unitary. The flavor eigenstates are then not orthonormal, but instead fulfill

$$\langle \nu_\alpha | \nu_\beta \rangle = \frac{(U^P U^{P\dagger})_{\beta\alpha}}{\sqrt{(U^P U^{P\dagger})_{\alpha\alpha}(U^P U^{P\dagger})_{\beta\beta}}} \,. \tag{3.28}$$

This affects the propagation of the flavor eigenstates and thus the oscillation probabilities. The free propagation of mass eigenstates, meaning in the vacuum, is given by the Hamiltonian H:

$$i\frac{d}{dt}|\nu_i\rangle = H|\nu_i\rangle \,, \tag{3.29}$$

and the orthonormality of the mass eigenbasis gives

$$\langle \nu_j | H | \nu_i \rangle = \delta_{ij} E_i \,, \tag{3.30}$$

with the energy eigenvalues E_i of the Hamiltonian. One can then project onto the energy eigenbasis:

$$i\frac{d}{dt}|\nu_i\rangle = \sum_j |\nu_j\rangle\langle\nu_j|H|\nu_i\rangle = E_i|\nu_i\rangle \,. \tag{3.31}$$

Since the flavor eigenbasis is not orthonormal, the evolution in this basis becomes

$$i\frac{d}{dt}|\nu_\alpha\rangle = H|\nu_\alpha\rangle = \sum_j |\nu_j\rangle\langle\nu_j|H|\nu_\alpha\rangle = \sum_\beta \frac{(U^{P*}E(U^{P*})^{-1})_{\alpha\beta}}{\sqrt{(U^P U^{P\dagger})_{\alpha\alpha}(U^P U^{P\dagger})_{\beta\beta}}} |\nu_\beta\rangle \,, \tag{3.32}$$

where E is a diagonal matrix with entries E_j, the energy of the state ν_j. Therefore the state produced as a flavor eigenstate $|\nu_\alpha\rangle$ at $t = 0$ ($L = 0$) evolves after a time T, corresponding to the length L, to the state

$$|\nu(L)\rangle = \sum_{i,\gamma} \frac{U^{P*}_{\alpha i} e^{iE_i L} (U^{P*})^{-1}_{i\gamma}}{\sqrt{(U^P U^{P\dagger})_{\alpha\alpha}(U^P U^{P\dagger})_{\gamma\gamma}}} |\nu_\gamma\rangle \,. \tag{3.33}$$

The oscillation probability of the neutrino with flavor α at $L = 0$ to be found as flavor

β at length L is then given by

$$P(\nu_\alpha \to \nu_\beta, L) = |\langle \nu_\beta | \nu(L) \rangle|^2 = \frac{|\sum_i U^{P*}_{\alpha i} e^{iE_i L} U^{P*}_{\beta i}|^2}{(U^P U^{P\dagger})_{\alpha\alpha}(U^P U^{P\dagger})_{\beta\beta}} \,. \tag{3.34}$$

Comparing this result to the one obtained in chapter 2 and section 3.1 respectively (see for example equation (3.3)) one obtains in the non-unitary case a so-called zero distance effect. This means that the probability of a transition of flavor α to β is nonzero at $L = 0$:

$$P(\nu_\alpha \to \nu_\beta, L = 0) = \frac{|(U^P U^{P\dagger})_{\beta\alpha}|^2}{(U^P U^{P\dagger})_{\alpha\alpha}(U^P U^{P\dagger})_{\beta\beta}} \neq 0 \,. \tag{3.35}$$

Also, the total probability does not sum up to one.

To correctly analyze oscillation data, also other effects have to be considered. As the propagation of the neutrinos of a certain flavor changes, the fluxes get modified. Furthermore, since the production and detection processes are charged or neutral current interactions, the cross-sections differ also from the unitary ones.

For neutrinos travelling in a medium the interactions with the matter particles get modified. This leads to a different interaction Hamiltonian. The calculation made in section 3.1.3 remains valid, only when changing from the flavor to the mass basis the responsible matrix is the non-unitary PMNS matrix and this again affects the propagation of the flavor eigenstates, analogously to the vacuum case. The non-unitarity of the mixing matrix then leads to a non-diagonal effective potential. For details see [44].

The oscillation data can then be reanalyzed under the assumption of a non-unitary PMNS matrix. One can derive constraints on the unitarity of the mixing matrix and derive the values of the mixing matrix from the experiments. This has been done in [44], yielding that U^P has to be unitary up to the percent level.

Electroweak decays on the other hand cannot determine the PMNS mixing matrix elements, as they are not sensitive to single neutrino eigenstates, but rather sums of products of U^P. They can however test the unitarity assumption through the zero distance effect, since the cross sections of charged and neutral current processes are modified by $(U^P U^{P\dagger})_{\alpha\beta}$ or $(U^{P\dagger} U^P)_{ij}$. In the following the decays of the W boson will be treated exemplarily.

The decay width of the W boson into a neutrino and a charged lepton is given by

$$\Gamma(W \to \ell_\alpha \nu_\alpha) = \sum_i \Gamma(W \to \ell_\alpha \nu_i) = \frac{G_F M_W^3}{6\sqrt{2}\pi} (U^P U^{P\dagger})_{\alpha\alpha} \,, \tag{3.36}$$

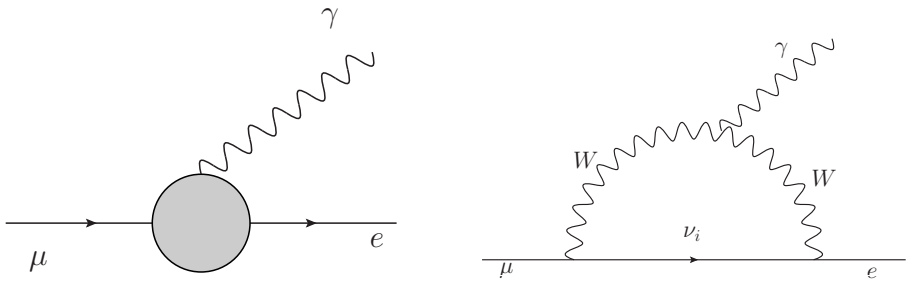

(a) Feynman diagram for $\mu \to e\,\gamma$ (b) possible diagram via neutrino mixing

Figure 3.9: Lepton flavor violating decay $\mu \to e\,\gamma$.

where the mixing elements have been absorbed to the definition of the decay width in the second step. G_F is the Fermi constant and M_W the mass of the W boson. Note that the Fermi constant is usually measured by the muon decay $\mu \to e\bar{\nu}_e\nu_\mu$, and this process also gets corrected by non-unitarity factors

$$G_F = \frac{G_\mu}{\sqrt{(U^P U^{P\dagger})_{ee}(U^P U^{P\dagger})_{\mu\mu}}}\,, \tag{3.37}$$

G_μ being the constant measured in the muon decay. The measured decay width of the W boson into different particles can therefore restrict the values of a combination of non-unitarity factors.

The existence of heavy sterile neutrinos changes the low energy electroweak observables, even when they cannot participate in the processes due to their large mass. These effects can be measured in various experiments, as for example in the LEP e^+e^- collider (Large Electron–Positron collider) that was studying weak processes. This can have interesting implications on for example the Z decay width, as its measured values at LEP differed from the SM values at about 2σ. This will be treated in chapter 5.

3.3 Lepton Flavor Violation

In the SM, as neutrinos are massless, lepton flavor is conserved. Only in the quark sector the quarks mix with each other and quark flavor is violated, but the quark-mixing matrix (CKM matrix) is almost diagonal, so the flavor violation in the SM is small.

Already when considering the existence of active neutrino masses as the beyond SM concept, lepton flavor violating decays, such as $\ell_\alpha \to \ell_\beta\,\gamma$, are induced by the mixing of the active neutrinos. The branching ratio however is tiny, as the mass squared differences are so small and the PMNS matrix is unitary, the amplitudes of the three processes cancel

out. A calculation of the process $\mu \rightarrow e\,\gamma$ induced by the three light neutrinos can be found in [45].

For light sterile neutrinos the same cancellation mechanism applies when their masses are much smaller than the mass of the mediator, which is the W-boson in this case (see figure 3.9b). The case for heavier sterile neutrinos will be treated in detail in section 5.4.1. Their contribution is proportional to the active–sterile mixing and therefore usually tiny for large masses (it is proportional to the mixing to the fourth power). Only when cancellations allow for a sizeable mixing, lepton flavor violating decays would become observable. This could be via a seesaw type II, where the triplet term cancels the contribution of the heavy sterile neutrinos in the light neutrino mass matrix:

$$m_\nu = M_L - m_D^T M_R^{-1} m_D\,, \tag{3.38}$$

or in case there is a cancellation of contribution from different heavy sterile neutrinos in the matrix

$$m_\nu = -m_D^T M_R^{-1} m_D \tag{3.39}$$

in a seesaw type I.

A review on the experimental status can be found in [46] or from the PDG [47]. The most stringend limits exist on the decay $\mu \rightarrow e\,\gamma$, coming from the MEG collaboration [48], where

$$B(\mu^+ \rightarrow e^+\gamma) \leq 2.4 \cdot 10^{-12} \tag{3.40}$$

at 90% confidence level.

3.4 Neutrinoless Double-Beta Decay

The neutrinoless double-beta decay $\beta\beta_{0\nu}$ is a process that is searched for to probe lepton number violation ($\Delta L = 2$). The nucleus with mass and charge number (A,Z) decays into a doubly charged nucleus and two electrons: (A,Z) $\rightarrow$ (A,Z+2) + 2 e^-. For some elements the simple beta decay is kinematically forbidden, but the double-beta decay is allowed. Then the process, without the two neutrinos in the final state, could be observed. The double-beta decay producing two neutrinos (so to say the SM process) has already been measured, its half-life is about 10^{20} years, depending on the nucleus. This is the main background for the process where the two neutrinos are missing in the

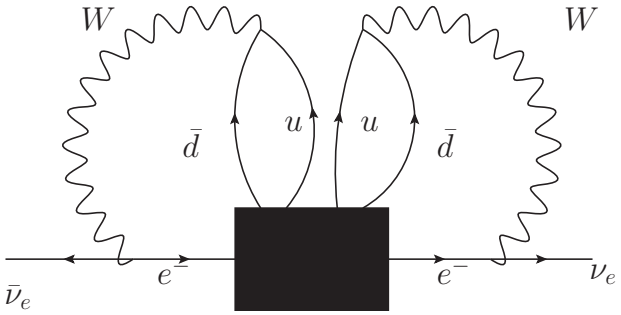

Figure 3.10: Schechter-Valle diagram illustrating the contribution of $\beta\beta_{0\nu}$ decay to the Majorana mass of the neutrino.

final state (compare [49]).

The rate of this process depends on the mechanism by which it is induced and can be divided into different parts. The decay rate is given by

$$\Gamma(\beta\beta_{0\nu}) = G_x(Q, \mathrm{Z})|M_x(\mathrm{A}, \mathrm{Z})\eta_x|^2\,, \tag{3.41}$$

where the x indicates the dependence on the mechanism. η_x depends on the particle physics parameters which are involved in the decay, M_x is the nuclear matrix element, describing the properties of the nucleus and $G_x(Q, \mathrm{Z})$ is the phase space factor. A and Z are again mass and charge number, Q is the value of energy that is released in the process. One can calculate these values for different mechanisms.

If neutrinoless double-beta decay is observed, neutrinos have to be Majorana particles, even though the process might be related to some other new physics beyond the SM (not a Majorana mass term of the light neutrinos). The Schechter-Valle theorem [20] states, that by a black-box diagram, $\beta\beta_{0\nu}$ decay necessarily leads to a Majorana mass for neutrinos, though it might be tiny, as it is induced by a four loop process. The diagram is shown in figure 3.10.

The so-called standard interpretation, the most investigated mechanism, is that $\beta\beta_{0\nu}$ is caused by three light Majorana neutrinos, which make up the active neutrinos. The Feynman diagram is shown in figure 3.11. Hereby one neglects possible other contributions from the physics that generate the light neutrino masses (e.g. heavy right-handed Majorana neutrinos or a Higgs triplet). It is usually a good approximation, as for example the right-handed neutrinos in the seesaw type I are typically very heavy and their contribution then suppressed (which will be shown in the following). This means that the masses of the exchanged neutrinos are much smaller than the scale of the momen-

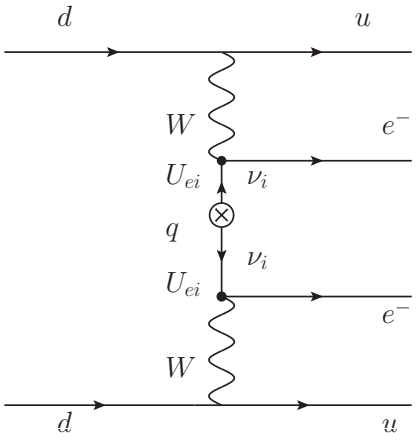

Figure 3.11: Feynman diagram for $\beta\beta_{0\nu}$ induced by Majorana neutrinos ν_i with mixing U_{ei} to the electron neutrino.

tum transfer, which is about 100 MeV. One can then make an approximation in the amplitude of the process, which is proportional to the propagator:

$$\mathcal{A} \propto \frac{m_i}{q^2 - m_i^2} \propto \begin{cases} \frac{m_i}{q^2} & m_i^2 \ll q^2\,, \\ \frac{1}{m_i} & m_i^2 \gg q^2\,. \end{cases} \tag{3.42}$$

This means that the decay rate becomes (index 3ℓ for three light neutrinos)

$$\Gamma_{3\ell} = G_{3\ell}(Q, Z)|M_{3\ell}|^2 \frac{\langle m_{ee}\rangle^2}{m_e^2}\,, \tag{3.43}$$

where m_{ee} is the effective electron neutrino mass, which is defined below. From the Feynman diagram in figure 3.11, we can read off the full dependence of the amplitude for the process in the V–A interaction:

$$\mathcal{A}_{3\ell} \propto \sum_{i=1}^{3} G_F^2 U_{ei}^2 \gamma_\mu P_R \frac{\not{q} + m_i}{q^2 - m_i^2} \gamma_\nu P_L = \sum_{i=1}^{3} G_F^2 U_{ei}^2 \frac{m_i}{q^2 - m_i^2} \gamma_\mu P_R \gamma_\nu \tag{3.44}$$

$$\approx \sum_{i=1}^{3} G_F^2 U_{ei}^2 \frac{m_i}{q^2} \gamma_\mu P_R \gamma_\nu\,. \tag{3.45}$$

G_F is the Fermi constant, U_{ei} the mixing element of the i-th neutrino of mass m_i with the electron neutrino and q^2 is the average neutrino momentum. $P_{L,R} = \frac{1}{2}(1 \pm \gamma_5)$ are the left and right projection operators and $\gamma_{\mu,\nu}$ the gamma matrices. This leads to an

effective neutrino mass of

$$\langle m_{ee} \rangle = \left| \sum_{i=1}^{3} U_{ei}^2 m_i \right| = \left| m_1 |U_{e1}|^2 + m_2 |U_{e2}|^2 e^{i\alpha_1} + m_3 |U_{e3}|^2 e^{i\alpha_2} \right| , \tag{3.46}$$

where $\alpha_{1,2}$ are the Majorana phases, compare equation (3.13). Depending on these phases, the effective mass can therefore cancel to zero. This is only possible in the normal hierarchy case; in the inverted hierarchy, there is a minimal value, as also in the quasi-degenerate case, see [49].

The contribution of sterile neutrinos to the $\beta\beta_{0\nu}$ decay strongly depends on the scale of their masses. For light sterile neutrinos one can make the same approximation as before, light meaning $m_i^2 \ll q^2$, well below 100 MeV. These just add to the three light (active) neutrinos that were considered before. For n light neutrinos (3 active and $(n-3)$ sterile states) this leads to

$$\Gamma_{n\ell} = G_{n\ell}(Q, Z) |M_{n\ell}|^2 \frac{\langle m_{ee} \rangle^2}{m_e^2} , \tag{3.47}$$

with

$$\langle m_{ee} \rangle = \left| \sum_{i=1}^{n} U_{ei}^2 m_i \right| . \tag{3.48}$$

For heavy sterile states ($m_i^2 \gg q^2$) the Feynman diagram for the process is still the same as in figure 3.11, but since the masses of these neutrinos are much bigger than the momentum scale, the amplitude becomes inversely proportional to the mass:

$$\mathcal{A}_h \propto \frac{1}{m_i} . \tag{3.49}$$

The maximal rate for this process can actually be expected for masses at the momentum scale, so around 100 MeV, since the decay rate is for small masses proportional to m^2 and for large masses to m^{-2}, meaning that there is a peak where the one approximation takes over the other. For heavy sterile neutrinos the decay rate becomes proportional to

$$\Gamma_h \propto \left| \sum_i \frac{U_{ei}^2}{m_i} \right|^2 , \tag{3.50}$$

where U_{ei} is here the active-sterile mixing, the mixing of the heavy mass eigenstates with the electron neutrino, which is usually small. This and the dependency on the inverse

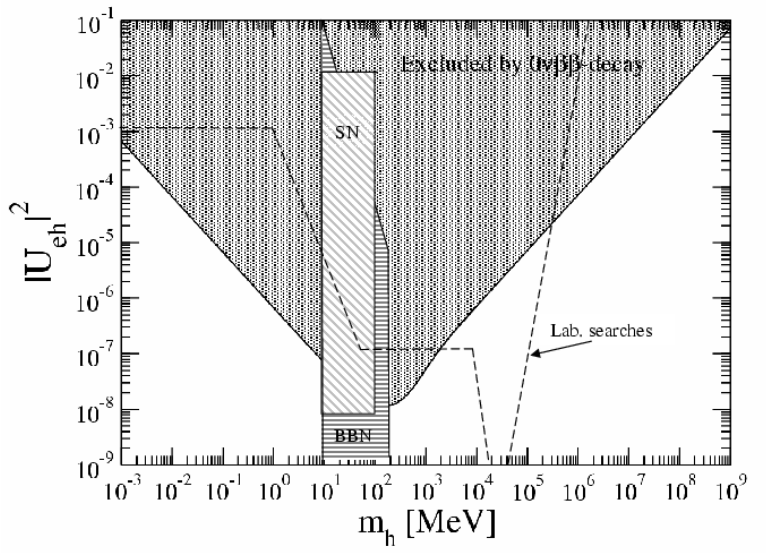

Figure 3.12: Exclusion limit on the mixing $|U_{eh}|^2$ of the heavy to the electron neutrino, m_h being its mass, from neutrinoless double-beta decay (dark shaded area). Also plotted are limits from the supernova SN1987A, Big Bang nucleosynthesis and laboratory searches. Taken from [50].

mass suppresses the contributions at higher sterile masses. The process here is of short range and therefore sensitive to the form factors (the finite size) of the nucleons.

In [50], an exclusion limit on the mixing of the heavy to the electron neutrino is plotted against the mass of the heavy state. The peak of the curve excludes mixing down to $|U_{ei}|^2 \simeq 10^{-8}$, see figure 3.12.

The seesaw type I contributes in two ways to the neutrinoless double-beta decay: directly through the exchange of heavy right-handed neutrinos and indirectly through the exchange of the light neutrinos. In case the right-handed neutrinos in the seesaw type I are also lighter than the momentum scale of $\beta\beta_{0\nu}$, the contributions cancel exactly, as the sum gives exactly the $(M_L)_{ee}$-entry in the neutrino mass matrix (see equation (2.16)), which is zero in a seesaw type I.

For a detailed review on neutrinoless double-beta decay and the contributions from different beyond the SM processes, see [49].

Most recent limits on the $\beta\beta_{0\nu}$ lifetime come from the EXO collaboration [51] and KamLAND-Zen [52], using ^{136}Xe:

$$T_{1/2}^{\beta\beta_{0\nu}}(^{136}\mathrm{Xe}) > 1.6 \cdot 10^{25}\ \mathrm{yr} \quad (90\%\ \mathrm{CL,\ EXO})\,, \tag{3.51}$$

$$T_{1/2}^{\beta\beta_{0\nu}}(^{136}\mathrm{Xe}) > 5.7 \cdot 10^{24}\ \mathrm{yr} \quad (90\%\ \mathrm{CL,\ KamLAND\text{-}Zen})\,. \tag{3.52}$$

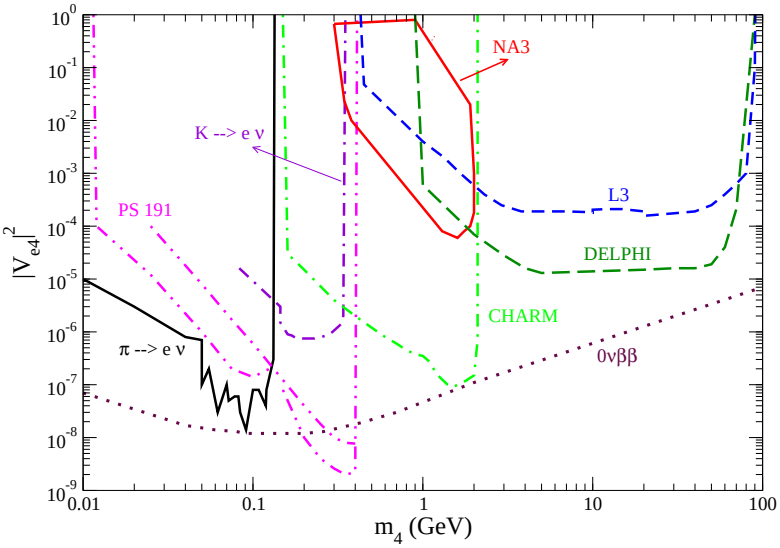

Figure 3.13: Bounds on $|U_{e4}|^2 = |V_{e4}|^2$ for masses of the heavy neutrino $M_4 = m_4$ in the range 10 MeV – 100 GeV from various experiments. Taken from [53].

In the standard interpretation this leads to an effective mass

$$\langle m_{ee} \rangle < 0.14 - 0.38 \text{ eV} \quad (90\% \text{ CL, EXO}) , \tag{3.53}$$

$$\langle m_{ee} \rangle < 0.3 - 0.6 \text{ eV} \quad (90\% \text{ CL, KamLAND-Zen}) . \tag{3.54}$$

3.5 Sterile Neutrinos at Colliders

The most stringend bounds on sterile neutrinos at colliders are found for steriles with masses up to $M_4 \lesssim 3$ GeV, where limits come from the decay of mesons. Also from Z decay $Z \rightarrow N + \nu$ upper limits can be found for $M_4 \lesssim M_Z$. The higher the mass of the sterile state, the shorter its lifetime, therefore the signature reconstruction becomes more difficult and the bounds weaker. The limits on the mixing elements squared $|U_{\alpha 4}|^2$ go from 10^{-7} for small M_4 to 10^{-3} and 10^{-1} for masses $M_4 \lesssim M_Z$. See [53] for a detailed overview and references therein. In figure 3.13 the limits on the mixing of the heavy neutrino to the electron neutrino are shown as an example.

There are not many experiments that can access higher masses. In the following, searches at LEP, Tevatron and LHC are discussed, since these searches will become relevant in section 5.4.2.

As the LEP collided e^+e^-, whereas Tevatron and LHC are hadron colliders, the detection channels for heavy Majorana neutrinos differ in these cases. At LEP there were

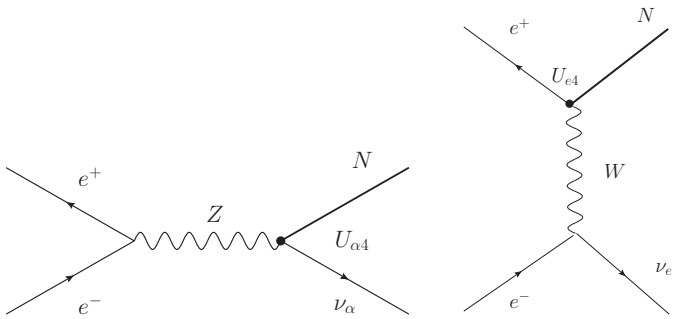

(a) s-channel (b) t-channel

Figure 3.14: Processes of e^+e^- leading to a heavy (mostly sterile) neutrino N in the final state.

two possible production channels for $e^+e^- \to \nu_\alpha N$: via the s-channel, see figure 3.14a, all mixing parameters $U_{\alpha 4}$ ($\alpha = e, \mu, \tau$) to the fourth, heavy neutrino N could be measured. The t-channel however is only sensitive to the mixing to the electron neutrino U_{e4}, see figure 3.14b. The heavy neutrino then decays into a W and a charged lepton or a Z boson and an active neutrino. Below the Z boson mass the bounds are much more stringend, but the L3 experiment at LEP also measured at higher energies and placed limits up to masses of the heavy neutrino of about 200 GeV (see section 5.4.2).

At hadron colliders, the production and detection of heavy Majorana neutrinos can occur via the two diagrams shown in figure 3.15. Both involve two leptons in the final state of equal sign and two jets (for oppositely charged leptons the SM background is significantly higher). In the s-channel the heavy neutrino is produced and subsequently decays. This is by far the dominant channel. The t-channel is in complete analogy to the $\beta\beta_{0\nu}$ Feynman diagram (compare the previous section 3.4). The theoretical calculation and the resulting bounds on the mixing elements from searches at Tevatron are discussed in [53]. For masses above the Z boson mass, the limits will be discussed in more detail in section 5.4.2, including measurements from LEP and LHC.

3.6 Loop Effects

In section 3.2, indirect effects of new physics at a high scale on low energy observables were described. The focus was on the non-unitarity of the theory, in this case the non-unitarity of the PMNS matrix. The so-called oblique corrections also encode indirect information arising from new physics. The effects can be seen in precision measurements, especially weak interaction parameters, as these are measured to very high accuracy. For

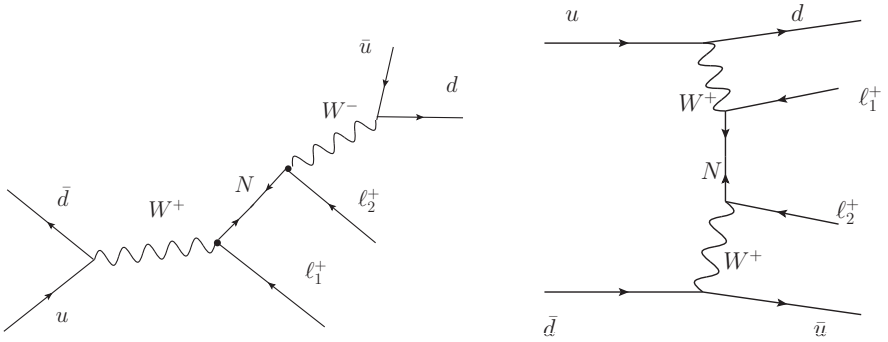

(a) s-channel (b) t-channel

Figure 3.15: Feynman diagram for the detection of a heavy sterile neutrino at a hadron collider.

example the rho parameter satisfies in the SM at tree level the relation

$$\rho = \frac{M_W^2}{M_Z^2 \cos^2(\theta_W)} = 1\,, \tag{3.55}$$

of the W and Z boson masses and the Weinberg angle θ_W. Loop corrections from SM and new particles will alter this relation. Since the SM contribution has been calculated very precisely, coming mainly from the top quark, new physics can be constrained by a measurement of this relation. For example, as mentioned in chapter 2, a Higgs triplet would shift the rho parameter. Such relations, as the one of the rho parameter, can restrict new physics even if only present in loop diagrams.

When the external particles in the experiments are light and we consider only processes of the weak interaction, one can neglect the vertex corrections and the box diagrams, as they are suppressed by an additional factor of m_f^2/M_Z^2, where m_f is the mass of the external particle. One can therefore concentrate on the vacuum polarization effects, the so-called oblique corrections (compare [54]). They can be quantified by the vacuum polarization tensors that have the form

$$\Pi_{xy}^{\mu\nu}(q^2) = \Pi_{xy}(q^2) g^{\mu\nu} + (q_\mu q_\nu\text{-terms})\,, \tag{3.56}$$

where x and y are the in- and outgoing gauge bosons γ, $W^\pm$ and Z, which can combine as $(\gamma\gamma)$, $(Z\gamma)$, (ZZ) and (WW), see figure 3.16. The $q_\mu q_\nu$-terms can be neglected in the W and Z propagators, also because the external fermions are light and the contraction with their currents suppress the terms by a factor m_f^2/M_Z^2. The $q_\mu q_\nu$-term of the photon propagator does not contribute due to the Ward identity (see [55]).

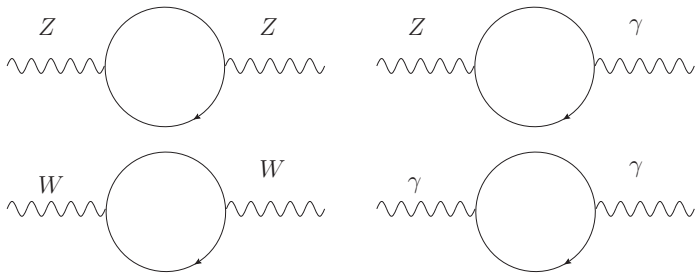

(a) Z and W boson self-energies. (b) Photon and photon–Z self energies.

Figure 3.16: Self-energy contribution to the Z and W boson and the photon from fermion loops.

Since SM processes also contribute to the vacuum polarization, one can write

$$\Pi_{xy}(q^2) = \Pi_{xy}^{SM}(q^2) + \delta\Pi_{xy}(q^2)\,, \tag{3.57}$$

where the new physics contribution is denoted as $\delta\Pi_{xy}(q^2)$. The Ward identity implies also that the photon self energies have to vanish at zero momentum:

$$\Pi_{Z\gamma}(0) = \Pi_{\gamma\gamma}(0) = 0\,. \tag{3.58}$$

In the on-shell scheme the self energies are renormalized by fixing the masses in the propagator to be the physical masses. This gives (renormalized quantities are denoted by a hat):

$$\Re\left(\hat{\Pi}_{WW}(M_W^2)\right) = \Re\left(\hat{\Pi}_{ZZ}(M_Z^2)\right) = \hat{\Pi}_{Z\gamma}(0) = \hat{\Pi}_{\gamma\gamma}(0) = 0\,. \tag{3.59}$$

In the following all self energies are assumed to be real, as resonances and decay width do not need to be considered in this context.

To parameterize the oblique corrections from the vacuum polarizations discussed above, three parameters are introduced that are called S, T and U. The correction residing purely in the electromagnetic sector is omitted, as only weak phenomena are considered. The parameters are defined in terms of the renormalized quantities as (see [56])

$$S = \frac{4s^2c^2}{M_Z^2}\left(\hat{\Pi}_{ZZ}(0) + \hat{\Pi}_{\gamma\gamma}(M_Z^2) - \frac{c^2-s^2}{cs}\hat{\Pi}_{Z\gamma}(M_Z^2)\right)\,, \tag{3.60}$$

$$T = \frac{\hat{\Pi}_{ZZ}(0)}{M_Z^2} - \frac{\hat{\Pi}_{WW}(0)}{M_W^2}\,, \tag{3.61}$$

$$U = 4s^2c^2 \left(\frac{1}{c^2} \frac{\hat{\Pi}_{WW}(0)}{M_W^2} - \frac{\hat{\Pi}_{ZZ}(0)}{M_Z^2} + \frac{s^2}{c^2} \frac{\hat{\Pi}_{\gamma\gamma}(M_Z^2)}{M_Z^2} - \frac{2s}{c} \frac{\hat{\Pi}_{Z\gamma}(M_Z^2)}{M_Z^2} \right) . \tag{3.62}$$

Here, s and c are the sine and cosine of the Weinberg angle, respectively.

Since the relations of the bare and the renormalized quantities are as follows (also see [56])

$$\hat{\Pi}_{WW}(q^2) = \Pi_{WW}(q^2) - \Pi_{WW}(M_W^2) + (q^2 - M_W^2) \left[\frac{c^2}{s^2} R - \Pi'_{\gamma\gamma}(0) \right] , \tag{3.63}$$

$$\hat{\Pi}_{ZZ}(q^2) = \Pi_{ZZ}(q^2) - \Pi_{ZZ}(M_W^2) + (q^2 - M_Z^2) \left[\left(\frac{c^2}{s^2} - 1 \right) R - \Pi'_{\gamma\gamma}(0) \right] , \tag{3.64}$$

$$\hat{\Pi}_{Z\gamma}(q^2) = \Pi_{Z\gamma}(q^2) - \Pi_{Z\gamma}(0) + q^2 \frac{c^2}{s^2} R , \tag{3.65}$$

$$\hat{\Pi}_{\gamma\gamma}(q^2) = \Pi_{\gamma\gamma}(q^2) - q^2 \Pi'_{\gamma\gamma}(0) , \tag{3.66}$$

where

$$R = \frac{\Pi_{ZZ}(M_Z^2)}{M_Z^2} - \frac{\Pi_{WW}(M_W^2)}{M_W^2} - 2\frac{s}{c} \frac{\Pi_{Z\gamma}(0)}{M_Z^2} , \tag{3.67}$$

the parameters S, T and U are related to the bare self energies through the equations

$$S = \frac{4s^2c^2}{M_Z^2} \left(\Pi_{ZZ}(0) - \Pi_{ZZ}(M_Z^2) + \Pi_{\gamma\gamma}(M_Z^2) - \frac{c^2 - s^2}{cs} \Pi_{Z\gamma}(M_Z^2) \right) , \tag{3.68}$$

$$T = \frac{\Pi_{ZZ}(0)}{M_Z^2} - \frac{\Pi_{WW}(0)}{M_W^2} - 2\frac{s}{c} \frac{\Pi_{Z\gamma}(0)}{M_Z^2} , \tag{3.69}$$

$$\begin{aligned} U = 4s^2c^2 \Bigg[& \frac{1}{c^2} \left(\frac{\Pi_{WW}(0)}{M_W^2} - \frac{\Pi_{WW}(M_W^2)}{M_W^2} \right) - \left(\frac{\Pi_{ZZ}(0)}{M_Z^2} - \frac{\Pi_{ZZ}(M_Z^2)}{M_Z^2} \right) \\ & + \frac{s^2}{c^2} \frac{\Pi_{\gamma\gamma}(M_Z^2)}{M_Z^2} - 2\frac{s}{c} \frac{\Pi_{Z\gamma}(M_Z^2)}{M_Z^2} \Bigg] . \end{aligned} \tag{3.70}$$

Note that in order to properly renormalize these quantities, a full theory has to be considered. This means for example that neutrino masses have to be introduced in a consistent way (in case of a Majorana mass for the left-handed neutrinos the triplet has to be taken into account, just as the doublet in the case of the Dirac mass). The neutrino masses then also determine their mixing; masses and mixing can not be considered to be independent.

The formalism of oblique corrections that was introduced can be applied to all types of new physics. In particular, it can also account for the radiative correction of heavy Majorana neutrinos. These can have interesting properties because of their Majorana

nature. The results of the contribution of heavy Majorana neutrinos to the parameters S, T and U will be quoted in section 5.1.1.

The last chapter has summarized the properties of sterile neutrinos at different scales. Light sterile neutrinos are special as they can oscillate with the active neutrinos. But also many other signatures differ a lot for light and heavy sterile neutrinos: For example the neutrinoless double-beta decay can be calculated in two different approximations: For neutrinos lighter or heavier than the momentum scale, which is at about 100 MeV. Similar for lepton flavor violation. When the mass squared differences of all neutrinos are very small, the amplitudes of the different diagrams contributing to the decays cancel out almost completely and lepton flavor violation is suppressed. The signatures of sterile neutrinos at colliders are better to identify, the smaller the masses are and can be produced in more processes. Therefore the most stringend bounds on active–sterile mixing can be placed at lower masses of the sterile states. An effect that is only relevant for heavy neutrinos is the non-unitarity of the PMNS matrix. If the sterile states cannot be produced in the considered processes, they nevertheless can be visible by the non-unitarity of the effective theory that is observed. In the case of neutrinos, the non-unitarity of the PMNS matrix is the strongest indicator of sterile neutrinos at a higher scale. Loop effects are also only relevant for heavy sterile neutrinos. They are an indirect measure of new physics and can be restricted because of the high precision of the measurements of weak observables.

In the following, the first of the main parts of this work, chapter 4, will examine the possibility of enhancing the active–sterile mixing in oscillations via the MSW effect. Oscillations of the electron to the sterile neutrino are considered, since there are some indications from short-baseline experiments pointing towards the existence of a fourth neutrino with a mass in the eV range, leading for example to $\bar{\nu}_e$ disappearance in reactor experiments (compare section 3.1.2). An enhanced mixing is obtained for a certain combination of energy and masses of the neutrinos and a certain baseline and density of the medium that is crossed. This combination can be found for atmospheric electron neutrinos traversing the Earth mixing with a sterile neutrino with a mass at about one to two eV.

In the second part, chapter 5, the effects of heavy sterile neutrinos on low energy observables is studied. The non-unitarity of the PMNS matrix leads to tree-level effects and via the vacuum polarization also loop effects are taken into account. Therefore, the

contribution of heavy sterile Majorana neutrinos to the self energies of the W and Z bosons have to be calculated. One can then summarize the contributions from tree-level and loops on electroweak observables and perform a χ^2-fit to the data to determine the best fit values for the masses and mixing of the sterile neutrinos. These parameters have to satisfy the constraints from above mentioned processes, like lepton flavor violating decays, double-beta decay and collider physics. The measured mass-squared differences and mixing of the active neutrinos have to be reproduced, too, which is ensured by using the Casas-Ibarra parameterization (see section 5.5.1). The model could explain the anomalous invisible decay width of the Z boson measured at LEP and the NuTeV anomaly, where the ratios of charged to neutral current interactions of (anti)neutrinos with nucleons were measured and did not agree with the SM predictions.

CHAPTER 4

Matter-enhanced Oscillation $\nu_e \leftrightarrow \nu_s$

As seen before in section 3.1.2, there are many hints to the existence of a sterile neutrino with a mass in the eV range and significant mixing to the active neutrinos. Especially the reactor neutrino anomaly motivates an oscillation of electron (anti)neutrinos to a sterile state. We will investigate the possible effects of a sterile neutrino mixing in particular to the electron neutrino on atmospheric neutrinos traversing the Earth. In this case, the mixing can be resonantly enhanced by the MSW effect (see section 3.1.3) for neutrino energies in the TeV range. Such oscillations could be observed by, for example, the IceCube experiment.

There have been studies about possible detection of enhanced $\nu_\mu \leftrightarrow \nu_s$ oscillation in IceCube by Smirnov and Razzaque ([57] and [58]). For the detection of oscillations to a sterile neutrino, the limitations of the IceCube experiment have been analysed to be in general restricted to systematic uncertainties [59]. In [60] a possible detection of oscillations with the best fit values from the global fit of Kopp et al. [37], that was discussed in section 3.1.2, with IceCube data is analysed.

The atmospheric electron neutrino flux after the neutrinos have traversed the Earth is calculated in the following. The existence of a fourth, sterile neutrino ν_s with mixing $U_{\alpha 4}$ to the active neutrinos is assumed, with a mass in the eV range.

4.1 Evolution Equation

To understand the evolution of the system of four neutrino flavors $\alpha = \mathrm{e}, \mu, \tau$ and s, its evolution equation has to be solved. As the sterile neutrino does not interact with the matter of the Earth, its interaction potential V vanishes. The electron neutrino interacts via charged and neutral currents and the muon and tau neutrino only through neutral current interactions. This leads to the following evolution equation

$$i\frac{d}{dx}\begin{pmatrix}\nu_e\\ \nu_\mu\\ \nu_\tau\\ \nu_s\end{pmatrix} = \left[\frac{1}{2E}U\begin{pmatrix}m_1^2 & 0 & 0 & 0\\ 0 & m_2^2 & 0 & 0\\ 0 & 0 & m_3^2 & 0\\ 0 & 0 & 0 & m_4^2\end{pmatrix}U^\dagger + \begin{pmatrix}V_{CC+NC} & 0 & 0 & 0\\ 0 & V_{NC} & 0 & 0\\ 0 & 0 & V_{NC} & 0\\ 0 & 0 & 0 & 0\end{pmatrix}\right]\begin{pmatrix}\nu_e\\ \nu_\mu\\ \nu_\tau\\ \nu_s\end{pmatrix}, \tag{4.1}$$

where V_{CC} and V_{NC}, the charged and neutral current potentials, depend on the matter density and thus on the coordinate x. E is the energy of the neutrinos and m_i are their masses. U describes the mixing between the neutrino flavour eigenstates and is parametrised by

$$U = \begin{pmatrix}U_{e1} & U_{e2} & U_{e3} & U_{e4}\\ U_{\mu 1} & U_{\mu 2} & U_{\mu 3} & U_{\mu 4}\\ U_{\tau 1} & U_{\tau 2} & U_{\tau 3} & U_{\tau 4}\\ U_{s1} & U_{s2} & U_{s3} & U_{s4}\end{pmatrix}. \tag{4.2}$$

The energy of the relativistic neutrinos was already approximated by $E_i \simeq p + m_i^2/2E$ and the term $p \cdot \mathbb{1}$ subtracted by absorbing it in an overall phase of the neutrino state (see section 3.1.1). One can repeat this for the neutral current potential V_{NC} and subtract also $m_1^2 \cdot \mathbb{1}$. This gives:

$$i\frac{d}{dx}\begin{pmatrix}\nu_e\\ \nu_\mu\\ \nu_\tau\\ \nu_s\end{pmatrix} = \left[U\begin{pmatrix}0 & 0 & 0 & 0\\ 0 & \frac{\Delta m_{21}^2}{2E} & 0 & 0\\ 0 & 0 & \frac{\Delta m_{31}^2}{2E} & 0\\ 0 & 0 & 0 & \frac{\Delta m_{41}^2}{2E}\end{pmatrix}U^\dagger + \begin{pmatrix}V_{CC} & 0 & 0 & 0\\ 0 & 0 & 0 & 0\\ 0 & 0 & 0 & 0\\ 0 & 0 & 0 & -V_{NC}\end{pmatrix}\right]\begin{pmatrix}\nu_e\\ \nu_\mu\\ \nu_\tau\\ \nu_s\end{pmatrix}. \tag{4.3}$$

When solving the evolution equation, the terms including the mass-squared differences, $\frac{\Delta m^2}{4E}L$, will enter as phases. At the energies that will be considered (in the TeV range) and as the travelled distance will be about 10^3 kilometers (1m $\approx 5/\mathrm{meV}$), the parameters

$\frac{\Delta m^2_{21}}{4E}L$, $\frac{\Delta m^2_{31}}{4E}L$ are much smaller than one and negligible compared to $\frac{\Delta m^2_{41}}{4E}L$, as they will appear as a very small phase shift ($\Delta m^2_{41} \gg \Delta m^2_{31}, \Delta m^2_{21}$). Therefore we can neglect the first two mass differences and set them to zero, thus obtaining a matrix with only the 44-element nonzero, namely $\frac{\Delta m^2_{41}}{2E}$. One can abbreviate this as:

$$\Delta \equiv \frac{\Delta m^2_{41}}{2E}\,. \tag{4.4}$$

By multiplying out this makes:

$$i\frac{d}{dx}\begin{pmatrix}\nu_e\\ \nu_\mu\\ \nu_\tau\\ \nu_s\end{pmatrix} = \begin{pmatrix} |U_{e4}|^2\Delta + V_{CC} & U_{e4}U^*_{\mu 4}\Delta & U_{e4}U^*_{\tau 4}\Delta & U_{e4}U^*_{s4}\Delta \\ U_{\mu 4}U^*_{e4}\Delta & |U_{\mu 4}|^2\Delta & U_{\mu 4}U^*_{\tau 4}\Delta & U_{\mu 4}U^*_{s4}\Delta \\ U_{\tau 4}U^*_{e4}\Delta & U_{\tau 4}U^*_{\mu 4}\Delta & |U_{\tau 4}|^2\Delta & U_{\tau 4}U^*_{s4}\Delta \\ U_{s4}U^*_{e4}\Delta & U_{s4}U^*_{\mu 4}\Delta & U_{s4}U^*_{\tau 4}\Delta & |U_{s4}|^2\Delta - V_{NC} \end{pmatrix}\begin{pmatrix}\nu_e\\ \nu_\mu\\ \nu_\tau\\ \nu_s\end{pmatrix} \tag{4.5}$$

$$= H(x)\nu(x)\,. \tag{4.6}$$

Note that, as there now is only one mass-squared difference, any phase in the resulting matrix can be absorbed in a redefinition of the neutrino states, so there is no possiblity of CP-violation [61].

The second and third columns and lines contain each $U_\mu^{(*)}$ or $U_\tau^{(*)}$ and a factor, so one can rotate the states ν_μ and ν_τ such that one of the new states decouples.

Define

$$\nu'_\mu = \cos(\beta)\nu_\mu + \sin(\beta)\nu_\tau\,, \tag{4.7}$$

$$\nu'_\tau = \cos(\beta)\nu_\tau - \sin(\beta)\nu_\mu\,. \tag{4.8}$$

This is equivalent to a rotation by the matrix V:

$$V = \begin{pmatrix} 1 & 0 & 0 & 0 \\ 0 & \cos(\beta) & \sin(\beta) & 0 \\ 0 & -\sin(\beta) & \cos(\beta) & 0 \\ 0 & 0 & 0 & 1 \end{pmatrix}\,. \tag{4.9}$$

The evolution equation then becomes

$$i\frac{d}{dx}\boldsymbol{\nu}(x) = H(x)\boldsymbol{\nu}(x) \qquad | \quad V\cdot \tag{4.10}$$

$$i\frac{d}{dx}\boldsymbol{\nu'}(x) = VH(x)V^\dagger\boldsymbol{\nu'}(x) = H'(x)\boldsymbol{\nu'}(x)\,, \tag{4.11}$$

$$\text{where} \qquad \boldsymbol{\nu}'(x) = V\boldsymbol{\nu}(x)\,. \tag{4.12}$$

As explained above, $H(x)$ has the form:

$$H = U \begin{pmatrix} 0 & 0 & 0 & 0 \\ 0 & 0 & 0 & 0 \\ 0 & 0 & 0 & 0 \\ 0 & 0 & 0 & \Delta \end{pmatrix} U^\dagger + \begin{pmatrix} V_{CC} & 0 & 0 & 0 \\ 0 & 0 & 0 & 0 \\ 0 & 0 & 0 & 0 \\ 0 & 0 & 0 & -V_{NC} \end{pmatrix}. \tag{4.13}$$

As the multiplication by V corresponds to a rotation in the 23-plane only, it commutes with the second matrix containing V_{CC} and V_{NC}, so the Hamiltonian becomes

$$H' = (VU) \begin{pmatrix} 0 & 0 & 0 & 0 \\ 0 & 0 & 0 & 0 \\ 0 & 0 & 0 & 0 \\ 0 & 0 & 0 & \Delta \end{pmatrix} (VU)^\dagger + \begin{pmatrix} V_{CC} & 0 & 0 & 0 \\ 0 & 0 & 0 & 0 \\ 0 & 0 & 0 & 0 \\ 0 & 0 & 0 & -V_{NC} \end{pmatrix}. \tag{4.14}$$

One can define a matrix U' that contains the rotation:

$$U' = VU = \begin{pmatrix} U_{e1} & U_{e2} & U_{e3} & U_{e4} \\ U'_{\mu 1} & U'_{\mu 2} & U'_{\mu 3} & U'_{\mu 4} \\ U'_{\tau 1} & U'_{\tau 2} & U'_{\tau 3} & U'_{\tau 4} \\ U_{s1} & U_{s2} & U_{s3} & U_{s4} \end{pmatrix} \tag{4.15}$$

with

$$U'_{\mu i} = U_{\mu i}\cos(\beta) + U_{\tau i}\sin(\beta)\,, \tag{4.16}$$

$$U'_{\tau i} = U_{\tau i}\cos(\beta) - U_{\mu i}\sin(\beta)\,. \tag{4.17}$$

This leads to

$$H' = \begin{pmatrix} |U_{e4}|^2\Delta + V_{CC} & U_{e4}U'^*_{\mu 4}\Delta & U_{e4}U'^*_{\tau 4}\Delta & U_{e4}U^*_{s4}\Delta \\ U'_{\mu 4}U^*_{e4}\Delta & |U'_{\mu 4}|^2\Delta & U'_{\mu 4}U'^*_{\tau 4}\Delta & U'_{\mu 4}U^*_{s4}\Delta \\ U'_{\tau 4}U^*_{e4}\Delta & U'_{\tau 4}U'^*_{\mu 4}\Delta & |U'_{\tau 4}|^2\Delta & U'_{\tau 4}U^*_{s4}\Delta \\ U_{s4}U^*_{e4}\Delta & U_{s4}U'^*_{\mu 4}\Delta & U_{s4}U'^*_{\tau 4}\Delta & |U_{s4}|^2\Delta - V_{NC} \end{pmatrix}. \tag{4.18}$$

Therefore, in order for ν'_τ to decouple from the evolution equation (to obtain only a

three state system that is easier to solve), one has to set

$$U'_{\tau 4} \equiv 0 \tag{4.19}$$

$$\Leftrightarrow \quad \tan(\beta) = \frac{U_{\tau 4}}{U_{\mu 4}}\,. \tag{4.20}$$

Now, the evolution equation involves only a three-state system:

$$i\frac{d}{dx}\begin{pmatrix}\nu_e\\ \nu'_\mu\\ \nu_s\end{pmatrix} = \begin{pmatrix}|U_{e4}|^2\Delta + V_{CC} & U_{e4}U'^*_{\mu 4}\Delta & U_{e4}U^*_{s4}\Delta\\ U'_{\mu 4}U^*_{e4}\Delta & |U'_{\mu 4}|^2\Delta & U'_{\mu 4}U^*_{s4}\Delta\\ U_{s4}U^*_{e4}\Delta & U_{s4}U'^*_{\mu 4}\Delta & |U_{s4}|^2\Delta - V_{NC}\end{pmatrix}\begin{pmatrix}\nu_e\\ \nu'_\mu\\ \nu_s\end{pmatrix} \tag{4.21}$$

$$= \begin{pmatrix}H_{ee} & H_{e\mu'} & H_{es}\\ H^*_{e\mu'} & H_{\mu'\mu'} & H_{\mu' s}\\ H^*_{es} & H^*_{\mu' s} & H_{ss}\end{pmatrix}\begin{pmatrix}\nu_e\\ \nu'_\mu\\ \nu_s\end{pmatrix}\,. \tag{4.22}$$

In the framework of coherent elastic forward scattering, this describes the evolution of the states ν_e, ν'_μ and ν_s, the only approximations being the neglect of the mass-squared differences Δm_{21}, Δm_{31} and the expansion of the energy.

We have a system of three coupled differential equations:

$$i\frac{d}{dx}\nu_e = H_{ee}\nu_e + H_{e\mu'}\nu'_\mu + H_{es}\nu_s\,, \tag{4.23}$$

$$i\frac{d}{dx}\nu'_\mu = H^*_{e\mu'}\nu_e + H_{\mu'\mu'}\nu'_\mu + H_{\mu' s}\nu_s\,, \tag{4.24}$$

$$i\frac{d}{dx}\nu_s = H^*_{es}\nu_e + H^*_{\mu' s}\nu'_\mu + H_{ss}\nu_s\,. \tag{4.25}$$

Since matter-enhanced $\nu_e \leftrightarrow \nu_s$ oscillations shall be considered here, the energy range will be the one where the corresponding resonance condition is fulfilled. In this region the probability of oscillations from muon neutrino (primed) states to electron neutrinos $P(\mu' \to e)$ is small: The resonance condition for $\nu_e \leftrightarrow \nu'_\mu$ is fulfilled at comparatively small energies. Its resonance energy is proportional to $(|U_{\mu' 4}|^2 - |U_{e4}|^2)$, while $\nu_e \leftrightarrow \nu_s$ goes with $(|U_{s4}|^2 - |U_{e4}|^2)$ and $|U_{\mu' 4}|\,, |U_{e4}| \ll |U_{s4}|$. The same argument applies for $\nu_s \leftrightarrow \nu'_\mu$ oscillations, where the resonance condition is even only fulfilled for antineutrinos.

So taking into account that at the relevant energies (in the TeV range) the initial atmospheric muon neutrino flux ($\nu'_\mu = \cos(\beta)\nu_\mu + \sin(\beta)\nu_\tau$) is much larger than the electron neutrino flux (see e.g. [62], the factor is about 20) and the original flux of sterile neutrinos is even zero[1], one can neglect the oscillation of $\nu_{e,s} \to \nu'_\mu$, but not $\nu'_\mu \to \nu_{e,s}$.

[1]Sterile neutrinos are not produced in interactions, only via the oscillations from active neutrinos.

This means that the evolution of ν_μ becomes independent of ν_e and ν_s and can be solved independently:

$$i\frac{d}{dx}\nu'_\mu = |U_{\mu' 4}|^2 \Delta\, \nu'_\mu \tag{4.26}$$

$$\Rightarrow \quad \nu'_\mu(x) = \nu'_\mu(0) e^{-i|U_{\mu' 4}|^2 \Delta \cdot x} \tag{4.27}$$

At the same time one can treat the conversion of $\nu'_\mu \to \nu_{e,s}$ as a source term for $\nu_{e,s}$:

$$i\frac{d}{dx}\begin{pmatrix}\nu_e \\ \nu_s\end{pmatrix} = \begin{pmatrix}H_{ee} & H_{es} \\ H^*_{es} & H_{ss}\end{pmatrix}\begin{pmatrix}\nu_e \\ \nu_s\end{pmatrix} + \begin{pmatrix}f_e \\ f_s\end{pmatrix} \tag{4.28}$$

$$\Leftrightarrow i\frac{d}{dx}\begin{pmatrix}\tilde{\nu}_e \\ \tilde{\nu}_s\end{pmatrix} = \begin{pmatrix}\frac{H_{ee}-H_{ss}}{2} & H_{es} \\ H^*_{es} & \frac{H_{ss}-H_{ee}}{2}\end{pmatrix}\begin{pmatrix}\tilde{\nu}_e \\ \tilde{\nu}_s\end{pmatrix} + e^{(i/2)\int_0^x H_{ee}(x')+H_{ss}(x')dx'}\begin{pmatrix}f_e \\ f_s\end{pmatrix}, \tag{4.29}$$

where

$$f_e = f_e(x) = H_{e\mu'}\nu'_\mu(x)\,, \tag{4.30}$$

$$f_s = f_s(x) = H^*_{\mu' s}\nu'_\mu(x)\,, \tag{4.31}$$

and the tilde marks a phase shift of the states. The Hamiltonian matrix was made traceless by subtracting the trace (a term proportional to the unit matrix only results in an overall phase marked by the tilde). In the following the tilde on the states is neglected, as it is physically irrelevant. For simplicity in notation call

$$\tilde{f}_e = e^{(i/2)\int_0^x H_{ee}(x')+H_{ss}(x')dx'} f_e\,, \tag{4.32}$$

$$\tilde{f}_s = e^{(i/2)\int_0^x H_{ee}(x')+H_{ss}(x')dx'} f_s\,. \tag{4.33}$$

To solve this system of coupled differential equations it is usefull to introduce the evolution matrix $S(x, x_0)$ of the homogeneous evolution equation (omitting the source term $f(x)$).

4.1.1 Evolution Matrix

First some general properties of the evolution matrix are summarised.

One can express the evolution of a state $\nu(x)$ through a matrix S:

$$\nu(x) = S(x, x_0)\nu(x_0)\,. \tag{4.34}$$

Then the evolution of $\nu(x)$,

$$i\frac{d}{dx}\nu(x) = H(x)\nu(x) \tag{4.35}$$

determines the evolution of $S(x, x_0)$:

$$i\frac{d}{dx}S(x, x_0) = H(x)S(x, x_0) \tag{4.36}$$

with the initial condition

$$S(x_0, x_0) = \mathbb{1}\,. \tag{4.37}$$

As the states are normalised, the evolution matrix (S-matrix) must be unitary

$$S(x, x_0)S^\dagger(x, x_0) = S^\dagger(x, x_0)S(x, x_0) = \mathbb{1}\,. \tag{4.38}$$

Additionally, it has to fulfill the following properties:

$$S(x, x_0) = S(x, x_1)S(x_1, x_0) \quad \text{for any } x_1\,, \tag{4.39}$$

$$S(x, x_0) = S^{-1}(x_0, x)\,. \tag{4.40}$$

Differentiating the equation $\nu(x) = S(x, x_0)\nu(x_0)$ with respect to x_0 gives, using equations (4.36) and (4.35):

$$i\frac{d}{dx_0}\nu(x) = i\frac{d}{dx_0}(S(x, x_0)\nu(x_0)) \tag{4.41}$$

$$= \left\{\left(i\frac{d}{dx_0}S(x, x_0)\right) + S(x, x_0)H(x_0)\right\}\nu(x_0)\,. \tag{4.42}$$

Since $i\frac{d}{dx_0}\nu(x) = 0$, it has to follow

$$i\frac{d}{dx_0}S(x, x_0) = -S(x, x_0)H(x_0)\,. \tag{4.43}$$

4.1.2 Solution of the Evolution Equation

To obtain the evolution of the simplified system of two flavors developed before (compare equation (4.29)), the inhomogeneous differential equation has to be solved

$$i\frac{d}{dx}\nu(x) = H(x)\nu(x) + \tilde{f}(x) \tag{4.44}$$

$$\Leftrightarrow \quad i\frac{d}{dx}\begin{pmatrix}\nu_e\\ \nu_s\end{pmatrix} = \begin{pmatrix}\frac{H_{ee}-H_{ss}}{2} & H_{es}\\ H_{es}^* & \frac{H_{ss}-H_{ee}}{2}\end{pmatrix}\begin{pmatrix}\nu_e\\ \nu_s\end{pmatrix} + \begin{pmatrix}\tilde{f}_e\\ \tilde{f}_s\end{pmatrix} . \tag{4.45}$$

The homogeneous equation with its solution ν_0

$$i\frac{d}{dx}\nu_0(x) = H(x)\nu_0(x) \tag{4.46}$$

is solved by the evolution matrix we introduced above

$$\nu_0(x) = S(x, x_0)\nu_0(x_0)\,. \tag{4.47}$$

The evolution matrix can be obtained by numerical integration of its differential equation.

Then one has to solve the full equation including the source term:

$$i\frac{d}{dx}\nu(x) = H(x)\nu(x) + \tilde{f}(x)\,. \tag{4.48}$$

The solution $\nu(x)$ is a superposition of the solutions of the homogeneous ($\nu_0(x)$) and the inhomogeneous equation ($\nu_1(x)$)

$$\nu(x) = \nu_0(x) + \nu_1(x)\,. \tag{4.49}$$

This means that a solution of the inhomogeneous equation has to be found

$$i\frac{d}{dx}\nu_1(x) = H(x)\nu_1(x) + \tilde{f}(x)\,. \tag{4.50}$$

One can make the ansatz (taking $x_0 = 0$)

$$\nu_1(x) = S(x, 0)g(x) \tag{4.51}$$

where $S(x, 0)$ is the evolution matrix of the homogeneous equation and the function $g(x)$ has to be determined in the following. Equation (4.50) gives

$$i\frac{d}{dx}\nu_1(x) = i\left\{\left(\frac{d}{dx}S(x,0)\right)\cdot g(x) + S(x,0)\cdot\frac{d}{dx}g(x)\right\} \tag{4.52}$$

$$= H(x)S(x,0)g(x) + \tilde{f}(x) \tag{4.53}$$

$$\Leftrightarrow \qquad i\frac{d}{dx}g(x) = S^{-1}(x,0)\cdot\tilde{f}(x) \tag{4.54}$$

$$= S(0,x)\cdot\tilde{f}(x)\,. \tag{4.55}$$

From the second to the third line the property

$$i\frac{d}{dx}S(x,x_0) = H(x)S(x,x_0)$$

was used and S^{-1} was multiplied from the left.

$g(x)$ then becomes

$$g(x) = -i\int_0^x S(0,x')\tilde{f}(x')dx' \tag{4.56}$$

$$= -i\int_0^x \begin{pmatrix} S_{ee}(0,x') & S_{es}(0,x') \\ S_{se}(0,x') & S_{ss}(0,x') \end{pmatrix} \begin{pmatrix} \tilde{f}_e(x') \\ \tilde{f}_s(x') \end{pmatrix} dx' \,, \tag{4.57}$$

where

$$\tilde{f}_e = \tilde{f}_e(x') = H_{e\mu'}\,\nu'_\mu(0)\,e^{(i/2)\int_0^{x'}(H_{ee}(y)+H_{ss}(y)-2H_{\mu'\mu'})dy}\,, \tag{4.58}$$

$$\tilde{f}_s = \tilde{f}_s(x') = H_{\mu' s}\,\nu'_\mu(0)\,e^{(i/2)\int_0^{x'}(H_{ee}(y)+H_{ss}(y)-2H_{\mu'\mu'})dy}\,. \tag{4.59}$$

This gives for ν_1

$$\nu_1(x) = S(x,0)g(x) \tag{4.60}$$

$$= -iS(x,0)\int_0^x S(0,x')\tilde{f}(x')dx' \tag{4.61}$$

$$= -i\int_0^x S(x,x')\tilde{f}(x')dx'\,. \tag{4.62}$$

The full solution for the evolution equation then is

$$\nu(x) = \nu_0(x) + \nu_1(x) \tag{4.63}$$

$$= S(x,0)\nu(0) - i\int_0^x S(x,x')\tilde{f}(x')dx'\,, \tag{4.64}$$

where one can identify $\nu_0(0) = \nu(0)$, as $\nu_1(0) = 0$.

Note that when calculating the flux of the electron (or sterile) neutrinos the two parts of the solution do not add up coherently, as ν_1 describes the conversion of muon to electron (sterile) neutrinos and they are not produced coherently. The flux $\Phi_{e(s)}$ of electron or sterile neutrinos, which is proportional to $|\nu(x)|^2$ is thus:

$$\Phi_{e(s)} \propto |\nu_0(x)_{e(s)}|^2 + |\nu_1(x)_{e(s)}|^2\,, \tag{4.65}$$

where the index e indicates to take the first entry of the two-vector, s taking the second:

$$\nu = \begin{pmatrix} \nu_e \\ \nu_s \end{pmatrix} \tag{4.66}$$

as the first (second) entry corresponds to the electron (sterile) neutrino component of ν_1 and ν_0.

As explained in the beginning, the oscillation of atmospheric neutrinos crossing the Earth shall be considered here, as these oscillations can be resonantly enhanced and a deficit of electron neutrinos due to a new mass state that consist mainly of the sterile state at about one to two eV could be detected. One therefore has to calculate the length of the trajectories of the neutrinos through the Earth. The geometry of the Earth will be approximated by dividing it into a core and a mantle with a constant density profile in each region.

4.2 Solution for a Three-Layer Model of the Earth

4.2.1 Geometry

The density profile of the Earth can be approximated by dividing it into two regions, a core and a mantle, in which the densities vary only little (see e.g. the PREM Earth model [63]). Therefore, the neutrino trajectory traverses three layers: mantle, core and then mantle again (provided the angle ϕ_N is small enough).

The length of the total passage of the neutrinos through the Earth (L) is given by the length of a chord, where the angle of the trajectory is parametrized by the Nadir angle φ_N, as shown in figure 4.1. With R_E being the radius of the Earth, this makes:

$$L = 2R_E \cos(\varphi_N)\,. \tag{4.67}$$

The paths through the different layers for the core (l) and mantle (s) are given by the law of cosines, compare figure 4.1:

$$s = R_E \cos(\varphi_N) - \sqrt{(R_E \cos(\varphi_N))^2 - (R_E^2 - R_1^2)}\,, \tag{4.68}$$

$$l = 2\sqrt{(R_E \cos(\varphi_N))^2 - (R_E^2 - R_1^2)}\,, \tag{4.69}$$

where R_1 is the radius of the core. The neutrino-trajectory crosses the three layers, if the Nadir angle is smaller than $\varphi_N < \arcsin(R_1/R_e)$. Otherwise, it only crosses the mantle at a length given by L.

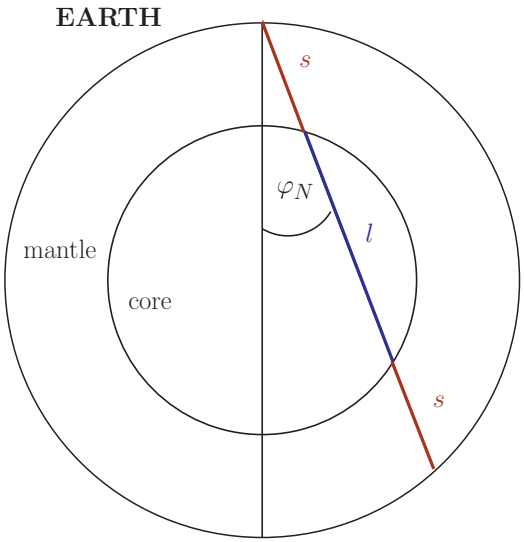

Figure 4.1: Trajectories through mantle (s) and core (l) of the Earth at Nadir angle φ_N

4.2.2 Solving the Two-Flavor System for a constant-Density Profile

First, the homogeneous equation for the evolution matrix in matter with constant density will be solved, meaning one drops the source term in (4.29). Then one can change to the eigensystem, diagonalising the Hamiltonian

$$H = \begin{pmatrix} \frac{H_{ee}-H_{ss}}{2} & H_{es} \\ H_{es}^* & \frac{H_{ss}-H_{ee}}{2} \end{pmatrix} . \tag{4.70}$$

Assuming $H_{es}^* = H_{es}$ (since only one mass-squared difference is considered, this is always possible, as there are no physical CP-violating phases) and taking the diagonalising matrix to be

$$W(\theta) = \begin{pmatrix} \cos(\theta) & \sin(\theta) \\ -\sin(\theta) & \cos(\theta) \end{pmatrix} . \tag{4.71}$$

Then, the mixing angle θ is then given by

$$\tan(2\theta) = \frac{2H_{es}}{H_{ss} - H_{ee}} , \tag{4.72}$$

while the eigenvalues $\Omega_{1,2}$ of the Hamiltonian are

$$\Omega_{1,2} = \pm\Omega , \tag{4.73}$$

$$\Omega = \frac{1}{2}\sqrt{(H_{ee} - H_{ss})^2 + 4H_{es}^2}\,, \tag{4.74}$$

$$W^\dagger H W = \begin{pmatrix} -\Omega & 0 \\ 0 & +\Omega \end{pmatrix} = H^d\,. \tag{4.75}$$

The evolution matrix is then given by (compare equation (3.10) in section 3.1.1):

$$S(x, x_0) = W e^{-iH^d(x-x_0)} W^\dagger = W \begin{pmatrix} e^{i\Omega\cdot(x-x_0)} & 0 \\ 0 & e^{-i\Omega\cdot(x-x_0)} \end{pmatrix} W^\dagger \tag{4.76}$$

$$= \begin{pmatrix} c_\theta^2 e^{i\Omega\cdot(x-x_0)} + s_\theta^2 e^{-i\Omega\cdot(x-x_0)} & -c_\theta s_\theta \left(e^{i\Omega\cdot(x-x_0)} - e^{-i\Omega\cdot(x-x_0)}\right) \\ -c_\theta s_\theta \left(e^{i\Omega\cdot(x-x_0)} - e^{-i\Omega\cdot(x-x_0)}\right) & s_\theta^2 e^{i\Omega\cdot(x-x_0)} + c_\theta^2 e^{-i\Omega\cdot(x-x_0)} \end{pmatrix} \tag{4.77}$$

$$= \begin{pmatrix} c_\phi + i c_{2\theta} s_\phi & -i s_{2\theta} s_\phi \\ -i s_{2\theta} s_\phi & c_\phi - i c_{2\theta} s_\phi \end{pmatrix}, \tag{4.78}$$

with the abbreviations

$$c_\theta = \cos(\theta)\,, \quad s_\theta = \sin(\theta)\,, \tag{4.79}$$

$$c_{2\theta} = \cos(2\theta)\,, \quad s_{2\theta} = \sin(2\theta)\,, \tag{4.80}$$

$$c_\phi = \cos(\phi)\,, \quad s_\phi = \sin(\phi)\,, \tag{4.81}$$

$$\phi = \Omega \cdot (x - x_0)\,. \tag{4.82}$$

The solution of the inhomogeneous equation was given by (see equation (4.62))

$$\nu_1(x) = -i \int_0^x S(x, x') \tilde{f}(x') dx'\,, \tag{4.83}$$

where $S(x, x')$ is the S-matrix solving the homogeneous equation obtained above. For matter of constant density one can also solve the integral in the source term $\tilde{f}$ analytically (see appendix A).

The three-layer solution of ν_0 and ν_1 is given in the appendix A.

4.2.3 Three-Flavor Solution

In order to quantify the approximation in treating the muon neutrino flux as a source term and neglecting the contributions from the conversions of electron and sterile neutrinos to muon neutrinos, one has to solve the three-flavor system numerically and compare the outcome graphically.

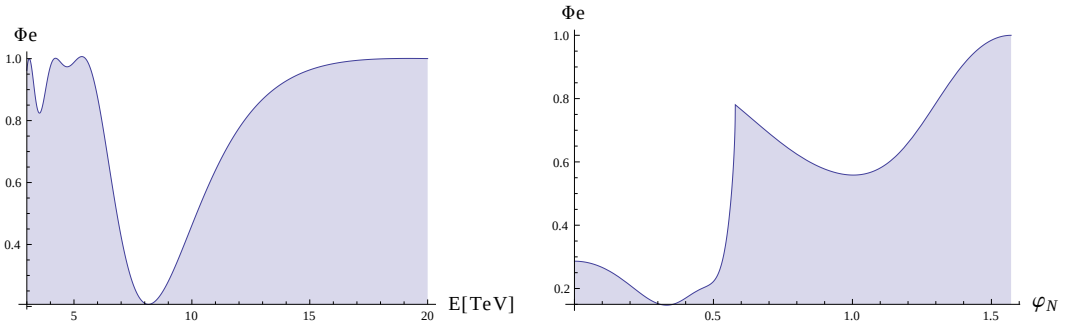

(a) Φ_e as a function of energy E at Nadir angle $\varphi_N = 0.2$

(b) Φ_e as a function of Nadir angle φ_N at energy $E = 8$ TeV

Figure 4.2: Electron neutrino flux varying the energy or the Nadir angle. $\Delta m^2_{41} = 2.5$ eV^2, $U_{\mu 4} = 0.1$ and $U_{e4} = 0.2$, for values of the other parameters used in the calculation, see table 4.1.

The system of equations (before the two-flavor approximation) is

$$i\frac{d}{dx}\begin{pmatrix}\nu_e\\ \nu'_\mu\\ \nu_s\end{pmatrix} = \begin{pmatrix}|U_{e4}|^2\Delta + V_{CC} & U_{e4}U'^*_{\mu 4}\Delta & U_{e4}U^*_{s4}\Delta\\ U'_{\mu 4}U^*_{e4}\Delta & |U'_{\mu 4}|^2\Delta & U'_{\mu 4}U^*_{s4}\Delta\\ U_{s4}U^*_{e4}\Delta & U_{s4}U'^*_{\mu 4}\Delta & |U_{s4}|^2\Delta - V_{NC}\end{pmatrix}\begin{pmatrix}\nu_e\\ \nu'_\mu\\ \nu_s\end{pmatrix} \tag{4.84}$$

$$= \begin{pmatrix}H_{ee} & H_{e\mu'} & H_{es}\\ H^*_{e\mu'} & H_{\mu'\mu'} & H_{\mu' s}\\ H^*_{es} & H^*_{\mu' s} & H_{ss}\end{pmatrix}\begin{pmatrix}\nu_e\\ \nu'_\mu\\ \nu_s\end{pmatrix}\,. \tag{4.85}$$

In matter with constant density the S-matrix is obtained by diagonalising the Hamiltonian (H^d being diagonal). When W is the matrix diagonalising H:

$$H^d = W^\dagger H W\,, \tag{4.86}$$

then the S-matrix is given by

$$S(x - x_0) = W e^{-iH^d(x-x_0)} W^\dagger\,, \tag{4.87}$$

As the elements of H depend on the energy and the density of the medium[2], the S-matrix differs for each layer. The electron neutrino flux entering the Earth is normalized to one and thus the muon neutrino flux becomes 20. The parameter values of the Earth and the entering neutrino flux are kept constant througout this work, see table 4.1. The plots are always shown in pairs of two, were the same values of model-parameters (mixing

[2]The density dependence enters with the potentials V_{NC} and V_{CC}, Δ carries the energy dependence.

and mass-squared difference) are used and the flux is plotted against energy and Nadir angle, as these are the two variables a detector could resolve. As the intention of this work is to study an enhanced $\nu_e \to \nu_s$ transition, only the electron neutrino flux Φ_e is considered.

In figure 4.2a the electron neutrino flux is plotted against the energy of the neutrinos in the TeV range, where the resonance can be expected, at a fixed Nadir angle of $\varphi_N = 0.2$. In this case, the trajectory crosses the core. One can see a resonant transition, missing electron neutrinos, at an energy of about 8 TeV. Therefore, in figure 4.2b the electron neutrino flux is plotted against the Nadir angle at a fixed neutrino energy of 8 TeV. At $\varphi_N \approx 0.58$ the trajectory no longer crosses the core of the Earth and the curve changes drastically. The electron neutrino deficit is much stronger for trajectories crossing the core, than for the ones that only cross the mantle.

Variable	Value
Δm^2_{41}	$2.5 \,/\, 2 \,/\, 1\,\mathrm{eV}^2$
U_{e4}	$0.2 \,/\, 0.1 \,/\, 0.05$
$U_{\mu 4}$	$0.1 \,/\, 0.15$
$U_{\tau 4}$	0
ρ_m	$4.5 \frac{g}{cm^3}$
ρ_c	$11.5 \frac{g}{cm^3}$
Y_{em}	0.49
Y_{ec}	0.467
R_E	$6371 \cdot 0.506842 \cdot 10^{10}$ eV
R_1	$3484 \cdot 0.506842 \cdot 10^{10}$ eV
$\nu_e(0)$	1
$\nu_s(0)$	0
$\nu_\mu(0)$	$\sqrt{20}$

Table 4.1: Values of the parameters used in the simulation of the oscillations for two and three flavors, index m for mantle, c for core.

4.2.4 Comparing the Two- and Three-Flavor Solutions

To solve the system of differential equations analytically, an approximation had to be made: The muon neutrino flux was treated as a source term for the electron and sterile neutrinos and oscillations from electron or sterile neutrinos to muon neutrinos were neglected. This approximation should be valid, as the muon neutrino flux in the TeV range is much higher than the electron neutrino flux and sterile neutrinos are not produced

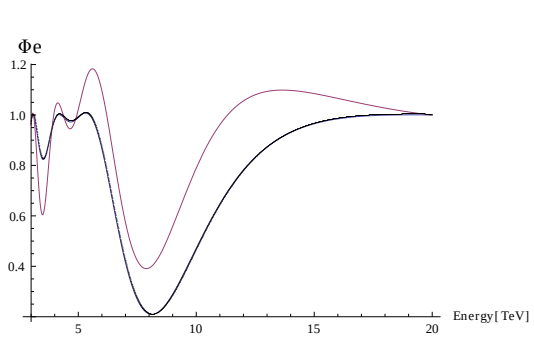

(a) Φ_e as a function of energy E at Nadir angle $\varphi_N = 0.2$, $U_{\mu 4} = 0.1$

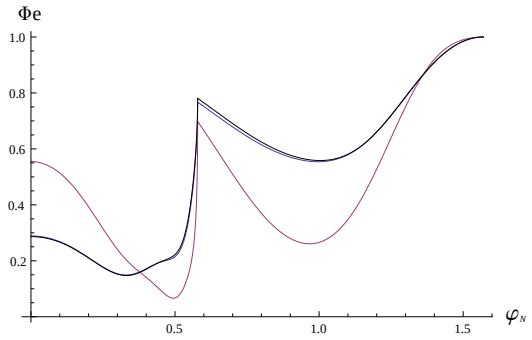

(b) Φ_e as a function of Nadir angle φ_N at energy $E = 8$ TeV, $U_{\mu 4} = 0.1$

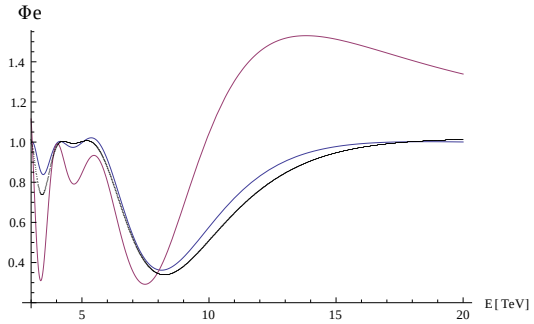

(c) Φ_e as a function of energy E at Nadir angle $\varphi_N = 0.4$, $U_{\mu 4} = 0.15$

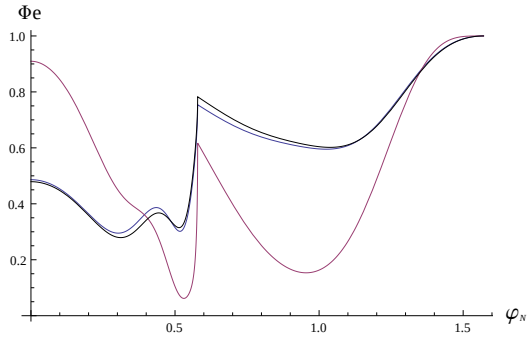

(d) Φ_e as a function of Nadir angle φ_N at energy $E = 8$ TeV, $U_{\mu 4} = 0.15$

Figure 4.3: Electron neutrino flux with $\Delta m^2_{41} = 2.5$ eV^2 and $U_{e4} = 0.2$. The black curve is the three-flavor numerical calculation, the blue and red curves are the two-flavor analytical calculation. (Note that the blue curve almost disappears behind the black one.)

in the interactions. Then the evolution equation of the muon neutrinos could be solved separately and one had to solve an inhomogeneous system of two coupled differential equations, for the electron and sterile neutrinos. Compare section 4.1. To check this approach the two-flavor solution will be compared to the three-flavor one. The parameter values are again given in table 4.1. It is to be expected that the approximation is valid only for small mixing to the fourth neutrino state, as this is the transition that has been neglected.

Figures 4.3a and 4.3b show that the approximation works very well for a mixing of the muon neutrino with the fourth mass eigenstate of $U_{\mu 4} = 0.1$; the black (three-flavor) and blue curve (two-flavor) almost coincide. The red curve shows the two flavor approximation when taking the solution of the homogeneous and inhomogeneous equation to be coherent. This ansatz is not correct, as already discussed before in section 4.1.2, which is confirmed by the figure 4.3.

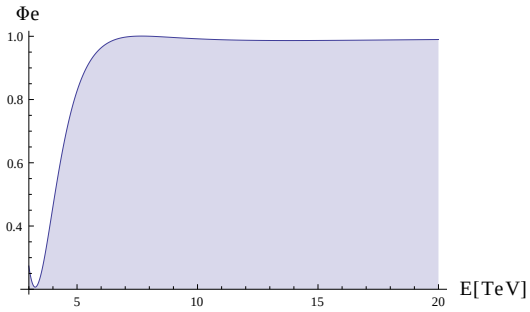

(a) Φ_e as a function of energy E at $\varphi_N = 0.2$, $\Delta m^2_{41} = 1$ eV^2

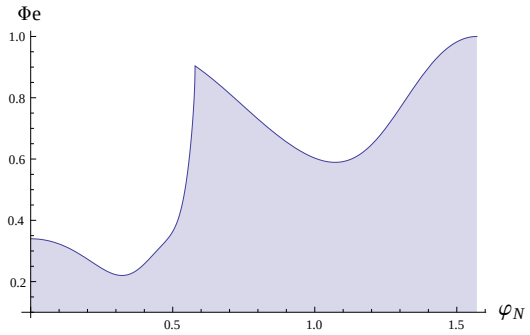

(b) Φ_e as a function of Nadir angle φ_N at $E = 3$ TeV, $\Delta m^2_{41} = 1$ eV^2

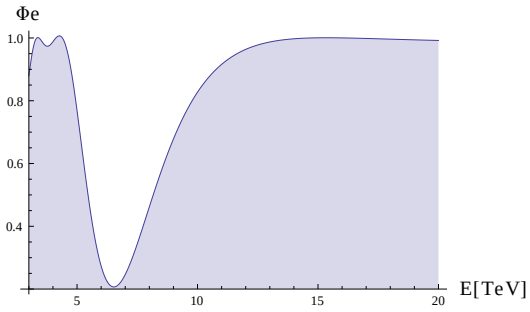

(c) Φ_e as a function of energy E at $\varphi_N = 0.2$, $\Delta m^2_{41} = 2$ eV^2

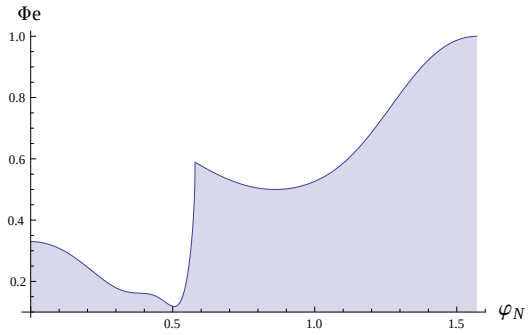

(d) Φ_e as a function of Nadir angle φ_N at $E = 7$ TeV, $\Delta m^2_{41} = 2$ eV^2

Figure 4.4: Electron neutrino flux varying the parameter Δm^2_{41}, which is taken to be 1 and 2 eV^2 respectively. ($U_{\mu 4} = 0.1$ and $U_{e4} = 0.2$, as before.)

When the mixing becomes larger, $U_{\mu 4} = 0.15$, the black and blue curves move apart, see figures 4.3c and 4.3d. For the approximation to two flavors to be valid, a small mixing of the muon neutrino with the fourth mass eigenstate has to be assumed.

4.2.5 Parameter Dependence of the Three-Flavor System

To see how the analysis depends on the parameters of the model, its most important parameters are varied here: the mass-squared difference Δm^2_{41} and the mixing of the electron to the fourth mass eigenstate, U_{e4}. This will be done for the three-flavor system.

Varying the mass-squared difference Δm^2_{41} one can see that at higher Δm^2_{41} the minimum in the electron neutrino flux Φ_e shifts to higher energies, compare figures 4.2 and 4.4. For $\Delta m^2_{41} = 1$ eV^2 the minimum is at about 3 TeV, for $\Delta m^2_{41} = 2$ eV^2 at about 6.5 TeV and for $\Delta m^2_{41} = 2.5$ eV^2 at about 8 TeV.

Varying the mixing parameter U_{e4}, the deficit in the electron neutrino flux decreases with a smaller the mixing: In figures 4.2 and 4.5 one can see that for a mixing of

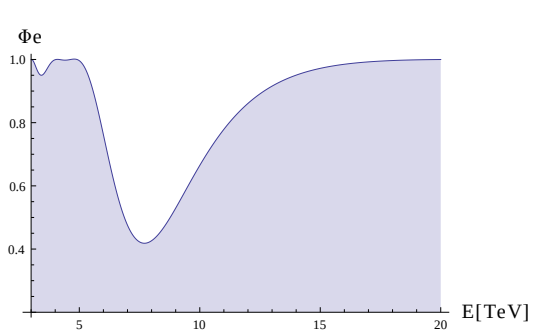

(a) Φ_e as a function of energy E at $\varphi_N = 0.2$, $U_{e4} = 0.1$

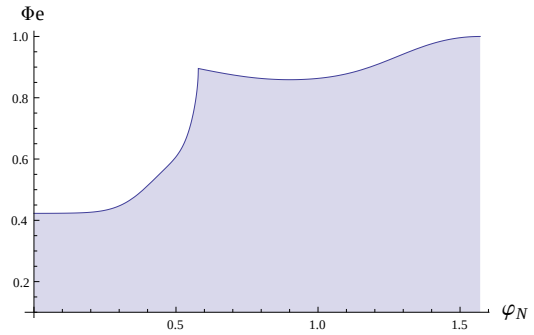

(b) Φ_e as a function of Nadir angle φ_N at $E = 8$ TeV, $U_{e4} = 0.1$

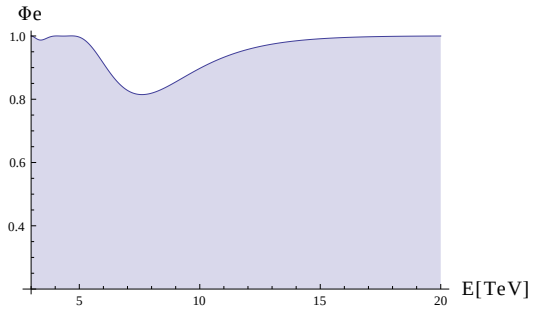

(c) Φ_e as a function of energy E at $\varphi_N = 0.2$, $U_{e4} = 0.05$

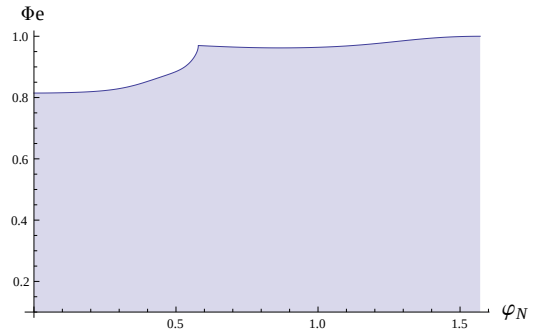

(d) Φ_e as a function of Nadir angle φ_N at $E = 8$ TeV, $U_{e4} = 0.05$

Figure 4.5: Electron neutrino flux varying the parameter U_{e4}, which is taken to be 0.1 and 0.05 respectively. ($U_{\mu 4} = 0.1$ and $\Delta m^2_{41} = 2.5$ eV^2, as before.)

$U_{e4} = 0.05$ the minimum is at only about 80% of the incoming electron neutrino flux, while it went down to 20% for $U_{e4} = 0.2$. Detecting the sterile neutrino via missing electron neutrino flux becomes more difficult, the smaller its mixing with the active neutrinos.

In this chapter the oscillation of the four-flavor system of the three active neutrinos with one sterile state has been studied. A matter background was parametrized by the charged and neutral current potentials in the framework of coherent elastic forward scattering. The system could be simplified to three flavors by rotating the muon and tau neutrino states. Atmospheric neutrinos were considered to traverse the Earth to enable a resonant enhancement of the transition of $\nu_e \to \nu_s$. Experiments such as the reactor anomaly and source experiments have motivated an oscillation of electron to sterile neutrinos at a mass-squared difference of a few eV^2. Therefore this work studies the possibility of an enhancement of exactly this transition by the interaction of neutrinos with matter.

It has been shown that the oscillation of electron to sterile neutrinos can be resonantly enhanced at neutrino energies of a few TeV, when traversing the Earth. The deficit of electron neutrinos can be as large as 80% of the original flux for a relatively large mixing with the fourth neutrino $U_{e4} = 0.2$. The oscillation is more difficult to observe the smaller this mixing, but the resonance is only shifted, when a different mass-squared difference is assumed. The direction to look for the deficit will be at small Nadir angle, when the trajectory of the neutrinos crosses the highly dense core of the Earth.

At resonably small mixing of the muon neutrino with the fourth state $U_{\mu 4}$ of about 0.1 the three-flavor system can be approximated to a two-flavor system that can be solved analytically. One can then treat the muon neutrino flux as a source term for the sterile and electron neutrino.

CHAPTER 5

Sterile Neutrinos above the Electroweak Scale

In the sections 3.2 and 3.6 the effects of heavy sterile neutrinos on the weak interactions were described. Depending on the masses of the sterile neutrinos and their mixing to the active ones, sterile neutrinos could notably influence electroweak precision measurements (the parameters of the weak interaction are known to a very high precision). In this chapter the effect of sterile neutrinos that are heavier than the Z boson on low energy observables will be calculated. These sterile states cannot be produced in the interaction, therefore leading to non-unitarity effects. They also alter the self-energies of the W and Z boson via loop diagrams, which is represented in the oblique corrections. The deviations from the SM predictions will be calculated in detail for two observables, namely the invisible decay width of the Z boson and the ratios of neutral to charged current events for neutrino–nucleon scattering. These observables are chosen because there have been experiments that found a deviation of the measured values compared to the expectations from the SM. This could be explained by the existence of heavy sterile neutrinos.

The experiments will now be introduced and the possible contribution of heavy sterile neutrinos will be calculated later, see sections 5.2 and 5.3. In section 5.1 the arising corrections to the SM parameters will be introduced, followed by the calculation for the two observables mentioned above. The constraints from other experiments are then quoted in section 5.4. The sterile neutrinos generate masses for the active neutrinos,

and thereby also their mixing, which is observed in neutrino oscillation experiments (see section 5.5). Finally, in section 5.6, all the contributions are collected, so that a χ^2-fit can be performed. It can reveal whether the introduction of heavy sterile neutrinos does lead to a better explanation of the measured parameters than the SM itself.

The LEP experiment tested the Standard Model with e^+e^- collisions, for collected results see [64]. The Z decay width was thouroughly measured and the decays into invisible channels determined. The measured ratio of invisible to leptonic decay width was

$$\frac{\Gamma_{inv}}{\Gamma_{ll}} = 5.942 \pm 0.016\,. \tag{5.1}$$

The SM prediction for the ratio of the partial decay width into neutrinos and charged leptons is (for one neutrino species)

$$\left(\frac{\Gamma_{\nu\nu}}{\Gamma_{ll}}\right)_{SM} = 1.9912 \pm 0.0012\,, \tag{5.2}$$

where $M_Z = 91.1875$ GeV and the error comes from the uncertainties in the top mass $m_t = 174.3 \pm 5.1$ GeV and the Higgs mass: 100 GeV $\leq m_H \leq$ 1000 GeV. This gives the number of neutrino species (being the ratio of these two values)

$$N_\nu = 2.9841 \pm 0.0083\,, \tag{5.3}$$

which is two sigma below the SM expected value of 3.

Introducing sterile neutrinos with masses higher than the one of the Z boson can effectively reduce the value of neutrino species in the invisible Z decay width, as will be demonstrated below. Since the mixing of active and sterile neutrinos also affects the coupling of the W and Z bosons, sterile neutrinos also affect the NuTeV experiment and could possibly explain the so called NuTeV anomaly.

In the NuTeV experiment [65] the ratios of NC to CC cross sections have been measured for neutrino and antineutrino scattering on nucleons, where N denotes the nucleons and X the scattering products:

$$R^\nu = \frac{\sigma(\nu N \to \nu X)}{\sigma(\nu N \to l^- X)} = (g_L^2 + r g_R^2)\,, \tag{5.4}$$

$$R^{\bar\nu} = \frac{\sigma(\bar\nu N \to \bar\nu X)}{\sigma(\bar\nu N \to l^+ X)} = (g_L^2 + r^{-1} g_R^2)\,, \tag{5.5}$$

where

$$r = \frac{\sigma(\bar{\nu}N \to l^+X)}{\sigma(\nu N \to l^-X)} \simeq \frac{1}{2}\,. \tag{5.6}$$

As the measurements were carried out with muon neutrinos, CC events were distinguished from NC events by their length: Muons are produced in CC events and thus create much longer tracks. The ratios of short to long events were measured to be

$$R^{\nu}_{exp} = 0.3916 \pm 0.0007\,, \tag{5.7}$$
$$R^{\bar{\nu}}_{exp} = 0.4050 \pm 0.0016\,. \tag{5.8}$$

When fitting the isoscalar combinations of effective[1] neutral current quark couplings $g^{\text{eff}}_{L,R}$ to R^{ν} and $R^{\bar{\nu}}$, $(g^{\text{eff}}_L)^2$ is 3 sigma below the SM prediction:

$$(g^{\text{eff}}_L)^2 = 0.30005 \pm 0.00137\,, \qquad (g^{\text{eff}}_L)^2_{SM} = 0.3042\,, \tag{5.9}$$
$$(g^{\text{eff}}_R)^2 = 0.03076 \pm 0.00110\,, \qquad (g^{\text{eff}}_L)^2_{SM} = 0.0301\,. \tag{5.10}$$

This discrepancy arises because both ratios R^{ν} and $R^{\bar{\nu}}$ were smaller than expected, meaning the NC events seemed suppressed compared to CC events.

A sterile neutrino that mixes with the active ones by ϵ would lead to a suppression of $(1-\epsilon^2)$ in the $Z\nu_l\nu_l$ coupling and only of $(1-\epsilon^2/2)$ in $Wl\nu_l$, which would explain the suppression of the ratios.

The effect of sterile neutrinos on the phenomenology of the two experiments will be described in more detail in sections 5.2 and 5.3.

5.1 Corrections to SM Parameters

The existence of sterile neutrinos affects various electroweak SM observables. When they involve neutrinos in their measurements, the corrections arise at tree-level, otherwise the electroweak parameters are only changed through the vacuum polarization effects, meaning the oblique corrections, that change the self-energies of the W and Z bosons. The model including these heavy sterile neutrinos can be compared to the SM by performing a χ^2-fit. Therefore the "SM predictions" have to be calculated. This is done by choosing well measured input parameters, usually the electromagnetic coupling constant α_{em}, the Fermi constant G_F, the strong coupling constant α_s, the Z boson mass M_Z and the

[1] Effective couplings meaning those who describe the experimentally observed ones, when the neutral current processes are calculated without electromagnetic radiative corrections.

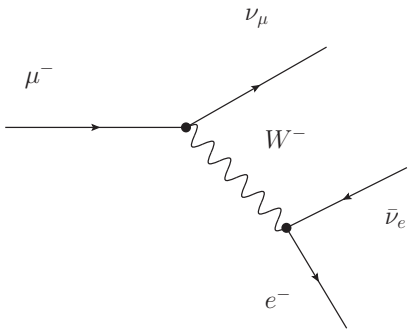

Figure 5.1: Feynman diagram of the muon decay

fermion masses m_f. The parameters that will influence the weak interactions are α_{em}, M_Z and G_F. The first two remain unaltered by the intoduction of sterile neutrinos. G_F however is determined from the muon lifetime in the decay $\mu \to e\bar{\nu}_e\nu_\mu$ and will be corrected by non-unitarity effects, as already mentioned in section 3.2. The process is shown in figure 5.1. This means that in the model including sterile neutrinos the value measured in the muon decay G_μ is different from the Fermi constant G_F:

$$G_F = \frac{G_\mu}{\sqrt{(U^P U^{P\dagger})_{ee}(U^P U^{P\dagger})_{\mu\mu}}} \approx G_\mu \left(1 + \frac{\varepsilon_e^2 + \varepsilon_\mu^2}{2}\right), \tag{5.11}$$

where the parameter ε_α is defined as

$$\varepsilon_e^2 = |U_{e4}|^2, \quad \varepsilon_\mu^2 = |U_{\mu 4}|^2, \quad \varepsilon_\tau^2 = |U_{\tau 4}|^2. \tag{5.12}$$

When there are more sterile neutrinos, say n_R, this changes to

$$\varepsilon_\alpha^2 = \sum_{i=4}^{n_R} |U_{\alpha i}|^2. \tag{5.13}$$

These parameters are a measure of the non-unitarity of the PMNS matrix:

$$(U^P U^{P\dagger})_{\alpha\alpha} = 1 - \varepsilon_\alpha^2. \tag{5.14}$$

The sum of the ε_α^2 is defined as

$$\varepsilon^2 = \sum_{\alpha=e,\mu,\tau} \varepsilon_\alpha^2 = \sum_{\alpha=e,\mu,\tau} |U_{\alpha 4}|^2 = \sum_{i=1}^{3} |U_{si}|^2 = 1 - |U_{s4}|^2, \tag{5.15}$$

where from the second equality on, this is only valid for one sterile neutrino.

All SM parameters that are calculated from G_F then have to be corrected by this factor coming from the non-unitarity of the PMNS matrix.

The observables of processes with neutrinos also get additional corrections. The invisible Z decay width has to be corrected by approximately

$$\Gamma_{inv} \approx (\Gamma_{inv})_{SM} \, (1 - \frac{2}{3}\varepsilon^2) \tag{5.16}$$

and the NuTeV observables, the neutral current quark couplings g_L^2 and g_R^2, get additionally corrected by a factor

$$g_{L,R}^2 = \left(g_{L,R}^2\right)_{SM} \cdot (1 - \varepsilon_\mu^2) \,, \tag{5.17}$$

as will be shown in the sections 5.2 and 5.3.

The contributions of the heavy sterile neutrino(s) to the oblique parameters S, T and U are also included in the considered corrections. See the next section 5.1.1 for results. The relation of the oblique parameters to the electroweak observables can be found in [66] and one can summarize tree-level and loop corrections to (compare [67]):

$$\frac{\Gamma_{lept}}{[\Gamma_{lept}]_{SM}} = 1 - 0.0021\, S + 0.0093\, T + 0.60\, \varepsilon_e^2 + 0.60\, \varepsilon_\mu^2 \,, \tag{5.18}$$

$$\frac{\Gamma_{inv}/\Gamma_{lept}}{[\Gamma_{inv}/\Gamma_{lept}]_{SM}} = 1 + 0.0021\, S - 0.0015\, T - 0.67\, \varepsilon_e^2 - 0.67\, \varepsilon_\mu^2 - 0.67\, \varepsilon_\tau^2 \,, \tag{5.19}$$

$$\frac{\sin^2(\theta_{eff}^{lept})}{[\sin^2(\theta_{eff}^{lept})]_{SM}} = 1 + 0.016\, S - 0.011\, T - 0.72\, \varepsilon_e^2 - 0.72\, \varepsilon_\mu^2 \,, \tag{5.20}$$

$$\frac{g_L^2}{[g_L^2]_{SM}} = 1 - 0.0090\, S + 0.022\, T + 0.41\, \varepsilon_e^2 - 0.59\, \varepsilon_\mu^2 \,, \tag{5.21}$$

$$\frac{g_R^2}{[g_R^2]_{SM}} = 1 + 0.031\, S - 0.0067\, T - 1.4\, \varepsilon_e^2 - 2.4\, \varepsilon_\mu^2 \,, \tag{5.22}$$

$$\frac{M_W}{[M_W]_{SM}} = 1 - 0.0036\, S + 0.0056\, T + 0.0042\, U + 0.11\, \varepsilon_e^2 + 0.11\, \varepsilon_\mu^2 \,, \tag{5.23}$$

where θ_{eff}^{lept} is the lepton effective Weinberg angle, effective meaning that all processes are calculated without radiative corrections and then fitted to the experimental results.

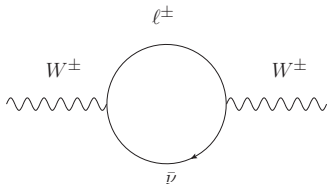

Figure 5.2: Contribution of neutrinos to the W boson self-energy.

5.1.1 Oblique Corrections from Sterile Majorana Neutrinos

In section 3.6 the oblique corrections were introduced. Their connection to the SM observables was described in the previous section 5.1. Here, the contribution to the self energies of the neutrinos and charged leptons are quoted, as well as the resulting parameters S, T and U. For details on the calculation, see [68].

The W boson self energy, see figure 5.2, is given by

$$\Pi^{\mu\nu}_{WW}(x,y) = \frac{e^2}{16\pi^2 \sin^2(\theta_W)} \sum_\alpha \sum_i U^\dagger_{i\alpha} U_{\alpha i} \left(q^\mu q^\nu P(q^2, m^2_{N_i}, m^2_\alpha) - g^{\mu\nu} Q(q^2, m^2_{N_i}, m^2_\alpha) \right) . \tag{5.24}$$

The functions P and Q are defined in appendix B. m_{N_i} is the mass of the i-th neutrino mass eigenstate, m_α the mass of the charged lepton ℓ_α. q is the external momentum of the W boson. The $q^\mu q^\nu$–term can be neglected, as argued in section 3.6, therefore the self energy takes the form

$$\Pi_{WW} = -\frac{e^2}{16\pi^2 \sin^2(\theta_W)} \sum_\alpha \sum_i U^\dagger_{i\alpha} U_{\alpha i} Q(q^2, m^2_{N_i}, m^2_\alpha) . \tag{5.25}$$

The contributions to the Z boson self energy are shown in figure 5.3a. Both the neutrinos and the charged leptons have to be considered.

$$\begin{aligned} \Pi_{ZZ} = \frac{-e^2}{32\pi^2 \cos^2(\theta_W) \sin^2(\theta_W)} \Bigg(& \sum_{i,j} \sum_{\alpha,\beta} U^\dagger_{i\alpha} U_{\alpha j} U^\dagger_{j\beta} U_{\beta i} Q(q^2, m^2_{N_i}, m^2_{N_j}) \\ & + \sum_{i,j} \sum_{\alpha,\beta} U^\dagger_{i\alpha} U_{\alpha j} U^\dagger_{i\beta} U_{\beta j} m_{N_i} m_{N_j} B_0(q^2, m^2_{N_i}, m^2_{N_j}) \\ & + [(1 - 2\sin^2(\theta_W))^2 + (2\sin^2(\theta_W))^2] \sum_\alpha Q(q^2, m^2_\alpha, m^2_\alpha) \\ & + 4\sin^2(\theta_W)(1 - 2\sin^2(\theta_W)) \sum_\alpha m^2_\alpha B_0(q^2, m^2_\alpha, m^2_\alpha) \Bigg) , \end{aligned} \tag{5.26}$$

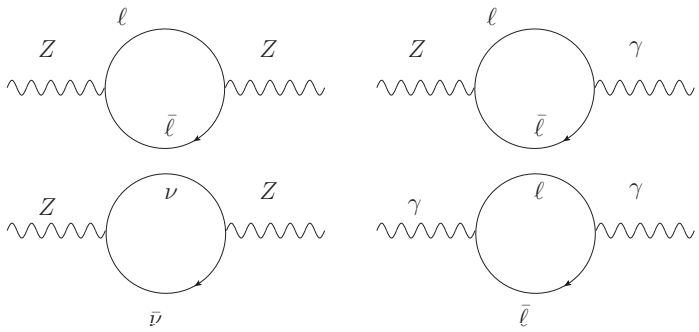

(a) Z boson self-energies from neutrinos and charged leptons.

(b) Photon and photon–Z self energies, same as in the SM.

Figure 5.3: Self-energy contribution to Z boson and photon from neutrinos and charged leptons.

where the first two lines correspond to the neutrino and the second two to the charged lepton contribution.

Since neutrinos do not contribute to the self energy of the photon and the one of the photon and Z boson, see figure 5.3b, these are the same as in the SM:

$$\Pi_{\gamma\gamma}(q) = \frac{-e^2}{4\pi^2}\sum_{\alpha}(Q(q^2, m_\alpha^2, m_\alpha^2) - m_\alpha^2 B_0(q^2, m_\alpha^2, m_\alpha^2))\,, \tag{5.27}$$

$$\Pi_{Z\gamma}(q) = \frac{4\sin^2(\theta_W) - 1}{4\cos(\theta_W)\sin(\theta_W)}\Pi_{\gamma\gamma}(q)\,. \tag{5.28}$$

In order to obtain only the beyond the SM contribution to the self energies the SM parts have to be subtracted. These are obtained by only considering the three massless SM neutrinos in the finite parts of Q and B_0, thus ensuring that the infinities still cancel out. Note that the PMNS matrix does then not enter, since mass and flavor bases coincide.

S, T, U Parameters

From these self energies one can now calculate the oblique correction parameters that are defined as in section 3.6. The on-shell renormalization scheme is used and the divergences cancel out (this has been checked), in the T parameter with the condition

$$|\sum_i U_{\alpha i} m_i U_{i\beta}^T|^2 = 0\,, \tag{5.29}$$

which is equivalent to the vanishing of $M_L = 0$ in the neutrino mass matrix for a seesaw type I.

The finite expression for T is

$$\begin{aligned}\alpha_{em} T = \frac{e^2}{32\pi^2 \sin^2\theta_W M_W^2} \Bigg\{ & \sum_{i,j}\sum_{\alpha,\beta} U^\dagger_{i\alpha} U_{\alpha j} U^\dagger_{j\beta} U_{\beta i} \cdot \\ & \cdot \frac{1}{4}\left(m^2_{N_i} + m^2_{N_j} - 2\frac{m^4_{N_i}\ln(m^2_{N_i}/M^2_W) - m^4_{N_j}\ln(m^2_{N_j}/M^2_W)}{m^2_{N_i} - m^2_{N_j}} \right) + \\ & + \sum_{i,j}\sum_{\alpha,\beta} U^\dagger_{i\alpha} U_{\alpha j} U^\dagger_{i\beta} U_{\beta j} m_{N_i} m_{N_j} \cdot \\ & \cdot \left(1 - \frac{m^2_{N_i}\ln(m^2_{N_i}/M^2_W) - m^2_{N_j}\ln(m^2_{N_j}/M^2_W)}{m^2_{N_i} - m^2_{N_j}} \right) - \\ & - \sum_\alpha m^2_\alpha \ln(m^2_\alpha/M^2_W) - \\ & - \sum_{\alpha,i} U^\dagger_{i\alpha} U_{\alpha i} \cdot \frac{1}{2}\left(m^2_{N_i} + m^2_\alpha - 2\frac{m^4_{N_i}\ln(m^2_{N_i}/M^2_W) - m^4_\alpha \ln(m^2_\alpha/M^2_W)}{m^2_{N_i} - m^2_\alpha} \right) \Bigg\} . \end{aligned} \tag{5.30}$$

S and U can be calculated analogously, also yielding lengthy expressions. The result will not be quoted here, see [68], for the entire expressions. Note that since S and U are related to the derivatives of the self-energies of the W and Z boson, whereas T is proportional to their difference, S and U are much smaller than T.

5.2 Z Pole

In this section the tree-level corrections of heavy sterile neutrinos to the Z decay width, that was measured at LEP [64], will be calculated. To understand possible implications of sterile neutrinos on this observable, one has to look at the interaction of the Z boson with neutrinos.

In the flavor basis, the weak neutral current interaction with the neutrinos is given by the Lagrangian:

$$\mathscr{L}_I^{NC} = -\sum_{\alpha=e,\mu,\tau} \frac{g}{4\cos(\theta_W)} \bar{\nu}_\alpha \gamma^\mu \left(1-\gamma_5\right) \nu_\alpha Z_\mu \,. \tag{5.31}$$

When now transforming from flavor to mass eigenstates the number of sterile neutrinos

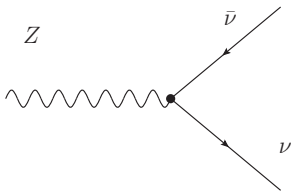

Figure 5.4: Decay of Z into two neutrinos.

assumed in this model has to be fixed. Only one sterile state s will be considered at first, so the following unitarity condition holds:

$$\sum_{\alpha=e,\mu,\tau,s} U^*_{\alpha i} U_{\alpha j} = \delta_{ij} \,. \tag{5.32}$$

Writing then $\nu_\alpha = \sum_i U_{\alpha i}\nu_i$ in the Lagrangian gives

$$\begin{aligned}
\mathscr{L}_I^{NC} &\propto \sum_{\alpha=e,\mu,\tau} \sum_{i=1}^{4}\sum_{j=1}^{4} U^*_{\alpha i}\bar{\nu}_{i_L}\gamma^\mu U_{\alpha j}\nu_{j_L} Z_\mu \\
&\propto \sum_{\alpha=e,\mu,\tau} \left(\sum_{i=1}^{4} U^*_{\alpha i} U_{\alpha i}\bar{\nu}_{i_L}\gamma^\mu \nu_{i_L} Z_\mu + \sum_{i\neq j}^{4} U^*_{\alpha i} U_{\alpha j}\bar{\nu}_{i_L}\gamma^\mu \nu_{j_L} Z_\mu \right) \\
&\propto \sum_{i=1}^{4} \bar{\nu}_{i_L}\gamma^\mu \nu_{i_L} Z_\mu \left(1 - U^*_{si}U_{si}\right) + \sum_{i\neq j}^{4} \bar{\nu}_{i_L}\gamma^\mu \nu_{j_L} Z_\mu \left(0 - U^*_{si}U_{sj}\right) \,.
\end{aligned} \tag{5.33}$$

The process to be calculated here is the decay of the Z boson into neutrinos, see figure 5.4. The decay width into neutrinos (invisible decay width) is proportional to the amplitude squared of these processes $|\mathcal{M}|^2$. Since only the corrections to the SM are relevant here, one can express the decay width in terms of the amplitudes of the decay in two light neutrinos (Γ_0), two heavy neutrinos (Γ_4) and one light and one heavy neutrino (Γ_{40}) and just consider the extra factors from the mixing of active and sterile neutrinos. This gives

$$\begin{aligned}
\Gamma_{inv} = \Gamma_0 \sum_{i=1}^{3} \left(1 - |U_{si}|^2\right)^2 + \Gamma_4 \left(1 - |U_{s4}|^2\right)^2 + \Gamma_0 \sum_{i\neq j}^{3} |U^*_{si}U_{sj}|^2 \\
+ \Gamma_{40} \sum_{i=1}^{3} |U^*_{si}U_{s4}|^2 + \Gamma_{40} \sum_{j=1}^{3} |U^*_{s4}U_{sj}|^2
\end{aligned}$$

$$= \Gamma_0 \left(\sum_{i=1}^{3} \left(1 - |U_{si}|^2\right)^2 + \sum_{i \neq j}^{3} |U_{si}^* U_{sj}|^2 \right) + \Gamma_4 \left(1 - |U_{s4}|^2\right)^2 + 2\Gamma_{40} \sum_{i=1}^{3} |U_{si}^* U_{s4}|^2 \,. \tag{5.34}$$

Recall the definition

$$\varepsilon^2 = \sum_{i=1}^{3} |U_{si}|^2 = \sum_{\alpha=e,\mu,\tau} |U_{\alpha 4}|^2 = 1 - |U_{s4}|^2 \,. \tag{5.35}$$

Use then

$$\sum_{i=1}^{3} |U_{si}|^4 + \sum_{i \neq j}^{3} |U_{si}^* U_{sj}|^2 = \sum_{i=1}^{4} |U_{si}|^4 + \sum_{i \neq j}^{4} |U_{si}^* U_{sj}|^2 - |U_{s4}|^4 - 2 \sum_{i=1}^{3} |U_{si}^* U_{s4}|^2 \tag{5.36}$$

together with the unitarity condition

$$\begin{aligned} 1 = \sum_{i=1}^{4} U_{\alpha i}^* U_{\alpha i} = \left(\sum_{i=1}^{4} U_{\alpha i}^* U_{\alpha i} \right)^2 &= \sum_{i=1}^{4} |U_{\alpha i}|^2 \sum_{j=1}^{4} |U_{\alpha j}|^2 \\ \Rightarrow \qquad \sum_{i=1}^{3} |U_{si}|^4 + \sum_{i \neq j}^{3} |U_{si}^* U_{sj}|^2 &= 1 - |U_{s4}|^4 - 2 \sum_{i=1}^{3} |U_{si}^* U_{s4}|^2 \\ &= 1 - |U_{s4}|^2 \left(|U_{s4}|^2 + 2 \sum_{i=1}^{3} |U_{si}|^2 \right) \\ &= 1 - (1 - \varepsilon^2)(1 - \varepsilon^2 + 2\varepsilon^2) = 1 - (1 - \varepsilon^4) = \varepsilon^4 \,, \end{aligned} \tag{5.37}$$

and the invisible Z decay width becomes

$$\Gamma_{inv} = \Gamma_0 (3 - 2\varepsilon^2 + \varepsilon^4) + \Gamma_4 \varepsilon^4 + 2\,\Gamma_{40}\, \varepsilon^2 (1 - \varepsilon^2) \,. \tag{5.38}$$

If the fourth (mainly sterile) neutrino is heavier than the Z boson, then the latter cannot decay into two heavy neutrinos or in a heavy and a light neutrino, meaning Γ_4 and Γ_{40} are kinematically forbidden and can thus be set to zero, and the decay width becomes:

$$\begin{aligned} \Gamma_{inv} &= \Gamma_0 (3 - 2\varepsilon^2 + \varepsilon^4) \\ &\approx 3\Gamma_0 (1 - \frac{2}{3}\varepsilon^2) \,. \end{aligned} \tag{5.39}$$

The value without any sterile neutrino would be $\Gamma_{inv} = 3\,\Gamma_0$, the SM value. Note also

that in case the fourth neutrino is as light as the three (active) ones, then the kinematics would give $\Gamma_4 \approx \Gamma_{40} \approx \Gamma_0$ and as terms cancel out this also also leads to $\Gamma_{inv} = 3\,\Gamma_0$.

Adding a heavy sterile state to the theory gives a negative contribution from non-unitarity effects of the 3×3 PMNS mixing matrix. As said above the LEP experiment [64] measured the number of active neutrinos to be smaller than three, $N_\nu = 2.9841 \pm 0.0083$, whereas three would be the SM value. The existence of a sterile neutrino could therefore be an explanation for this Z pole anomaly. But to reproduce the experimental value, a large mixing of active and sterile neutrinos is required and one has to take care of unitarity constraints and masses and mixing of the active neutrinos (to be treated in the sections 5.4 and 5.5).

To compare the theoretical result to the LEP data one needs the ratio $\Gamma_{inv}/\Gamma_{lept}$ of the invisible and the leptonic decay width of the Z boson. In the SM (see also [64]) and from the LEP experiment one gets

$$\frac{\Gamma_{inv}}{\Gamma_{lept}}_{SM} = 5.9736 \pm 0.0036\,, \tag{5.40}$$

$$\frac{\Gamma_{inv}}{\Gamma_{lept}}_{LEP} = 5.942 \pm 0.016\,. \tag{5.41}$$

When a heavy sterile neutrino is present, the invisible Z decay width gets shifted by $(1 - \frac{2}{3}\varepsilon^2 + \frac{1}{3}\varepsilon^4)$, whereas the leptonic decay width stays the same, meaning that the ratio of the two is shifted by the same factor:

$$\frac{\Gamma_{inv}}{\Gamma_{lept}}_{LEP} = \frac{\Gamma_{inv}}{\Gamma_{lept}}_{SM} \cdot \left(1 - \frac{2}{3}\varepsilon^2 + \frac{1}{3}\varepsilon^4\right)\,. \tag{5.42}$$

One can now estimate the necessary mixing, which would explain the Z pole anomaly. It is

$$\varepsilon^2 = \sum_{i=1}^{3} |U_{si}|^2 = \sum_{\alpha=e,\mu,\tau} |U_{\alpha 4}|^2 \approx 0.008\,. \tag{5.43}$$

As the presence of a sterile neutrino also changes other SM observables, ε^2 has to be fitted to several measurements. This makes the above value really just an approximation.

5.3 NuTeV

The NuTeV experiment [65] produces neutrino and antineutrino beams to measure the (anti)neutrino-nucleon cross sections and extracts the value of the Weinberg an-

gle $\sin^2(\theta_W)$. It compares the ratios of neutral to charged current cross sections via the event rate:

$$R^{\nu} = \frac{\sigma(\nu N \to \nu X)}{\sigma(\nu N \to l^- X)}\,, \tag{5.44}$$

$$R^{\bar{\nu}} = \frac{\sigma(\bar{\nu} N \to \bar{\nu} X)}{\sigma(\bar{\nu} N \to l^+ X)}\,. \tag{5.45}$$

The charged and neutral current interactions are described by the Lagrangians:

$$\mathscr{L}_{int}^{CC} = -\frac{g}{\sqrt{2}}\bar{\nu}_\alpha \gamma_\mu \left(\frac{1-\gamma_5}{2}\right) \ell_\alpha W^{+\mu} - \frac{g}{\sqrt{2}}\bar{\ell}_\alpha \gamma_\mu \left(\frac{1-\gamma_5}{2}\right) \nu_\alpha W^{-\mu} \tag{5.46}$$

$$\mathscr{L}_{int}^{NC} = -\frac{g}{4\cos(\theta_W)}\bar{\nu}_\alpha \gamma_\mu \left(1-\gamma_5\right) \nu_\alpha Z^{\mu} \tag{5.47}$$

Transforming from flavor to mass eigenstates and having one additional sterile neutrino gives (constant factors are set aside):

$$\mathscr{L}_{int}^{CC} \propto \sum_{j=1}^{4} U_{\alpha j}^{*} \bar{\nu}_j \gamma_\mu P_L \ell_\alpha W^{+\mu} + \sum_{i=1}^{4} \bar{\ell}_\alpha \gamma_\mu P_L U_{\alpha i} \nu_i W^{-\mu}\,, \tag{5.48}$$

$$\mathscr{L}_{int}^{NC} \propto \sum_{i=1}^{4}\sum_{j=1}^{4} U_{\alpha i}^{*} \bar{\nu}_{i_L} \gamma^{\mu} U_{\alpha j} \nu_{j_L} Z_\mu\,. \tag{5.49}$$

The experiment uses muon neutrinos, events from electron neutrinos are excluded or contribute to the experimental error. Therefore, one does not sum over flavors as in the invisible Z width, but rather has to consider only $\alpha = \mu$.

The cross sections are proportional to the corresponding amplitude squared $|\mathcal{M}|^2$ of the process. As can be seen from the Lagrangians above, charged current events (independent of the mediation via W^+ or W^-) get modified by a factor $\sum_i |U_{\alpha i}|^2$, while the neutral current events contain two neutrinos and thus have a factor of $\sum_i |U_{\alpha i}|^2 \sum_j |U_{\alpha j}|^2$.

$$|\mathcal{M}|_{CC}^2 \propto \sum_{i=1}^{4} |U_{\mu i}|^2\,, \tag{5.50}$$

$$|\mathcal{M}|_{NC}^2 \propto \sum_{i=1}^{4} |U_{\mu i}|^2 \sum_{j=1}^{4} |U_{\mu j}|^2\,. \tag{5.51}$$

These factors still only come from converting to mass eigenstates, because of unitarity they all give unity when omitting the kinematics. But when the sterile neutrino is too heavy to be produced, the sum goes only from one to three and one can use the unitarity

condition to write

$$\sum_{i=1}^{3} |U_{\alpha i}|^2 = 1 - |U_{\alpha 4}|^2 \tag{5.52}$$

$$\Rightarrow \qquad \sigma_{CC}^{\pm} \propto (1 - |U_{\mu 4}|^2) \tag{5.53}$$

$$\sigma_{NC} \propto (1 - |U_{\mu 4}|^2)^2 \approx (1 - 2\,|U_{\mu 4}|^2)\,. \tag{5.54}$$

To compare the NuTeV results to the SM predictions use the relation of the Weinberg angle and the cross sections:

$$\frac{1}{2} - \sin^2(\theta_W) = \frac{\sigma_{NC}^{\nu} - \sigma_{NC}^{\bar{\nu}}}{\sigma_{CC}^{\nu} - \sigma_{CC}^{\bar{\nu}}} \tag{5.55}$$

$$\Rightarrow \qquad \left(\frac{1}{2} - \sin^2(\theta_W)\right)_{NuTeV} = \left(\frac{1}{2} - \sin^2(\theta_W)\right)_{SM} \cdot \left(1 - |U_{\mu 4}|^2\right)\,. \tag{5.56}$$

In the NuTeV experiment $\sin^2(\theta_W)$ was determined by Monte Carlo simulations to be

$$\begin{aligned}\sin^2(\theta_W)_{NuTeV} &= 0.2277 \pm 0.00135(\text{stat}) \pm 0.00093(\text{syst}) \\ &\quad - 0.00022 \times \left(\frac{M_{top}^2 - (175\,GeV)^2}{(50\,GeV)^2}\right) + 0.00032 \times \ln\left(\frac{M_{Higgs}}{150\,GeV}\right)\,,\end{aligned} \tag{5.57}$$

while the best fit value from other electroweak measurements is ([64], p. 154 and [65], see references therein)

$$\sin^2(\theta_W)_{other} = 0.2227 \pm 0.0004\,. \tag{5.58}$$

The NuTeV value thus differs from other (neutrino-nucleon excluding) measurements by about $3\,\sigma$. When assuming that the other measurements correspond to the SM value and only NuTeV sees the influence of a heavy sterile neutrino, one can calculate the mixing of muon to sterile neutrino that is required to explain the deviation (again only an estimate):

$$|U_{\mu 4}|^2 = \varepsilon_{\mu}^2 = 0.018\,. \tag{5.59}$$

Note that later on a correction will be included, where next-to-next-to-leading order effects in the quark distribution functions are taken into account.

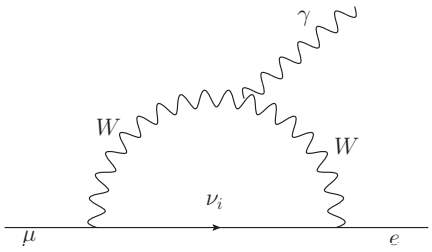

Figure 5.5: Lepton flavor violating decay $\mu \rightarrow e\,\gamma$, possible diagram via neutrino mixing.

5.4 Constraints

5.4.1 Lepton Flavor Violating Decay

One of the most stringend bounds on the mixing of active to sterile neutrinos is the experimental limit on the branching ratio of the decay $\mu \rightarrow e\,\gamma$, see section 3.3. It depends on the product of the mixing parameters of the electron and muon neutrino to the additional (mostly sterile) mass eigenstates $U^*_{ei}U_{\mu i}$ and on their masses M_i, $i = 4, .., N$.

The branching ratio of the $\mu \rightarrow e\gamma$ decay is given by (see [69], p. 244 ff.):

$$B(\mu \rightarrow e\gamma) = \frac{\Sigma(\mu \rightarrow e\gamma)}{\Sigma(\mu \rightarrow e\nu\bar{\nu})} = \frac{3\alpha_{em}}{32\pi}\delta_\nu^2\,, \tag{5.60}$$

$$\text{where} \quad \delta_\nu = 2\sum_{i=1}^{N} U^*_{ei}U_{\mu i}\, g\left(\frac{M_i^2}{M_W^2}\right) \tag{5.61}$$

$$\text{with} \quad g(x) = \int_0^1 \frac{(1-\alpha)d\alpha}{(1-\alpha)+\alpha x}[2(1-\alpha)(2-\alpha)+\alpha(1+\alpha)x]\,. \tag{5.62}$$

Since the masses of the active neutrinos are so small, one can approximate their contribution by

$$\frac{M_i^2}{M_W^2} \approx 0 \qquad \Rightarrow \qquad g\left(\frac{M_i^2}{M_W^2}\right) \approx g(0) = \frac{5}{3} \qquad \text{for } i = 1, 2, 3\,. \tag{5.63}$$

Assuming a fourth neutrino and using the unitarity relation one gets:

$$\sum_{i=1}^{4} U^*_{ei}U_{\mu i} = 0 \qquad \Rightarrow \qquad \sum_{i=1}^{3} U^*_{ei}U_{\mu i} = -U^*_{e4}U_{\mu 4}\,. \tag{5.64}$$

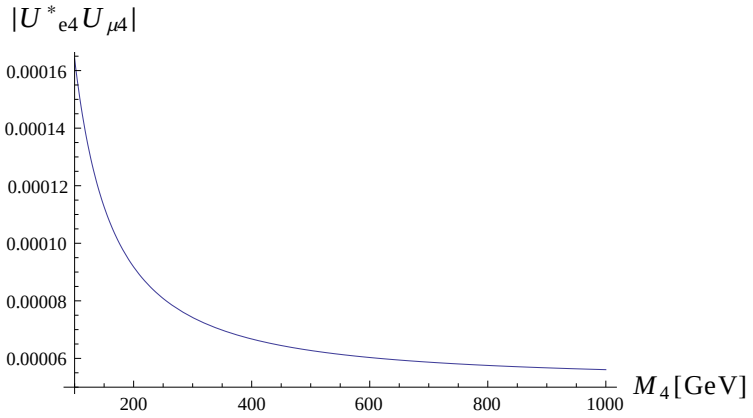

Figure 5.6: Upper limit of $|U^*_{e4}U_{\mu 4}|$ as a function of the mass of the fourth neutrino M_4 in GeV.

Therefore

$$\begin{aligned}\delta_\nu &= 2\left(\sum_{i=1}^{3} U^*_{ei}U_{\mu i}\right) g(0) + 2U^*_{e4}U_{\mu 4} g\left(\frac{M_4^2}{M_W^2}\right) \\ &= 2U^*_{e4}U_{\mu 4}\left(g\left(\frac{M_4^2}{M_W^2}\right) - \frac{5}{3}\right) . \end{aligned} \tag{5.65}$$

This gives the limit for $|U^*_{e4}U_{\mu 4}|$ when there is only a fourth neutrino. In case there should be more the product is replaced by the sum over all products:

$$\delta_\nu = 2U^*_{e4}U_{\mu 4}\left(g\left(\frac{M_4^2}{M_W^2}\right) - \frac{5}{3}\right) \quad \rightarrow \quad 2\sum_{i=1}^{N} U^*_{ei}U_{\mu i} \cdot \left(g\left(\frac{M_i^2}{M_W^2}\right) - \frac{5}{3}\right) . \tag{5.66}$$

The MEG collaboration [48] has determined the most recent upper bound on the branching ratio of $\mu \rightarrow e\,\gamma$ to be

$$B(\mu^+ \rightarrow e^+\gamma) \leq 2.4 \cdot 10^{-12} , \tag{5.67}$$

at 90% confidence level. This results in an upper limit for $U^*_{e4}U_{\mu 4}$ of about

$$|U^*_{e4}U_{\mu 4}| \approx 6 \cdot 10^{-5} , \tag{5.68}$$

where

$$M_W = 80.399\,\text{GeV} , \tag{5.69}$$

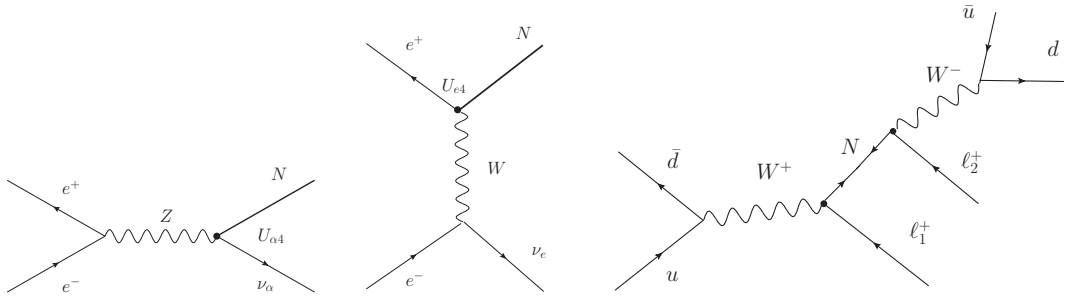

(a) e^+e^- s-channel (b) e^+e^- t-channel (c) Channel in hadron collider.

Figure 5.7: Feynman diagrams for the detection of heavy sterile neutrinos in colliders. (a,b): Processes of e^+e^- leading to a heavy (mostly sterile) neutrino N in the final state. (c): Feynman diagram for the detection of a heavy sterile neutrino at the LHC.

$$M_4 \lesssim 1\,\mathrm{TeV}\,. \tag{5.70}$$

In Figure 5.6 the limit of $|U_{e4}^* U_{\mu 4}|$ has been plotted against the mass of the fourth neutrino M_4. It converges for large masses to about $|U_{e4}^* U_{\mu 4}| \lesssim 6 \cdot 10^{-5}$.

5.4.2 Direct Collider Searches

Since sterile neutrinos with masses of order of the Z boson mass are considered here, there are not many bounds from collider searches. Measurements for masses $M_4 \gtrsim M_Z$ come from the L3 experiment at LEP [70]. The heavy (mostly sterile) neutrino is produced via

$$e^+e^- \;\to\; \nu_\alpha N\,. \tag{5.71}$$

Active neutrino of any flavor $\alpha = e$, μ, τ can be produced via the s-channel, but in the t-channel there are only electron neutrinos, see figures 5.7a and 5.7b and section 3.5. As the t-channel dominates, limits on $|U_{e4}|$ are much stronger than on the other mixing parameters and the production cross section via the s-channel even lies beneath LEP sensitivity. Thus, only $|U_{e4}|$ will be considered in the following.

Figure 5.8 shows the plot from the L3 experiment with upper limits for the mixing of the electron to a fourth (mostly sterile) neutrino. It varies from about 10^{-3} at masses $M_4 \approx 100$ GeV to about 10^{-2} around $M_4 \approx 160$ GeV.

The most recent limits from collider searches on the mixing parameter of muon and electron neutrino, U_{e4} and $U_{\mu 4}$, assuming no specific model (mixing and mass of the fourth neutrino are free parameters), are from the CMS collaboration at the LHC [71].

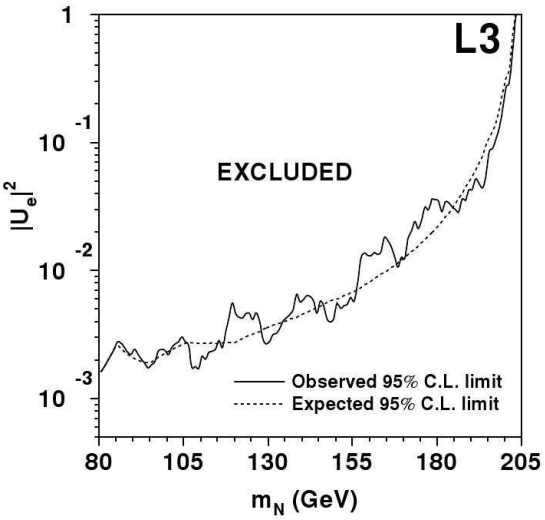

Figure 5.8: Upper bound of $|U_{e4}|^2 = |U_e|^2$) as a function of the mass of the fourth neutrino $M_4 = m_N$ in GeV as measured in L3 in the LEP experiment. Taken from [70].

The leading order Feynman diagram is shown in figure 5.7c, the charge conjugate process contributes also (compare section 3.5). The event contains two equally charged leptons μ or e (τ leptons are very difficult to reconstruct) and two jets in the final state.

The limits on U_{e4} and $U_{\mu 4}$ are calculated under the assumption that the other two mixing elements are zero. In other words, $U_{\tau 4}$ is always assumed to vanish. Figure 5.9 shows the plot from CMS.

In the region concerning this model here, at masses above the Z boson mass, the limit is $|U_{e4}|^2 \lesssim 10^{-3} - 10^{-1}$ and $|U_{\mu 4}|^2 \lesssim 4 \cdot 10^{-2}$. L3 imposed the best limits for U_{e4} and the only limits on $U_{\mu 4}$ come from CMS.

5.4.3 Lepton Universality

In the Standard Model the weak force is universal, meaning that the coupling constant g is the same for all particles. In some beyond SM scenarios, for example when adding sterile neutrinos that mix differently with the different active neutrinos, this relation gets modified and the coupling becomes flavor dependent.

$$\mathscr{L}_{int}^{CC} = -\sum_{\ell=e,\mu,\tau} \frac{g_\ell}{\sqrt{2}} \bar{\nu}_\ell \gamma_\mu \left(\frac{1-\gamma_5}{2}\right) \ell \, W^{+\mu} + h.c. \tag{5.72}$$

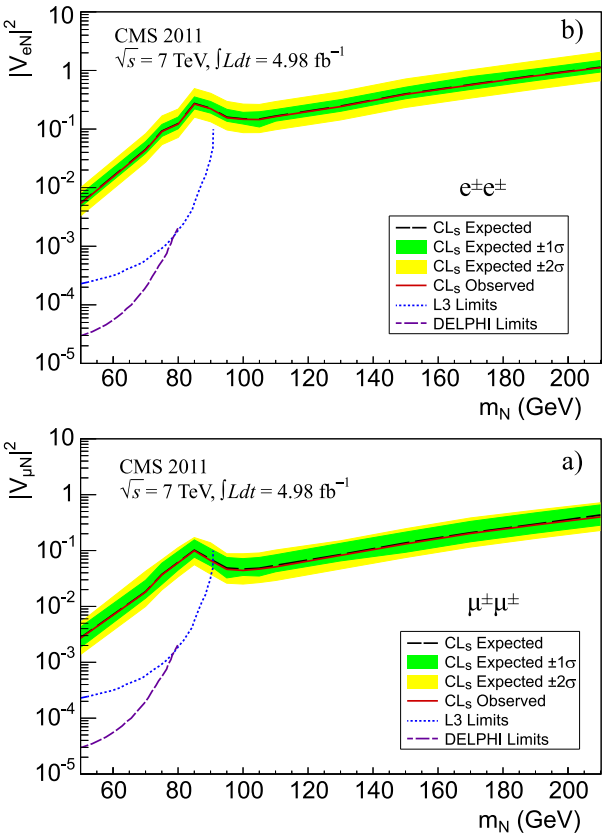

Figure 5.9: Limits on $|U_{e4}|^2 (= |V_{eN}|^2)$ and $|U_{\mu 4}|^2 (= |V_{\mu N}|^2)$ at 95% confidence level from the CSM collaboration at LHC, taken from [71].

Processes	Constraints
$W \to e\,\bar{\nu}_e$ $W \to \mu\,\bar{\nu}_\mu$ $W \to \tau\,\bar{\nu}_\tau$	$(g_\mu/g_e)_W = 0.999 \pm 0.011$ $(g_\tau/g_e)_W = 1.029 \pm 0.014$
$\mu \to e\,\bar{\nu}_e \nu_\mu$ $\tau \to e\,\bar{\nu}_e \nu_\tau$ $\tau \to \mu\,\bar{\nu}_\mu \nu_\tau$	$(g_\mu/g_e)_\tau = 0.9999 \pm 0.0021$ $(g_\tau/g_e)_{\tau\mu} = 1.0004 \pm 0.0022$
$\pi \to \mu\,\bar{\nu}_\mu$ $\pi \to e\,\bar{\nu}_e$ $\tau \to \pi\,\nu_\tau$	$(g_\mu/g_e)_\pi = 1.0021 \pm 0.0016$ $(g_\tau/g_\mu)_{\pi\tau} = 1.0030 \pm 0.0034$
$K \to \mu\,\bar{\nu}_\mu$ $\tau \to K\,\nu_\tau$	$(g_\tau/g_\mu)_{K\tau} = 0.979 \pm 0.017$

Table 5.1: Limits on lepton non-universality from different decays, determined from the ratios of the respective decay widths.

$\varepsilon_e^2 \approx 0$	$\varepsilon_\mu^2 \approx 0$
$-0.02 \leq \varepsilon_\mu^2 \leq 0.24$	$-0.24 \leq \varepsilon_e^2 \leq 0.02$
$-0.086 \leq \varepsilon_\tau^2 \leq 0.0036$	$-0.0036 \leq \varepsilon_e^2 - \varepsilon_\tau^2 \leq 0.086$
$-0.076 \leq \varepsilon_\mu^2 - \varepsilon_\tau^2 \leq 0.0128$	$-0.0128 \leq \varepsilon_\tau^2 \leq 0.076$

Table 5.2: Limits on the mixing parameters from lepton universality bounds.

The measurements of the decay widths constrain these scenarios. The lepton universality constraints are summarized in table 5.1, which are taken from [67].

Combining these constraints gives for the three ratios

$$0.988 \leq \frac{g_\mu}{g_e} \leq 1.01\,, \quad 0.9982 \leq \frac{g_\tau}{g_e} \leq 1.043\,, \quad 0.962 \leq \frac{g_\tau}{g_\mu} \leq 1.0064\,. \tag{5.73}$$

The ratios of the flavor dependent coupling constants are related to the mixing parameters ε_α as follows:

$$\frac{g_\mu}{g_e} = 1 + \frac{\varepsilon_e^2 - \varepsilon_\mu^2}{2}\,, \quad \frac{g_\tau}{g_\mu} = 1 + \frac{\varepsilon_\mu^2 - \varepsilon_\tau^2}{2}\,, \quad \frac{g_\tau}{g_e} = 1 + \frac{\varepsilon_e^2 - \varepsilon_\tau^2}{2}\,. \tag{5.74}$$

This gives

$$-0.24 \leq \varepsilon_e^2 - \varepsilon_\mu^2 \leq 0.02\,, \tag{5.75}$$

$$-0.0036 \leq \varepsilon_e^2 - \varepsilon_\tau^2 \leq 0.086\,, \tag{5.76}$$

$$-0.076 \leq \varepsilon_\mu^2 - \varepsilon_\tau^2 \leq 0.0128\,. \tag{5.77}$$

As has been argued in section 5.4.1, the product of $|U_{e4}^* U_{\mu 4}|$ has to be very small to satisfy the limit from the lepton flavor violating decay $\mu \to e\,\gamma$. Therefore either ε_e^2 or ε_μ^2 have to be tiny and one can distinguish two scenarios: $\varepsilon_e \approx 0$ or $\varepsilon_\mu \approx 0$. The respective bounds on the remaining parameters are shown in table 5.2.

5.4.4 Non-Unitarity

In a theory with additional sterile neutrinos the mixing matrix of the active neutrinos, the PMNS matrix, becomes non-unitary. One can constrain the non-unitarity from measurements of oscillations of the active neutrinos. This was done in [44]. But as it turns out these constraints are much less stringent than the lepton universality bounds presented above (which can also be translated to bounds on non-unitarity, but this is of no need here). These bounds are therefore not considered here.

5.4.5 Neutrinoless Double-Beta Decay

Sterile neutrinos contribute to neutrinoless double-beta decay in two ways: Directly via the exchange of the sterile neutrinos and indirectly by giving a Majorana mass to the active neutrinos and those are then the mediator of the decay. This has been shown in section 3.4.

The indirect contribution will be treated first. When considering the masses and mixing of the active neutrinos listed in the next section 5.5, one can estimate the corresponding contribution to the effective mass with the equation (3.46):

$$\langle m_{ee} \rangle = \left| \sum_{i=1}^{3} U_{ei}^2 m_i \right| = \left| m_1 |U_{e1}|^2 + m_2 |U_{e2}|^2 e^{i\alpha_1} + m_3 |U_{e3}|^2 e^{i\alpha_2} \right| . \tag{5.78}$$

The masses are taken to be the same as in table 5.4 and the mixing as in table 5.3. Thus, three different cases are treated, the normal and inverse hierarchy (NH, IH), each with the lowest mass set to zero, and the degenerate case (DC), where all masses are at about 0.1 eV. One can estimate the largest possible contribution of each case, by assuming that the Majorana phases vanish, $\alpha_1 = \alpha_2 = 0$. The values are

$$\langle m_{ee}^{\mathrm{NH}} \rangle^{\max} = 0.003\,\mathrm{eV}\,, \tag{5.79}$$

$$\langle m_{ee}^{\mathrm{IH}} \rangle^{\max} = 0.048\,\mathrm{eV}\,, \tag{5.80}$$

$$\langle m_{ee}^{\mathrm{DC}} \rangle^{\max} = 0.100\,\mathrm{eV}\,. \tag{5.81}$$

Since the sensitivity of experiments now is at about 0.38 eV (EXO conservative bound, see section 3.4), the contributions in the normal and inverse hierarchy cases can be neglected. The maximal contribution in the degenerate case could be important, depending on the direct contribution of the sterile neutrinos. One can also estimate the minimal contribution to be $\langle m_{ee}^{\mathrm{DC}} \rangle^{\min} \approx \cos(2\theta_{12}) \cdot m_1 \approx 0.04\,\mathrm{eV}$ (compare [49]). The Majorana phases could also lead to a cancellation, making the active neutrino contribution in the degenerate case negligible, too.

For heavy sterile neutrinos, meaning with masses well above the momentum scale of about 100 MeV, the decay rate becomes proportional to

$$\Gamma_h \propto \left| \sum_i \frac{U_{ei}^2}{m_i} \right|^2 , \tag{5.82}$$

where m_i are their masses and U_{ei} their mixing to the electron neutrino (compare also section 3.4). Because of the large mass of the mediator, the process is of short range and

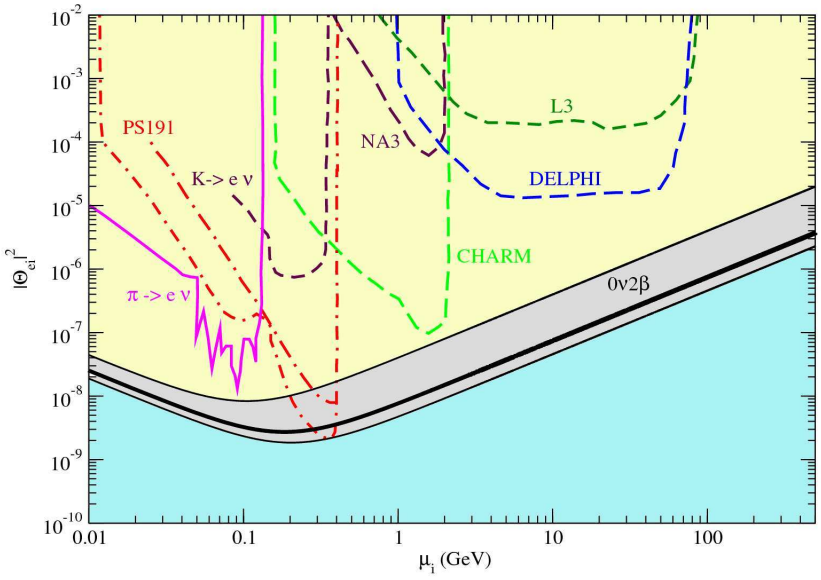

Figure 5.10: Bound on the mixing of one heavy sterile neutrino to the electron neutrino from neutrinoless double-beta decay. Taken from [74].

therefore becomes sensitive to the finite size of the nucleons. The nuclear form factors in this case become very sensitive to the mass of the sterile neutrinos, see e.g. [72].

In a seesaw type I, for a mass range of about 100 GeV to 1 TeV, one can nevertheless approximate the direct contribution of the heavy sterile neutrinos to the effective mass:

$$|\langle m_{ee}\rangle| \approx \left|\sum_i (U^P D_{\sqrt{m_\nu}} R^*)^2_{ei} \cdot \frac{m_a^2}{m_i^2} f(A, m_i)\right|, \tag{5.83}$$

where the active sterile mixing is parameterized in the Casas-Ibarra form, see section 5.5.1: U^P is the PMNS matrix, $D_{\sqrt{m_\nu}}$ a 3×3 matrix with the square roots of the light neutrino masses on the diagonal. R contains parameters of the Dirac mass matrix. m_a is here a mass-parameter that has a value of about 0.9 GeV. $f(A, m_i)$ depends on the mass number of the element and has a weak dependence on the mass m_i. It can be approximated by $f(A, m_i) \lesssim 0.08$. For details see [73].

To illustrate the bound from neutrinoless double-beta decay on the mixing of the heavy sterile neutrinos to the electron neutrino, a plot for the case of a single sterile neutrino is shown in figure 5.10 (from [74]).

5.5 Masses and Mixing Angles of the Active Neutrinos

In order to obtain a consistent model in the χ^2-fit it has to be assured that the model satisfies the bounds on active neutrino masses and reproduces their mass-squared differences and their mixing (the PMNS matrix).

As was mentioned in chapter 2 the light neutrino mass eigenstates can be normal ordered $m_1 < m_2 < m_3$ or inverse ordered $m_3 < m_1 < m_2$ (also called normal or inverse hierarchy):
(NH) $m_1 = m_{min} = m$, $m_2 = \sqrt{m^2 + \Delta m^2_{\odot}}$ and $m_3 = \sqrt{m^2 + \Delta m_{atm}}$,
(IH) $m_3 = m_{min} = m$, $m_1 = \sqrt{m^2 + \Delta m^2_{atm} - \Delta m^2_{\odot}}$ and $m_2 = \sqrt{m^2 + \Delta m^2_{atm}}$.

In the normal hierarchy, the atmospheric mass-squared difference corresponds to Δm^2_{31}, while in the inverse hierarchy it is Δm^2_{32} (and negative). The best fit values can also differ slightly. For the χ^2-fit the masses and mixing of the active neutrinos from [75] were used, they are quoted in table 5.3.

Parameter	Value
Δm^2_{21}	$7.50 \cdot 10^{-5}\text{eV}^2$
Δm^2_{31} (NH)	$2.47 \cdot 10^{-3}\text{eV}^2$
Δm^2_{32} (IH)	$-2.43 \cdot 10^{-3}\text{eV}^2$
$\sin^2(\theta_{12})$	0.30
$\sin^2(\theta_{23})$	0.41
$\sin^2(\theta_{13})$	0.023
δ_{CP}	240°

Table 5.3: Values of the parameters used in the χ^2-fit, taken from [75].

The PMNS matrix U^P is defined as in equation 3.12, with the angles as in table 5.3 this gives (the Majorana phases are neglected):

$$U^P = \begin{pmatrix} 0.844 & 0.515 & -0.076 + 0.131i \\ -0.379 + 0.067i & 0.708 + 0.041i & 0.591 \\ 0.363 + 0.090i & -0.479 + 0.055i & 0.793 \end{pmatrix}. \tag{5.84}$$

In the χ^2-fit, three scenarios will be considered: The normal and inverse hierarchy (NH and IH) where the smallest mass is set to zero and the so-called degenerate case (DC), where all masses are of the same order, thus a lot bigger than the mass-squared differences (the value for the mass in the degenerate case is taken from the PDG [5]). The resulting values for the masses are listed in table 5.4

	m_1 [eV]	m_2 [eV]	m_3 [eV]
NH	0	0.00866	0.0497
IH	0.0485	0.0493	0
DC	0.1	0.1004	0.11210

Table 5.4: Masses of the light neutrinos in the normal and inverse hierarchy (with the smallest mass set to zero) and in the degenerate, also normal ordered, case. All values are in eV.

The active neutrino masses will be generated in a seesaw type I scenario, where three heavy right handed neutrinos are assumed. The right handed neutrinos have to be heavier than the Z boson, thus have masses $\gtrsim 10^2$ GeV. The specific values of the masses will be determined in the χ^2-fit. Note that the active–sterile mixing will be quite large compared to "natural" seesaw expectation. When calculating the tree-level contribution of the sterile neutrinos to the Z decay width and the neutral to charged current event-ratios, a leading order expansion in the mixing was made. For example, the sum over all active-sterile mixing parameters in the Z decay width was about

$$\varepsilon^2 = \sum_{i=1}^{3} |U_{si}|^2 = \sum_{\alpha=e,\mu,\tau} |U_{\alpha 4}|^2 \approx 0.008\,. \tag{5.85}$$

This was calculated for one sterile neutrino, for more than one it has to be summed over their contributions. One can now estimate the contribution that a 10^2 GeV heavy sterile neutrino with this mixing makes to the light neutrino masses via the seesaw type I. When the mixing to, say, the first mass eigenstate m_1 is taken to be $|U_{s1}|^2 \approx 0.002$, this corresponds in the seesaw to $(m_D/M_R)^2$. Since M_R is at least 10^2 GeV and the light neutrino masses are given by $m_1 \approx m_D^2/M_R$ this gives:

$$m_1 \gtrsim \frac{m_D^2}{M_R^2} \cdot M_R \approx 0.003 \cdot 10^2 \text{ GeV} \approx 0.3 \text{ GeV}\,. \tag{5.86}$$

This means that in order to reproduce the measured parameters of the active neutrinos, there must be a huge cancellation between the contributions of the different sterile states. The model is thus very fine-tuned.

To ensure that the given parameters are met when performing the fit, the Casas-Ibarra parameterization is used. It will be explained in the following.

5.5.1 Casas-Ibarra Parameterization

A useful parameterization, first introduced in [76], isolates the remaining degrees of freedom, when fixing the PMNS matrix of the active neutrinos and their masses, as well as the masses of the sterile neutrinos in a seesaw type I scenario. These are parameters in the Dirac mass matrix.

The Dirac mass term comes from the Yukawa coupling $y\,(\bar{L}\langle\phi\rangle\nu_R)$, where L is the lepton doublet, $\langle\phi\rangle$ the VEV of the neutral component of the Higgs field and ν_R the right-handed neutrino. The Dirac mass matrix is then given by

$$m_D = y\langle\phi\rangle\,.$$

Note that y is a matrix, whereas $\langle\phi\rangle$ is a scalar. In the seesaw type I mechanism one can integrate out the heavy sterile states and get the light neutrino mass matrix (compare chapter 2)

$$M_{light} = m_D^T M_R^{-1} m_D = y^T M_R^{-1} y \cdot \langle\phi\rangle^2\,. \tag{5.87}$$

One can choose a basis where M_R is diagonal, $M_R = D_{M_R}$. $\hat{U}$ is taken to be the matrix diagonalising M_{light} : $\hat{U}^T M_{light}\hat{U} = D_{m_\nu}$ (the diagonal matrices are indicated by D, the index marks the diagonal elements). From the seesaw formula one gets the connection of $\hat{U}$ to the PMNS matrix[2]:

$$U_{PMNS} = \sqrt{1 - BB^\dagger}\hat{U} \approx (1 - \frac{1}{2}BB^\dagger)\,\hat{U}\,. \tag{5.88}$$

This means that at first order $\hat{U}$ can be approximated to be the PMNS matrix. The equation for the neutrino masses becomes

$$D_{m_\nu} = \hat{U}^T y^T D_{M_R^{-1}} y\hat{U}\langle\phi\rangle^2 = \hat{U}^T y^T D_{\sqrt{M_R^{-1}}} D_{\sqrt{M_R^{-1}}} y\hat{U}\langle\phi\rangle^2\,, \tag{5.89}$$

where $D_{\sqrt{M_R^{-1}}}$ is a diagonal matrix with the elements $1/\sqrt{M_{R_i}}$.

By multiplying with $D_{\sqrt{m_\nu^{-1}}}$ from left and right one obtains:

$$\mathbb{1} = \left[D_{\sqrt{M_R^{-1}}} y\hat{U} D_{\sqrt{m_\nu^{-1}}}\right]^T \left[D_{\sqrt{M_R^{-1}}} y\hat{U} D_{\sqrt{m_\nu^{-1}}}\right]\langle\phi\rangle^2\,. \tag{5.90}$$

[2]Compare here section 2.1, equation (2.28). Note that the notation is slightly different: $\hat{U} \equiv U_{light}$

So one can write $D_{\sqrt{M_R^{-1}}} y \hat{U} D_{\sqrt{m_\nu^{-1}}} \langle\phi\rangle = R$, where R is an orthogonal matrix, $R^T R = \mathbb{1}$ and then the general form of the Yukawa matrix is:

$$y = \langle\phi\rangle^{-1} D_{\sqrt{M_R}} R D_{\sqrt{m_\nu}} \hat{U}^\dagger \,. \tag{5.91}$$

The Yukawa couplings thus depend on the low energy parameters contained in m_ν and $\hat{U}$, on the masses of the right handed neutrinos in M_R and on the complex parameters defining R. There are three complex parameters, when the number of sterile neutrinos is taken to be three. R is then a 3×3 matrix. When a different number of right handed neutrinos is assumed, this changes the number of complex parameters in R and R is then not a square matrix.

In the χ^2-fit the number of right handed neutrinos is taken to be three. The orthogonal matrix R is defined as a rotation around three complex angles $\theta_j = z_j + i\, Z_j$, where j=1,2,3. R then reads

$$R = R_1(\theta_1) R_2(\theta_2) R_3(\theta_3) \,, \tag{5.92}$$

where

$$R_1 = \begin{pmatrix} 1 & 0 & 0 \\ 0 & \cos(\theta_1) & -\sin(\theta_1) \\ 0 & \sin(\theta_1) & \cos(\theta_1) \end{pmatrix} \,, \quad R_2 = \begin{pmatrix} \cos(\theta_2) & 0 & -\sin(\theta_2) \\ 0 & 1 & 0 \\ \sin(\theta_2) & 0 & \cos(\theta_2) \end{pmatrix} \,,$$
$$R_3 = \begin{pmatrix} \cos(\theta_3) & -\sin(\theta_3) & 0 \\ \sin(\theta_3) & \cos(\theta_3) & 0 \\ 0 & 0 & 1 \end{pmatrix} \,. \tag{5.93}$$

Since the relevant parameters in this model are the values of the active-sterile mixing, the form of the Casas-Ibarra parameterization will be changed. The active-sterile mixing B is in the seesaw type I at first order given as

$$B = (M_R^{-1} m_D)^\dagger \,. \tag{5.94}$$

In the above notation the Dirac matrix is

$$m_D = i\, D_{\sqrt{M_R}} R D_{\sqrt{m_\nu}} \hat{U}^\dagger \,, \tag{5.95}$$

where the formula for the light masses was changed to its correct form $M_{light} = -m_D^T M_R^{-1} m_D$ by introducing the factor i. By multiplying from the left with M_R^{-1}, assuming it to be

diagonal, thus equal to $D_{M_R^{-1}}$, the active-sterile mixing is obtained:

$$D_{M_R^{-1}} m_D = i\, D_{\sqrt{M_R^{-1}}} R D_{\sqrt{m_\nu}} \hat{U}^\dagger \tag{5.96}$$

$$\Leftrightarrow \qquad B = (D_{M_R^{-1}} m_D)^\dagger = -i \hat{U} D^*_{\sqrt{m_\nu}} R^\dagger D^*_{\sqrt{M_R^{-1}}}\,. \tag{5.97}$$

When the masses of the neutrinos are real, one can drop the complex conjugation.

5.6 χ^2-Fit

The model that includes sterile neutrinos will be compared to the SM by performing a χ^2-fit to measured observables. A χ^2-fit compares the predictions of a theory $T_i(\vec{x})$, that vary with some parameters $x_i (i = 1, ..., p) \to \vec{x}$, to the observed values in experiments D_i:

$$\chi^2(\vec{x}) = \sum_{i=1}^{N} \left(\frac{D_i - T_i(\vec{x})}{\sigma_i} \right)^2 , \tag{5.98}$$

where σ_i is the error of the experimental values. The number of obervables that are fitted is N. Then the best fit is found by minimizing $\chi^2(\vec{x})$ for the theoretical parameters x_i. When the theoretical predictions have errors σ_i^t, the formula changes to

$$\chi^2(\vec{x}) = \sum_{i=1}^{N} \frac{(D_i - T_i(\vec{x}))^2}{(\sigma_i^t)^2 + (\sigma_i)^2}\,. \tag{5.99}$$

This is valid when neglecting off-diagonal elements in the covariance matrix that are describing the correlations of the errors.

A χ^2 distribution is obtained (assuming no open theoretical parameters x_i), when the theoretical predictions T_i are the mean values of a Gaussian distribution, σ_i their errors and D_i random variables that are normally distributed. Then one gets a χ^2 distribution with N degrees of freedom (d.o.f.) and its value should be

$$\langle \chi^2 \rangle \approx N\,. \tag{5.100}$$

When considering a theory depending on the parameters x_i, the minimal χ^2 should follow a χ^2 distribution with $(N - p)$ d.o.f., where N is the number of observables and p the number of parameters. Note that the central limit theorem states that for a sufficient amount of observables N, the χ^2 analysis is also valid even if the data is not normally

Parameter	exp. values	SM pred.
Γ_{lept} [MeV]	83.984 ± 0.086	84.005 ± 0.015
$\Gamma_{\text{inv}}/\Gamma_{\text{lept}}$	5.942 ± 0.016	5.9721 ± 0.0002
$\sin^2(\theta_{\text{eff}})^{\text{lept}}$	0.2324 ± 0.0012	0.23150 ± 0.0001
g_L^2	0.3026 ± 0.0012	0.3040 ± 0.0002
g_R^2	0.033 ± 0.001	0.0300 ± 0.0002
M_W [GeV]	80.385 ± 0.015	80.359 ± 0.011

Table 5.5: Experimental values and SM predictions used for the χ^2-fit.

distributed.

In the model considered here, the masses of the sterile neutrinos and their mixing to the active neutrinos are the open theoretical parameters. Note, however, that masses and mixing are not independent. The Casas-Ibarra parameterization separates the low-energy from the high-energy parameters. When fixing the low-energy observables (active neutrino masses and mixing), only the three masses of the sterile neutrinos and three complex parameters are open in the fit. This would mean there are nine theoretical parameters. In the corrections of the SM (section 5.1) it becomes however apparent, that with S, T, U and ε_e, ε_μ and ε_τ only six independent parameters enter the fit. Of these, S and U tend to be so small that they effectively do not change the observables and one can thus count four effective physical parameters in the considered theory: ε_e, ε_μ, ε_τ and T. Since six observables are fitted (see table 5.5), this leads to an effective number of d.o.f of $6 - 4 = 2$.

The best fits χ^2_{min} are compared to the SM, where the χ^2_{SM} is obtained by setting the active–sterile mixing parameters to zero. The active neutrinos then become massless. The number of d.o.f. of the SM fit is here equal to the number of observables, thus being six. The improvement of the fit including the sterile neutrinos compared to the SM is quantified by the change $\Delta\chi^2$ per degree of freedom. This should be bigger than one.

The SM values are taken from the Gfitter group [77] and from the fit of the PDG [5]. They use as input values the electromagnetic coupling constant α_{em}, the Fermi constant G_F, the strong coupling constant α_s, the Z boson mass M_Z and the fermion masses m_f, compare [78]. Apart from the Fermi constant G_F, these quantities remain unaltered by the existence of additional sterile neutrinos, as they are measured in processes where no neutrinos appear.

The measured values are taken from the PDG [5], except for g_L and g_R, where the

NuTeV values [65] are used, which have been corrected in the form suggested in [79][3]. For the Weinberg angle on the other hand[4] a value is chosen that was measured in hadronic processes, so that it should not be influenced by the introduction of the sterile neutrinos.

5.7 Summary

The value χ^2_{SM} is obtained for negligibly small active-sterile mixing to be

$$\chi^2_{SM} \simeq 7.5 \tag{5.101}$$

for six degrees of freedom. It is independent of the mass hierarchy of the light neutrinos. Since in g_L^2 and g_R^2 and $\Gamma_{\text{inv}}/\Gamma_{\text{lept}}$ the NuTeV anomaly and the smaller than expected invisible decay width of the Z boson are fitted, the value is quite large.

In the χ^2-fits including the sterile neutrinos, the different light neutrino mass scenarios have different impact on the fit parameters.

5.7.1 Normal Mass Hierarchy

In figure 5.11, the fit parameters ε_τ^2 and ε_μ^2 and ε_τ^2 and ε_e^2, respectively, are shown. The color denotes the value of χ^2, but only values for $\chi^2 \leq \chi^2_{SM}$ are chosen. The bound from the decay $\mu \to e\gamma$ implies that either ε_e^2 or ε_μ^2 must be very tiny. In figure 5.11a, the mixing of the sterile neutrinos to the electron neutrino is negligible, while in figure 5.11b this is the case for the mixing to the muon neutrino.

For almost vanishing mixing to the electron neutrino more points in the parameter space are found. Larger mixing to the active neutrino is favored, resulting in a better fit to the above mentioned anomalies. In the case where ε_μ^2 is suppressed, the largest possible values are only at about $1.2 \cdot 10^{-3}$, for higher values some or the constraints are violated. Note that since the mixing to either the electron or muon neutrino has to be negligibly small, the effective number of d.o.f. becomes three. The improvement compared to the SM is then for the best points, with $\chi^2 \approx 4.5$, about one per d.o.f., being not significant.

Note that the fit improves very much, wenn the W boson mass is not included, see figure 5.12. The mean value of χ^2 goes down to less than two and the improvement

[3] In this work next-to-next-to-leading order effects in the quark distribution functions are taken into account, where charge and isospin violation are included.

[4] The Weinberg angle could also represent the NuTeV measurement, but here g_L and g_R are chosen and θ_W should not be affected by the sterile neutrinos.

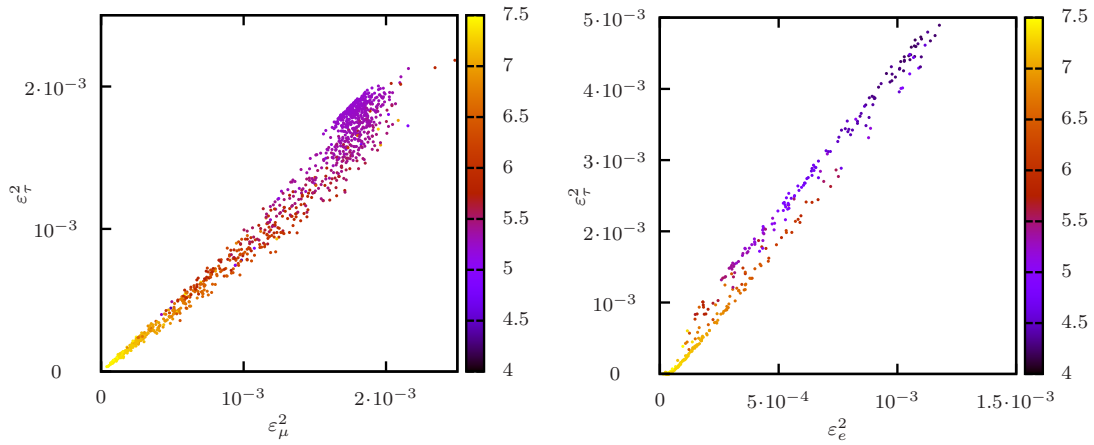

(a) ε_τ^2 and ε_μ^2 are shown, $\varepsilon_e^2 \approx 0$

(b) ε_τ^2 and ε_e^2 are shown, $\varepsilon_\mu^2 \approx 0$

Figure 5.11: Parameters ε_α^2 with $\chi^2 \leq \chi^2_{SM}$ for the case of the normal hierarchy of light neutrino masses. The color denotes the value of χ^2.

compared to the SM becomes almost two per d.o.f..

5.7.2 Inverse Mass Hierarchy

For the case of the inverse mass hierarchy of the light neutrinos, the case of negligibly small ε_μ^2 leads to tiny mixings to the electron and tau neutrino as well, thus resulting in the same fit as for the SM. Figure 5.13a therefore only shows the case of small mixing to the electron neutrino, $\varepsilon_e^2 \approx 0$. The smallest values of χ^2 are ≈ 5.5, leading to no improvement of the fit compared to the SM, as $\Delta\chi^2$ per d.o.f. is smaller than one.

This changes again radically, if the mass of the W boson is not included in the fit, see figure 5.13b. The best values of χ^2 are ≈ 1.5, therefore the fit improves compared to the SM by two per d.o.f..

5.7.3 Degenerate Masses

In the case of degenerate light neutrino masses, there are almost no points for non-negligible mixing of the sterile neutrinos the the muon neutrino, thus $\varepsilon_\mu^2 \approx 0$ and figure 5.14 shows only ε_τ^2 and ε_e^2. The smallest values of χ^2 are ≈ 5, leading to no improvement of the fit compared to the SM, as $\Delta\chi^2$ per d.o.f. is again smaller than one. The fit does not improve when not including the mass of the W boson and it is therefore not shown here.

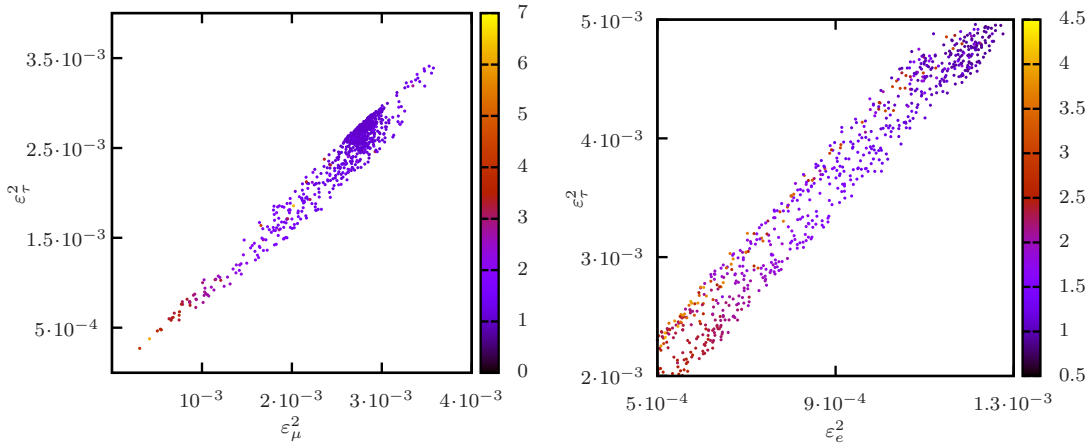

(a) ε_τ^2 and ε_μ^2 are shown, $\varepsilon_e^2 \approx 0$

(b) ε_τ^2 and ε_e^2 are shown, $\varepsilon_\mu^2 \approx 0$

Figure 5.12: Parameters ε_α^2 with $\chi^2 \leq \chi^2_{SM}$ for the case of the normal hierarchy of light neutrino masses. The color denotes the value of χ^2. The W boson mass is not included in the fit here.

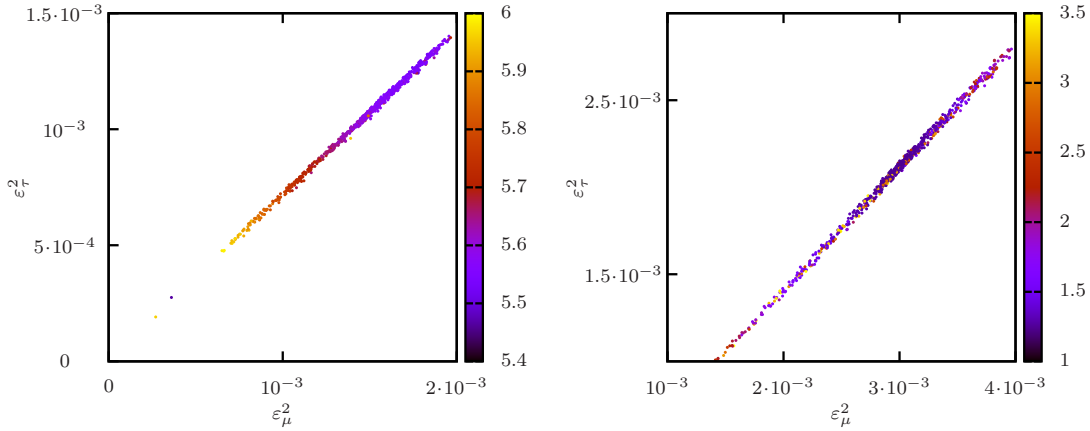

(a) ε_τ^2 and ε_μ^2 are shown, $\varepsilon_e^2 \approx 0$

(b) ε_τ^2 and ε_μ^2 are shown, $\varepsilon_e^2 \approx 0$, M_W not included.

Figure 5.13: Parameters ε_τ^2 and ε_μ^2 with $\chi^2 \leq \chi^2_{SM}$ for the case of the inverse hierarchy of light neutrino masses. The mixing to the electron neutrino is negligible, $\varepsilon_e^2 \approx 0$. The color denotes the value of χ^2. In (b) the W boson mass is not included in the fit.

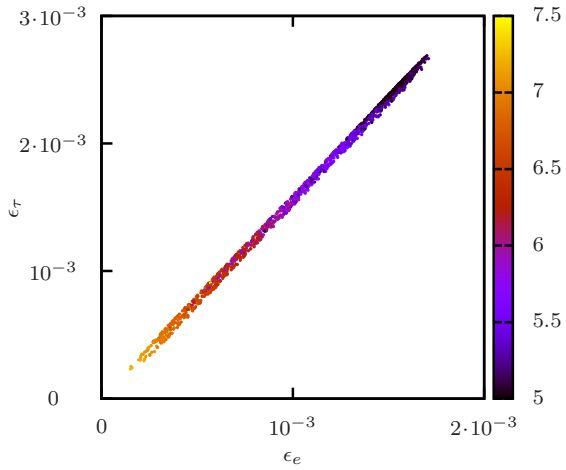

Figure 5.14: Parameters ε_τ^2 and ε_e^2 with $\chi^2 \leq \chi^2_{SM}$ for the case of degenerate light neutrino masses. The mixing to the muon neutrino is negligible, $\varepsilon_\mu^2 \approx 0$. The color denotes the value of χ^2.

5.7.4 Masses of the heavy Neutrinos

In figure 5.15 the distribution of the masses of the heavy neutrinos is shown. The points are fitted in the case of normal hierarchy of the light neutrino masses and almost vanishing mixing of the sterile states to the muon neutrino. The masses of the heavy neutrinos are all in the TeV range, and since $M_1 \approx M_3$, their medium value is plotted.

5.7.5 Discussion

The mass hierarchy of the light neutrinos seems to have a big impact on the quality of the fit. While for the inverse hierarchy and a degenerate mass spectrum the fit is worse compared to the SM, in the case of normal hierarchy it is at least as good as the SM. When omitting the mass of the W boson in the fit, the inclusion of heavy sterile neutrinos can lead to an improvement compared to the SM of two per d.o.f..

Note that for all points with χ^2 less than the SM value, the T parameter is quite sizeable and negative (between -0.1 and -0.2). In this range, the negative T parameter can screen the effect of the active-sterile mixing on parameters such as G_F that are measured at high precision and therefore constrain the mixing parameters. This interplay of tree-level and loop effects has already been studied in [67], [80] and [81], where the tree-level effects were induced by heavy sterile neutrinos, but the contributions to the S, T, U parameters were assumed to originate from different beyond the SM physics[5].

[5] They actually discussed the possibility of a negative T parameter coming from a very large Higgs mass, $M_H \gg 115$ GeV. This scenario however is excluded by now.

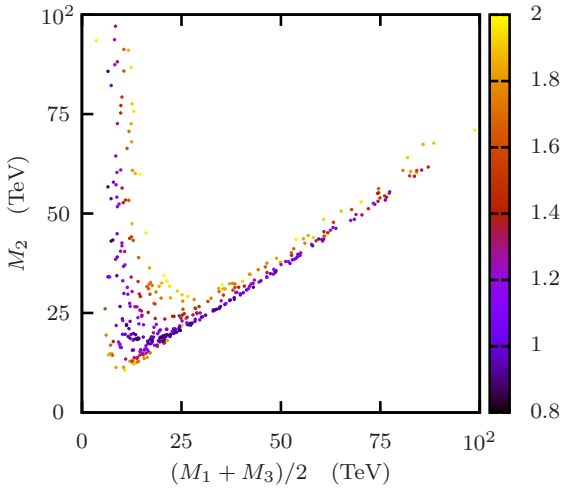

Figure 5.15: Masses M_1, M_2 and M_3 of the heavy neutrinos, in the case of normal hierarchy of the light masses and almost vanishing $\varepsilon_\mu^2 \approx 0$. Since the masses M_1 and M_3 are approximately equal, their medium value is plotted. The color denotes the value of χ^2.

Here all effects are induced only by adding sterile neutrinos to the particle content of the SM.

But the fits show that the large negative T paramter is in conflict with the experimental measurements of the W boson mass. The fits improve drastically, when M_W is omitted. This might motivate for example the introduction of a Higgs triplet, as it can have a notable effect on the W boson mass and additionally lead to a cancellation of contributions to the active neutrino masses.

Note also that some of the best fit values have quite a large contribution to neutrinoless double-beta decay. The resulting effective electron neutrino mass is close to the current bounds and could be detected in future experiments.

The type I seesaw extension of the SM can only improve the fits compared to the SM when the experimental value of the W boson mass is omitted. Therefore it should be investigated how the shift in the W boson mass could be compensated by additional beyond the SM physics.

CHAPTER 6

Conclusions

In this work it has been shown that sterile neutrinos can have a wide spectrum of phenomenological implications on observables in different processes. Although they are sterile, i.e. singlets under the SM gauge groups, they interact through their mixing to the active neutrinos. Given the current precision of experiments, the signatures of sterile neutrinos could be observed, for example in electroweak precision measurements or oscillation experiments.

The introduction of sterile neutrinos has been motivated by the observation that neutrinos have tiny, but non-vanishing masses. As verified now in numerous experiments, neutrinos oscillate into each other and thereby one can measure their mass-squared differences. In addition to providing the mass term for neutrinos, sterile neutrinos can have impact on various processes.

Very light sterile neutrinos, with masses at the eV scale, can oscillate with the SM neutrinos, leading to new oscillation patterns and missing active neutrino flux. There have even been some (controversial) observations that could be explained by the existence of a light sterile neutrino. Neutrinoless double-beta decay is a process that can only occur when lepton number is violated. It is forbidden in the SM and would thus be a clear signature of beyond the SM physics. Sterile neutrinos can contribute to this decay in two ways: They have a direct contribution that strongly depends on whether

their masses are above or below the scale of momentum transfer (which is about 100 MeV). Furthermore, when they are responsible for the light neutrino masses, they have an indirect contribution through the exchange of light Majorana neutrinos.

Other processes that are forbidden in the SM and could be induced by sterile neutrinos are decays that violate lepton flavor. The muon decay $\mu \to e\gamma$ has not been observed so far and thus places strong bounds on the mixing of active and sterile neutrinos. In colliders, sterile neutrinos can be observed in meson decays, when the masses of the former are small enough. Up to masses of about 90 GeV they can still be produced via the decay of W and Z bosons. At higher masses fusion processes and virtual gauge bosons can produce sterile neutrinos. But the bigger the mass, the more difficult becomes the observation. Therefore, bounds from collider physics above 150 GeV are not competitive with indirect measurements. When the mass of a sterile neutrino is so big that it cannot be produced in interactions, they leave indirect traces. The mixing matrix of the light neutrinos becomes then non-unitary and electroweak cross-sections can be suppressed. As virtual particles, the sterile neutrinos can propagate in loops, thus affecting the self-energies of the W and Z bosons. This is represented by the so-called oblique corrections. Since the precision in electroweak measurements has become so impressively high, even these small effects could be detected.

In this thesis, two scales of sterile neutrino masses have been picked up. In chapter 4 a very light sterile neutrino was considered. When the mass of the sterile state is at a few eV, oscillation phenomena can be observed, as the state remains coherent with the active neutrinos. Especially an oscillation of a sterile neutrino and the electron neutrino is motivated by observations in reactor experiments and in calibrations of detectors, where a deficit in the electron (anti)neutrino flux compared to (also controversial) theoretical predictions has been observed. To detect this oscillation, the interaction of neutrinos with matter could be used. Through the MSW effect, oscillations can be resonantly enhanced by coherent forward scattering of neutrinos on the particles of the medium. This effect depends on the baseline of the experiment, the energies of the neutrinos and the matter density and relative abundance of electrons in the medium. It has been investigated, whether such an enhancement of $\nu_e \leftrightarrow \nu_s$ oscillation could be present for neutrinos produced in the atmosphere that subsequently cross the Earth. The Earth has herein been treated as an object with two different density regions, the core and the mantle.

For quite a sizeable mixing of the electron and sterile neutrino of $U_{e4} = 0.2$, the oscillation could be enhanced such that the deficit in the electron neutrino flux is as large as 80% at a neutrino energy of about 8 TeV and for trajectories that cross the core of the

earth. For a smaller mixing, the deficit decreases rapidly, for $U_{e4} = 0.05$ it is maximally 20% of the original electron neutrino flux. The deficit is however independent of the mass of the sterile neutrino, the minimum in the flux is only shifted to lower energies for smaller mass-squared differences.

Since the IceCube detector would be very suitable to look for these oscillations, in future work one should take into account the energy and angular resolution of the detector to quantify whether the IceCube experiment could place competitive bounds on the active–sterile mixing of a light sterile neutrino with the electron neutrino or even detect the sterile state. This analysis has been done in [57] and [58] for the oscillation of muon to sterile neutrinos.

In the second part of this work, indirect effects of heavy sterile neutrinos in electroweak processes were studied. Tree-level effects are induced by the resulting non-unitarity of the light neutrino (PMNS) mixing matrix, modifying electroweak observables that are measured in processes including neutrinos. Sterile neutrinos propagating in loops modify the self-energies of the W and Z boson. These have been calculated for Majorana neutrinos and the S, T, U parameters have been summarized.

The study of these effects was motivated by the observations of two experiments. The LEP experiments measured the decay width of the Z boson into invisible particles, and the extracted number of neutrinos coupling to the Z boson was determined to be smaller than three by 2σ. The NuTeV experiment measured the ratios of neutral to charged current cross sections of (anti)neutrino–nucleon scattering. Since both ratios were slightly smaller than expected, the extracted Weinberg angle differed from the value measured in other experiments by 3σ. Since sterile neutrinos with masses above the Z boson mass suppress the coupling of the SM neutrinos to the Z and W boson, both of these effects could be caused by heavy sterile neutrinos.

To test this hypothesis, the corrections induced by the tree-level and one-loop effects were summarized and a χ^2-fit was performed on six electroweak observables. For a sizeable mixing of active and sterile neutrinos, the fit could be improved by a $\Delta\chi^2$ of about two per degree of freedom it the mass of the W boson is not included. In this case, however, the model becomes very fine-tuned, as the contributions of the sterile neutrinos to the masses of the light neutrinos had to cancel at many orders of magnitude.

Models with a large mixing of the active neutrinos with heavy sterile neutrinos are in general strongly constained by their impact on electroweak precision observables, such as the Fermi constant G_F. But when taking the self-energy corrections into account, one can see that the tree-level effects could be "screened" by a sizeable negative T parameter. This has already been investigated in [67], [80] and [81], but they assumed

that the contributions to the S, T, U parameters came from some other beyond the SM physics, rather than sterile neutrinos. In the analysis of the corrections from heavy Majorana neutrinos, certain points in the parameter space of masses and mixing of the sterile neutrinos were discovered, that led to a sizeable negative T parameter.

In future work it would be interesting to study the effect of a triplet Higgs on the analysis. It can have notable effects on the mass of the W boson, the parameter that is limiting the improvement of the χ^2-fit in the scenario with only heavy sterile neutrinos. Furthermore it could also lead to cancellations in the contributions to the light neutrino masses. The model building aspect could also be interesting to explore. If a symmetry would impose the cancellations in the light neutrino masses and the corrections to quantities like G_F, but would not affect the invisible decay width and the neutrino–nucleon cross sections, this could lead to the above described phenomenology.

Appendices

APPENDIX A

Three-Layer Calculation for the Two-Flavor Approximation

A.1 Solution of the homogeneous Equation

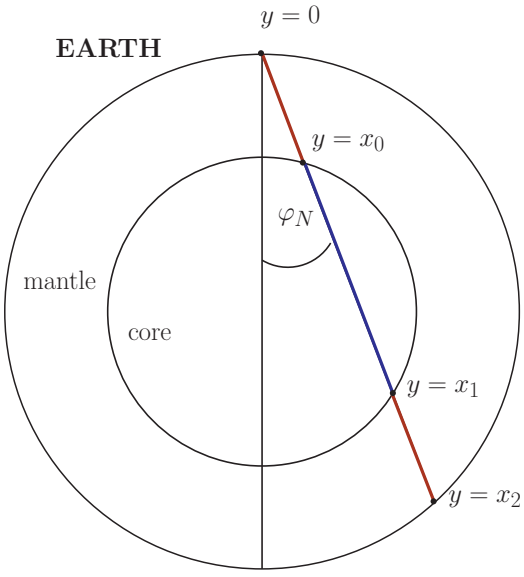

Figure A.1: Definition of the points $y = 0, x_0, x_1, x_2$ of the passage through the Earth.

For the solution of the homogeneous equation

$$\nu_0(x) = S(x,0)\nu(0) \tag{A.1}$$

use the multiplicative property of the evolution matrix. The points 0, x_0, x_1 and x_2 are defined as in Figure A.1. Therefore, for small enough angles φ_N, the neutrinos first pass through the mantle from 0 to x_0, then through the core from x_0 to x_1 and then through the mantle again from x_1 to x_2. The density is taken to be constant in each of these layers. As the parameters θ and ϕ in the S-matrix, see equation 4.78, both depend on the density, the S-matrix depends on whether the neutrinos move through the core or the mantle. These two possiblities are indicated by an index S_m for the mantle and S_c for the core.

This gives then for $y = x_2$:

$$\nu_0(x_2) = S_m(x_2,x_1)S_c(x_1,x_0)S_m(x_0,0)\cdot\nu(0)\,. \tag{A.2}$$

Note that for each constant-density layer the S-matrix

$$S(x,x_0) = S(x-x_0) \tag{A.3}$$

depends only on the interval $x - x_0$ and therefore the evolution of ν_0 depends only on the lengths of the passages that we called $s = x_2 - x_1 = x_0 - 0$ through the mantle and $l = x_1 - x_0$ through the core. With this one can write:

$$\nu_0(x_2) = S_m(s)S_c(l)S_m(s)\cdot\nu(0)\,. \tag{A.4}$$

The three-layer solution for the inhomogeneous equation will become more complicated though, as here we have to integrate over the position y.

A.2 Solution of the inhomogeneous Equation

The solution $\nu_1(x)$ of the inhomogeneous equation was given by (equation 4.62)

$$\nu_1(x) = -iS(x,0)\int_0^x S(0,y)\tilde{f}(y)dy \tag{A.5}$$

$$= -i\int_0^x S(x,y)\tilde{f}(y)dy\,, \tag{A.6}$$

where both the S-matrix and the source term $\tilde{f}$ depend on the density of the medium. One has to be careful about the different densities in mantle and core, therefore the notation in equation A.5 will be more useful.

Since the S-matrix is multiplicative and the integral adds up over different intervals one gets for three layers (points 0, x_0, x_1 and x_2 are defined as before):

$$\begin{aligned}\nu_1(x_2) = &-iS_m(x_2,x_1)S_c(x_1,x_0)S_m(x_0,0) \qquad \text{(A.7)}\\ &\left\{\int_0^{x_0} S_m^{-1}(y,0)\tilde{f}_{m1}(y)dy + \int_{x_0}^{x_1} S_m^{-1}(x_0,0)S_c^{-1}(y,x_0)\tilde{f}_c(y)dy\right.\\ &\left.+\int_{x_1}^{x_2} S_m^{-1}(x_0,0)S_c^{-1}(x_1,x_0)S_m^{-1}(y,x_1)\tilde{f}_{m2}(y)dy\right\}\\ = &-iS_m(x_2,x_1)S_c(x_1,x_0)S_m(x_0,0)\cdot\int_0^{x_0} S_m^{-1}(y,0)\tilde{f}_{m1}(y)dy \qquad \text{(A.8)}\\ &-iS_m(x_2,x_1)S_c(x_1,x_0)\cdot\int_{x_0}^{x_1} S_c^{-1}(y,x_0)\tilde{f}_c(y)dy\\ &-iS_m(x_2,x_1)\cdot\int_{x_1}^{x_2} S_m^{-1}(y,x_1)\tilde{f}_{m2}(y)dy\\ = &-iS_m(x_2,x_1)S_c(x_1,x_0)\cdot\int_0^{x_0} S_m(x_0,y)\tilde{f}_{m1}(y)dy \qquad \text{(A.9)}\\ &-iS_m(x_2,x_1)\cdot\int_{x_0}^{x_1} S_c(x_1,y)\tilde{f}_c(y)dy\\ &-i\cdot\int_{x_1}^{x_2} S_m(x_2,y)\tilde{f}_{m2}(y)dy\,,\end{aligned}$$

where from the first to the second equation all S-matrices that do not depend on y were pulled out of the integral, which then cancel with their inverse. The source terms $\tilde{f}$ are for the three layers given by:

$$\tilde{f}_{m1}(y) = H_{e\mu'}\nu'_\mu(0)e^{(i/2)(H^m_{ee}+H^m_{ss}-2H_{\mu'\mu'})\cdot y} \qquad \text{(A.10)}$$

$$\tilde{f}_c(y) = H_{e\mu'}\nu'_\mu(0)e^{(i/2)\left\{(H^m_{ee}+H^m_{ss}-2H_{\mu'\mu'})\cdot(x_0-0)+(H^c_{ee}+H^c_{ss}-2H_{\mu'\mu'})\cdot(y-x_0)\right\}} \qquad \text{(A.11)}$$

$$\tilde{f}_{m2}(y) = H_{e\mu'}\nu'_\mu(0)e^{(i/2)\left\{(H^m_{ee}+H^m_{ss}-2H_{\mu'\mu'})\cdot(x_0+(y-x_1))+(H^c_{ee}+H^c_{ss}-2H_{\mu'\mu'})\cdot(x_1-x_0)\right\}} \qquad \text{(A.12)}$$

The indices m and c denote again the mantle and core regions and indicate those parameters that depend on the densities. Note that the points x_0, x_1 and x_2 depend on the Nadir angle φ_N

These are now the three-layer expressions for the homogenous and inhomogenous term of the neutrino evolution in the two-flavor case.

APPENDIX B

One-Loop Integrals

The dimensionally regularized one-loop integrals for the one- and two-point functions are quoted here. The metric $g_{\mu\nu} = (+,-,-,-)$ is used. The dimensions are $d = 4 - 2\epsilon$. Note the difference between ϵ and ε. For original references, see [82] (note that the metric is defined differently) and see [83].

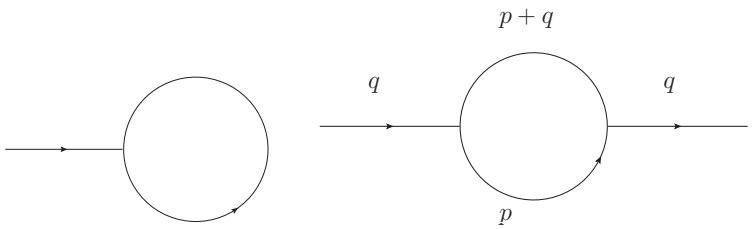

(a) Tadpole diagram (one-point function).

(b) Two-point function

Figure B.1: Loop diagrams for the one- and two-point functions.

B.1 One-Point Function

The scalar one-point function (see figure B.1a) is defined as

$$A(m) = \frac{\mu^{4-d}}{i\pi^2} \int d^d p \frac{1}{p^2 - m^2 + i\varepsilon} \,. \tag{B.1}$$

μ is here the renormalization parameter. In the limit $\epsilon \to 0$ this gives

$$A(m) = m^2 \left(\Delta - \ln\left(\frac{m}{\mu^2}\right) + 1 \right) , \tag{B.2}$$

where Δ is defined as

$$\Delta = \frac{1}{\epsilon} - C + \ln(4\pi) \tag{B.3}$$

and $C = 0.577216$ is the Euler constant.

B.2 Two-Point Functions

The two-point function is given by the integral

$$B(q, m_1, m_2) = \int \frac{d^d p}{(2\pi)^d} \frac{p^\mu q^\nu + p^\nu q^\mu + 2p^\mu q^\nu - g^{\mu\nu}(p \cot(p+q)) + g^{\mu\nu} m_1 m_2}{(p^2 - m_1^2 + i\varepsilon)((p+q)^2 - m_2^2 + i\varepsilon)} \,, \tag{B.4}$$

where m_1 and m_2 are the masses of the particles in the loop, with the respective momenta p and $p+q$, see figure B.1b. For simplicity one divides this integral in different parts and solves them individually.

$$B(q, m_1, m_2) = \frac{i\pi^2}{\mu^{4-d}} \frac{1}{(2\pi)^d} \Big[(q^\alpha B^\beta(q, m_1, m_2) + B^{\alpha\beta}(q, m_1, m_2)) \cdot \tag{B.5}$$

$$(g_{\mu\alpha} g_{\nu\beta} + g_{\mu\beta} g_{\alpha\nu} - g_{\mu\nu} g_{\alpha\beta}) + g_{\mu\nu} m_1 m_2 B_0(q, m_1, m_2)] \tag{B.6}$$

$$= \frac{i\pi^2}{\mu^{4-d}} \frac{1}{(4\pi)^d} \big[(B_1(q, m_1, m_2) + B_{21}(q, m_1, m_2))(2q_\mu q_\nu - g_{\mu\nu} q^2) + \tag{B.7}$$

$$B_{22}(q, m_1, m_2)(2-d) g_{\mu\nu} + g_{\mu\nu} m_1 m_2 B_0(q, m_1, m_2)] \tag{B.8}$$

$$= \frac{i\pi^2}{\mu^{4-d}} \frac{1}{(2\pi)^d} \left[q_\mu q_\nu P(q, m_1, m_2) + g_{\mu\nu} (Q(q, m_1, m_2) + m_1 m_2 B_0(q, m_1, m_2)) \right] , \tag{B.9}$$

where

$$P(q,m_1,m_2) = 2B_1(q,m_1,m_2) + 2B_{21}(q,m_1,m_2)\,, \tag{B.10}$$

$$Q(q,m_1,m_2) = (d-2)B_{22}(q,m_1,m_2) + q^2[B_1(q,m_1,m_2) + B_{21}(q,m_1,m_2)]\,. \tag{B.11}$$

The loop integrals are defined as

$$B_0(q,m_1,m_2) = \frac{\mu^{4-d}}{i\pi^2}\int d^dp \frac{1}{(p^2-m_1^2+i\varepsilon)((p+q)^2-m_2^2+i\varepsilon)}\,, \tag{B.12}$$

$$q^\mu B_1(q,m_1,m_2) = \frac{\mu^{4-d}}{i\pi^2}\int d^dp \frac{p^\mu}{(p^2-m_1^2+i\varepsilon)((p+q)^2-m_2^2+i\varepsilon)}\,, \tag{B.13}$$

$$q^\mu q^\nu B_{21}(q,m_1,m_2) + g^{\mu\nu}B_{22}(q,m_1,m_2) = \frac{\mu^{4-d}}{i\pi^2}\int d^dp \frac{p^\mu p^\nu}{(p^2-m_1^2+i\varepsilon)((p+q)^2-m_2^2+i\varepsilon)}\,. \tag{B.14}$$

B_0 can be expanded in order of ϵ, using the Feynman parametrization

$$B_0(q,m_1,m_2) = \Delta - \int_0^1 dx \ln\left(\frac{x^2q^2 - x(q^2+m_1^2-m_2^2)+m_1^2-i\varepsilon}{\mu^2}\right) + \mathcal{O}(d-4)\,, \tag{B.15}$$

where Δ is defined as before in equation (B.3). In the limit $d \to 3$ this gives the following identities (omitting imaginary parts):

$$B_0(q,0,0) = \Delta - \ln\left(\frac{|q^2|}{\mu^2}\right) + 2 \tag{B.16}$$

$$B_0(0,0,m) = B_0(0,m,0) = \Delta - \ln\left(\frac{m^2}{\mu^2}\right) + 1 = \frac{1}{m^2}A(m^2) \tag{B.17}$$

Useful relations between the above introduced quantities are

$$B_1(q,m_1,m_2) = \frac{1}{2q^2}[A(m_1) - A(m_2) + (m_2^2 - m_1^2 - q^2)B_0(q,m_1,m_2)]\,, \tag{B.18}$$

$$B_{21}(q,m_1,m_2) = \frac{1}{3q^2}\left[A(m_2) - m_1^2B_0(q,m_1,m_2) - \right. \tag{B.19}$$

$$\left. -2(q^2+m_1^2-m_2^2)B_1(q,m_1,m_2) - \frac{1}{2}(m_1^2+m_2^2-q^2/3)\right]\,, \tag{B.20}$$

$$B_{22}(q,m_1,m_2) = \frac{1}{6}\left[A(m_2) - 2m_1^2B_0(q,m_1,m_2) + \right. \tag{B.21}$$

$$\left. +(q^2+m_1^2-m_2^2)B_1(q,m_1,m_2) + m_1^2+m_2^2-q^2/3\right]\,. \tag{B.22}$$

Bibliography

[1] R. Davis, Phys.Rev.Lett. **12**, 303 (1964).

[2] SNO Collaboration, Q. Ahmad *et al.*, Phys.Rev.Lett. **87**, 071301 (2001), nucl-ex/0106015.

[3] W. Grimus, Lect.Notes Phys. **629**, 169 (2004), hep-ph/0307149.

[4] R. Mohapatra and P. Pal, World Sci.Lect.Notes Phys. **60**, 1 (1998).

[5] Particle Data Group, J. Beringer *et al.*, Phys.Rev. **D86**, 010001 (2012).

[6] S. Kanemura and K. Yagyu, Phys.Rev. **D85**, 115009 (2012), 1201.6287.

[7] W. Grimus, R. Pfeiffer, and T. Schwetz, Eur.Phys.J. **C13**, 125 (2000), hep-ph/9905320.

[8] V. Aseev *et al.*, Phys.Atom.Nucl. **75**, 464 (2012).

[9] C. Kraus *et al.*, Eur.Phys.J. **C40**, 447 (2005), hep-ex/0412056.

[10] KATRIN Collaboration, J. Formaggio, AIP Conf.Proc. **1441**, 426 (2012).

[11] V. Hannen, J.Phys.Conf.Ser. **375**, 042004 (2012).

[12] P. Minkowski, Phys.Lett. **B67**, 421 (1977).

[13] T. Yanagida, Conf.Proc. **C7902131**, 95 (1979).

[14] R. N. Mohapatra and G. Senjanovic, Phys.Rev. **D21**, 3470 (1980).

[15] M. Gell-Mann, P. Ramond, and R. Slansky, Conf.Proc. **C790927**, 315 (1979).

[16] G. Lazarides, Q. Shafi, and C. Wetterich, Nucl.Phys. **B181**, 287 (1981).

[17] M. Magg and C. Wetterich, Phys.Lett. **B94**, 61 (1980).

[18] R. N. Mohapatra and G. Senjanovic, Phys.Rev. **D23**, 165 (1981).

[19] W. Grimus and L. Lavoura, JHEP **0011**, 042 (2000), hep-ph/0008179.

[20] J. Schechter and J. Valle, Phys.Rev. **D25**, 2951 (1982).

[21] F. Bezrukov, H. Hettmansperger, and M. Lindner, Phys.Rev. **D81**, 085032 (2010), 0912.4415.

[22] T. Asaka and M. Shaposhnikov, Phys.Lett. **B620**, 17 (2005), hep-ph/0505013.

[23] T. Asaka, S. Blanchet, and M. Shaposhnikov, Phys.Lett. **B631**, 151 (2005), hep-ph/0503065.

[24] F. Bezrukov, A. Kartavtsev, and M. Lindner, (2012), 1204.5477.

[25] K. Abazajian *et al.*, (2012), 1204.5379.

[26] E. Akhmedov, D. Hernandez, and A. Smirnov, JHEP **1204**, 052 (2012), 1201.4128.

[27] LSND Collaboration, C. Athanassopoulos *et al.*, Nucl.Instrum.Meth. **A388**, 149 (1997), nucl-ex/9605002.

[28] H. Gemmeke *et al.*, Nucl.Instrum.Meth. **A289**, 490 (1990).

[29] LSND Collaboration, A. Aguilar-Arevalo *et al.*, Phys.Rev. **D64**, 112007 (2001), hep-ex/0104049.

[30] KARMEN Collaboration, B. Armbruster *et al.*, Phys.Rev. **D65**, 112001 (2002), hep-ex/0203021.

[31] MiniBooNE Collaboration, A. Aguilar-Arevalo *et al.*, Nucl.Instrum.Meth. **A599**, 28 (2009), 0806.4201.

[32] MiniBooNE Collaboration, A. Aguilar-Arevalo *et al.*, Phys.Rev.Lett. **105**, 181801 (2010), 1007.1150.

[33] C. Giunti and M. Laveder, Phys.Rev. **C83**, 065504 (2011), 1006.3244.

[34] P. Huber, Phys.Rev. **C84**, 024617 (2011), 1106.0687.

[35] Nucifer Collaboration, A. S. Cucoanes, J.Phys.Conf.Ser. **375**, 042063 (2012).

[36] MINOS Collaboration, D. Michael *et al.*, Nucl.Instrum.Meth. **A596**, 190 (2008), 0805.3170.

[37] J. Kopp, M. Maltoni, and T. Schwetz, Phys.Rev.Lett. **107**, 091801 (2011), 1103.4570.

[38] NOMAD Collaboration, P. Astier *et al.*, Nucl.Phys. **B611**, 3 (2001), hep-ex/0106102.

[39] F. Dydak *et al.*, Phys.Lett. **B134**, 281 (1984).

[40] MiniBooNE Collaboration, A. Aguilar-Arevalo *et al.*, (2012), 1207.4809.

[41] M. Antonello *et al.*, (2012), 1209.0122.

[42] L. Wolfenstein, Phys.Rev. **D17**, 2369 (1978).

[43] S. Mikheev and A. Y. Smirnov, Nuovo Cim. **C9**, 17 (1986).

[44] S. Antusch, C. Biggio, E. Fernandez-Martinez, M. Gavela, and J. Lopez-Pavon, JHEP **0610**, 084 (2006), hep-ph/0607020.

[45] T. Cheng and L. Li, *Gauge theory of elementary particle physics* (Oxford University Press, USA, 1985).

[46] W. J. Marciano, T. Mori, and J. M. Roney, Ann.Rev.Nucl.Part.Sci. **58**, 315 (2008).

[47] Particle Data Group, C. Amsler *et al.*, Phys.Lett. **B667**, 1 (2008).

[48] MEG collaboration, J. Adam *et al.*, Phys.Rev.Lett. **107**, 171801 (2011), 1107.5547.

[49] W. Rodejohann, Int.J.Mod.Phys. **E20**, 1833 (2011), 1106.1334.

[50] P. Benes, A. Faessler, F. Simkovic, and S. Kovalenko, Phys.Rev. **D71**, 077901 (2005), hep-ph/0501295.

[51] EXO Collaboration, M. Auger *et al.*, Phys.Rev.Lett. **109**, 032505 (2012), 1205.5608.

[52] KamLAND-Zen Collaboration, A. Gando, (2012), 1205.6130.

[53] A. Atre, T. Han, S. Pascoli, and B. Zhang, JHEP **0905**, 030 (2009), 0901.3589.

[54] M. E. Peskin and T. Takeuchi, Phys.Rev. **D46**, 381 (1992).

[55] M. E. Peskin and D. V. Schroeder, *An Introduction to quantum field theory* (Westview Press, 1995).

[56] B. A. Kniehl and H.-G. Kohrs, Phys.Rev. **D48**, 225 (1993).

[57] S. Razzaque and A. Y. Smirnov, JHEP **1107**, 084 (2011), 1104.1390.

[58] S. Razzaque and A. Y. Smirnov, Phys.Rev. **D85**, 093010 (2012), 1203.5406.

[59] F. Halzen, (2011), 1111.0918.

[60] V. Barger, Y. Gao, and D. Marfatia, Phys.Rev. **D85**, 011302 (2012), 1109.5748.

[61] C. Giunti, Phys.Lett. **B686**, 41 (2010), 1001.0760.

[62] V. Agrawal, T. Gaisser, P. Lipari, and T. Stanev, Phys.Rev. **D53**, 1314 (1996), hep-ph/9509423.

[63] A. Dziewonski and D. Anderson, Phys.Earth Planet.Interiors **25**, 297 (1981).

[64] ALEPH Collaboration, DELPHI Collaboration, L3 Collaboration, OPAL Collaboration, LEP Electroweak Working Group, SLD Heavy Flavor Group, (2002), hep-ex/0212036.

[65] NuTeV Collaboration, G. Zeller *et al.*, Phys.Rev.Lett. **88**, 091802 (2002), hep-ex/0110059.

[66] J. Hewett, T. Takeuchi, and S. D. Thomas, (1996), hep-ph/9603391.

[67] W. Loinaz, N. Okamura, S. Rayyan, T. Takeuchi, and L. Wijewardhana, Phys.Rev. **D70**, 113004 (2004), hep-ph/0403306.

[68] E. Akhmedov, A. Kartavtsev, M. Lindner, L. Michaels, and J. Smirnov, (2013), in preparation.

[69] T. Cheng and L. Li, *Gauge theory of elementary particle physics: Problems and solutions* (Oxford University Press, USA, 2000).

[70] L3 Collaboration, P. Achard *et al.*, Phys.Lett. **B517**, 67 (2001), hep-ex/0107014.

[71] CMS Collaboration, S. Chatrchyan *et al.*, Phys.Lett. **B717**, 109 (2012), 1207.6079.

[72] M. Blennow, E. Fernandez-Martinez, J. Lopez-Pavon, and J. Menendez, JHEP **1007**, 096 (2010), 1005.3240.

[73] A. Ibarra, E. Molinaro, and S. Petcov, JHEP **1009**, 108 (2010), 1007.2378.

[74] M. Mitra, G. Senjanovic, and F. Vissani, Nucl.Phys. **B856**, 26 (2012), 1108.0004.

[75] M. Gonzalez-Garcia, M. Maltoni, J. Salvado, and T. Schwetz, (2012), 1209.3023.

[76] J. Casas and A. Ibarra, Nucl.Phys.Proc.Suppl. **95**, 268 (2001).

[77] M. Baak *et al.*, (2012), 1209.2716.

[78] M. Baak *et al.*, Eur.Phys.J. **C72**, 2003 (2012), 1107.0975.

[79] M. Traini, Phys.Lett. **B707**, 523 (2012), 1110.3594.

[80] W. Loinaz, N. Okamura, T. Takeuchi, and L. Wijewardhana, Phys.Rev. **D67**, 073012 (2003), hep-ph/0210193.

[81] T. Takeuchi and W. Loinaz, (2004), hep-ph/0410201.

[82] G. Passarino and M. Veltman, Nucl.Phys. **B160**, 151 (1979).

[83] M. Plumacher, (1998), hep-ph/9807557.

Erklärung:

Ich versichere, dass ich diese Arbeit selbstständig verfasst habe und keine anderen als die angegebenen Quellen und Hilfsmittel benutzt habe.

Heidelberg, den 15.12.2012 .....

(Lisa Michaels)